1-1-1979

Propagation in pulsar magnetospheres: effects of a shearing plasma.

Alice K. Harding
University of Massachusetts Amherst

PROPAGATION IN PULSAR MAGNETOSPHERES:

EFFECTS OF A SHEARING PLASMA

A Dissertation Presented

By

ALICE KUST HARDING

Submitted to the Graduate School of the
University of Massachusetts in partial fulfillment
of the requirements for the degree of

DOCTOR OF PHILOSOPHY

September 1979

Astronomy

PROPAGATION IN PULSAR MAGNETOSPHERES:

EFFECTS OF A SHEARING PLASMA

A Dissertation Presented

By

ALICE KUST HARDING

Approved as to style and content by:

Eugene H. Tademaru
Chairperson of Committee

Joseph H. Taylor, Member

William M. Irvine, Member

Ting-Wei Tang, Member

Frederick W. Byron, Jr.
Head, Department of Physics
and Astronomy

ACKNOWLEDGEMENTS

There are several people whose work and ideas made essential contributions to this thesis. First, I thank my adviser Eugene Tademaru for his physical insights, tireless discussions and sustained encouragement throughout my graduate studies. I am most grateful to Ian Lerche for laying the foundations and for his continued interest in the problem. I would like to thank James Cordes for providing support and encouragement, many helpful comments, and access to both published and unpublished data. Discussions and friendships with my colleagues, especially Peter Backus, Lee Fowler and Joel Weisberg, were also of great benefit.

I am grateful to the AAUW Educational Foundation for providing a fellowship to support part of this research. I also thank Nellie Bristol for an excellent typing job.

Finally, I thank my husband, Dave, for being a constant source of support and understanding.

ABSTRACT

Propagation in Pulsar Magnetospheres: Effects of a Shearing Plasma

(September 1979)

Alice Kust Harding, B.A., Bryn Mawr College,
M.S., University of Massachusetts
Ph.D., University of Massachusetts

Directed by: Professor Eugene H. Tademaru

According to current theories of the pulsar magnetosphere, it is likely that regions of relativistic velocity shear exist either in the emission region or near the light cylinder. The propagation of radiation through these relativistically moving media is a problem of major importance regarding the interpretation of the observed signals. Numerical models are developed in which to investigate the propagation of time dependent, polarized radiation through regions of shearing plasma. Maxwell's equations and the Minkowski relations are used to solve explicitly for the radiation fields in stratified media having symmetric velocity profiles.

The simplest model is a Gaussian modulated wave packet incident on a field-free plasma undergoing laminar shear. This medium is found to be birefringent: a pulse polarized in the plane of shear undergoes multiple reflections from velocity gradients and a pulse polarized perpendicular to the plane of shear is unaffected by the motion. Resonances appear in the transmission coefficient of the parallel mode in a narrow frequency range above the plasma frequency, causing periodic temporal

modulations in the transmitted pulse. The birefringence produces polarization fluctuations which are correlated with the intensity variations, whose period is found to be a function of frequency.

A constant magnetic field parallel to the velocity introduces more complex propagation modes which are neither linearly polarized nor constant through the medium. A shearing magneto-plasma does, however, preserve the orthogonality of the incident polarized modes and can convert linear to circular polarization. The period of the time structure in the transmitted pulse is frequency independent in the limit of a strong field, but in the weak field regime, shows the frequency dependence seen in the field-free case. Due to the presence of more than one cutoff frequency, the periodic temporal modulations can occur in several widely spaced, though still narrow, frequency bands.

The addition of turbulent velocity fluctuations to the shearing motion results in broadband temporal modulations above the cutoff frequencies. The modulation (or resonance) bandwidth is related to the degree of turbulence and the spatial correlation length of the fluctuations for the cases of mildly relativistic and highly relativistic turbulence. The period of the modulations is variable from one realization of the random process to the next, due to the dependence of the velocity gradients on the instantaneous structure of the turbulent fluctuations.

A more realistic shot noise model for the incident radiation produces a variability in the extent to which the modulations are expressed in the transmitted pulse structure. The effects of both broadband and narrow-band shot noise are explored.

When the results of these calculations are compared to single pulse

observations, it is found that some of the properties of microstructure can be explained in the context of the shearing plasma model. It is suggested that periodic micropulses and their associated polarization properties may result from propagation effects in magnetospheric shearing regions. This model predicts that the bandwidth of microstructure should be smaller than the total flux bandwidth and that the period might be frequency dependent. Observational tests and possible limits on magnetospheric parameters are discussed.

TABLE OF CONTENTS

LIST OF TABLES

LIST OF FIGURES

CHAPTER I

INTRODUCTION

Pulsars were discovered eleven years ago as radio sources emitting highly periodic pulses of radiation. General agreement now exists that they are rotating neutron stars, the only model capable of accounting for the short and stable periods observed. Neutron stars are collapsed cores of evolved stars, compact enough to withstand the huge centrifugal forces resulting from a rapid rotation rate. These stars are believed to possess extremely strong surface magnetic fields of order 10^{12} gauss and magnetospheres of charged particles.

The presence of the magnetosphere was first suggested by Goldreich and Julian (1969) who showed that a rotating, uniformly magnetized and infinitely conducting star cannot be surrounded by vacuum but must supply charged particles to the space around it. They showed also that this magnetosphere (magnetic field + particles) would corotate with the star out to distances where the linear velocities approach the speed of light, c. The locus of all points comoving at the speed of light is a cylinder of radius $R_L = c/\Omega$, where Ω is the star's rotation rate. In the vicinity of the light cylinder, the energy density of the particles becomes comparable to the energy density of the magnetic field, which grows weaker with distance from the star. At this point, the field can no longer maintain corotation, since the particles are able to move across field lines. The field is thought to be predominantly dipolar in the corotation zone, but as the particles lag behind, the field lines are swept out into a toroidal pattern. These field lines intersecting the light cylinder are called "open", because they form a bridge be-

tween the corotating and non-corotating zones, allowing particles to escape from the magnetosphere.

Sturrock (1971) pointed out that a toroidal field pattern requires a current flow to maintain it, and large electric fields must exist above the polar cap which will be available to accelerate particles to high energies along the open field lines. These electric fields may be the result of the nonzero space-charge, and surface-charge densities induced by the star's rotation. According to his model, the radiation we observe from pulsars is emitted by the energetic particles as they move along curved field lines. Since this idea was proposed, there have been various mechanisms suggested for the acceleration and radiation, none of which has been generally accepted. The models which are best able to explain properties of the pulsed radio emission propose that coherent radiation is produced above the polar cap, the area of the stellar surface where the open field lines originate.

Single pulses have been observed in some detail and show a number of interesting features which have yet to be explained in any proposed radiation model. A pulse from a typical pulsar shows three basic constituents with different characteristic time scales. The shortest time scale variations seen with the highest resolution are micropulses, intense spikes of several hundred microsecond duration, often showing periodicities. Subpulses are of longer duration, typically a few milliseconds, and seem to occur at preferred positions of pulse longitude. Subpulses and micropulses are modulated by a pulse window which is the extent in longitude of the mean profile, obtained by summing $\sim 10^3$ single pulses. Mean profiles are extremely stable and, at least

in some pulsars, seem to be a measure of the frequency of subpulse occurrence with longitude. On the other hand, single pulse structure varies drastically from one pulse to the next. Rickett (1975) has proposed that the pulsar signal be modeled as a white Gaussian noise process, and that the pulse structures observed, including micropulses and subpulses, are envelopes modulating the noise. Statistical analysis of the signals with 12 μs time resolution indicates that the radiation is consistent with an amplitude modulated shot noise model (Cordes 1976 a,b), each pulse being one realization of a random process. The noise is evidently an intrinsic property of the emission mechanism, but the short time scale amplitude modulations could be explained as either emission or propagation effects.

Aside from the problem of the emission mechanism for pulsars is the question of how radiation propagates through the magnetosphere after emission. The characteristics of the radiation we observe presumably result from a combination of these two independent processes. To ultimately determine the nature of the emission mechanism, it is necessary to know what propagation effects, if any, influence the signals we observe. The interstellar medium causes dispersion of the pulse and Faraday rotation of the polarization position angle, both effects of a low density plasma which are relatively well understood. The magnetosphere is a much higher density plasma in a strong magnetic field, with particles moving at relativistic velocities. Its equilibrium state must include at least one region of rapid shearing, where velocities approaching c at the light cylinder decrease to the particle velocities of the interstellar medium. Velocity shearing may also occur in the

radial streaming motions of accelerated particles along the dipole field lines near the star. Particle energies of γmc^2 with $\gamma = 10^{6-7}$, as predicted by some models, imply highly relativistic streaming velocities. There is no reason to believe that these motions are ordered; some degree of turbulence could exist as well. If the pulsar signals originate within the light cylinder, as is held by most theories, then they must travel through regions of shearing plasma before being observed. Details of the geometry of these regions are not known, but it seems clear that the propagation of radiation through such relativistically moving media is a problem of major importance regarding the interpretation of observed signals.

The theory of electromagnetic wave propagation in moving media was first formulated by Minkowski (1910). His constitutive relations for the fields in a moving medium of constant index of refraction implied that the properties of waves are changed substantially by the motion. Various problems concerning the electrodynamics of moving media have since been considered (Tai 1964, Chen and Cheng 1966, Yeh and Casey 1966) but ultimately applied to non-relativistic situations. Problems involving wave propagation in moving plasmas have also been of interest in their applicability to phenomena in the earth's magnetosphere and to the solar corona (Bailey 1950, Scarf 1961, Chawla and Unz 1971).

The basic physics of wave propagation in shearing media has been investigated in a series of papers by Ian Lerche (1974 I - X, Lee and Lerche 1974 XI, 1975 XII). The motivation for his extensive work in this area is to provide a basis for understanding the propagation of

radiation in pulsar magnetospheres. His calculations yield a variety of possible effects on ray paths, fluxes, and polarization of plane waves in a shearing medium. All of these effects are relativistic, arising from differences in the index of refraction measured by an observer locally comoving with the medium and the index of refraction measured by an observer at rest. The rapid motion of the medium makes possible permanent exchanges of energy between the medium and the radiation, a process which could have very interesting consequences.

Lerche has approached the problem of plane wave propagation in a differentially shearing medium in two ways. Both methods start with Maxwell's Equations and the Minkowski constitutive formulae for moving media. In the first method, he extracts the propagation characteristics of the medium from the equations by invoking the geometrical optics approximation. In this approximation, it is assumed that the scale length of variations in the medium, L, due to velocity shearing are large compared to the wavelength of the radiation, λ, or $kL \ll 1$ where $k = 2\pi/\lambda$. All fields can then be eliminated from the equations to give a dispersion relation for the wave and a differential equation for the phase velocity direction (Lerche 1974 I). This expression describes the behavior of the ray path in a medium of constant index of refraction, which undergoes plane shearing. He finds that for a velocity field in the +x direction which is a monotonically increasing function of y, the phase velocity changes direction. For constant index of refraction, $n > 1$, a ray entering the medium at $y = 0$ is bent in the direction of the velocity and turns directly downstream as $\beta \to 1$ ($\beta = v/c$). For $n < 1$, the ray path bends against the direction of flow and there is a

critical level, $\beta = n$, beyond which rays at some angles of incidence will not propagate, but turn directly upstream with infinite phase speed. The approximation, in fact, breaks down at the critical levels and does not adequately describe the true behavior of waves in their vicinity. Another disadvantage of the geometrical optics approximation is that one cannot determine fluxes or polarization changes of the waves as they pass through the medium.

The second approach is to derive exact equations for the wave fields and look for solutions in certain simple cases (Lerche 1974 VII). Due to the overwhelming complexity of the equations (in general, fourth order differential equations with non-constant coefficients), Lerche was able to find an exact solution only for constant n and normal incidence. He was, however, able to produce results showing that the ray paths do indeed bend as found in the geometrical optics approximation. It was also found that a finite amount of power flows past the critical level, because the wave is exponentially damped in this region, causing a surface layer phenomenon. Furthermore, the waves do not bend directly upstream but approach at a finite angle and the phase velocity remains finite. This method retains all information on the phases and amplitudes of the fields, therefore giving information on the polarization of waves in the medium.

In this work, we use the latter approach to apply Lerche's theory to propagation in a pulsar magnetosphere. We explore the possible effects of the magnetosphere, in particular the effect of a shearing plasma, on pulsar signals. Our results are then compared with the observational data on single pulses to determine if any of the observed

phenomena can be explained by such propagation effects.

We have constructed a numerical model in which to investigate the propagation of time dependent, polarized radiation through regions of shearing plasma. In Chapter II, we present a derivation of Lerche's equations for plane wave propagation and the methods used to calculate the propagation of pulses. The simplest case of a Gaussian modulated plane wave incident on a shearing field-free plasma is described in Chapter III. In Chapter IV, the effects of a strong magnetic field are introduced, requiring a new derivation of the field equations and boundary conditions. Chapters V and VI introduce two variations on the model: turbulent shearing and shot noise radiation. We discuss, in Chapter VII, the possible geometry of the shearing regions in pulsar magnetospheres and relate this to our simplified model. In Chapter VIII, the results obtained are compared to single pulse observations and it is suggested that the model offers an explanation for some of the properties of microstructure. Finally, we discuss in Chapter IX the observations which could possibly verify this explanation, the conclusions to be drawn if it is correct, and what could be learned about magnetospheric structure from the properties of single pulses.

CHAPTER II

PULSE PROPAGATION IN A SHEARING MEDIUM

We describe here the methods used to calculate the propagation of time dependent, polarized radiation through a shearing medium. Lerche (1974 VII, Lee and Lerche 1975 XII) has derived equations in three dimensions for the electric and magnetic fields of plane waves in inhomogeneous, moving media. We develop a numerical scheme for solving these equations in two dimensional form, making the simplification that the waves propagate in the same plane as the velocity shearing.

1. Plane Wave Propagation

We outline in this section the derivation of Lerche's equations for waves in moving media. Consider a plane medium as in Figure 2-1 having a velocity $\vec{v} = v(y)\hat{x}$, as measured by an inertial observer, P, who is at rest. Assume that the radiation is incident on the medium at $y = 0$ and propagates in the positive y direction with wave vector $\vec{k}$. If an observer comoving with the medium at height y measures $\vec{D}' = \varepsilon\vec{E}'$ and $\vec{B}' = \mu\vec{H}'$, then the Minkowski formulae give the relations between the fields as measured by observer P:

$$\vec{D} + \frac{\vec{v}}{c} \times \vec{H} = \varepsilon(\vec{E} + \frac{\vec{v}}{c} \times \vec{B}) \tag{2.1}$$

$$\vec{B} - \frac{\vec{v}}{c} \times \vec{E} = \mu(\vec{H} - \frac{\vec{v}}{c} \times \vec{D}) \tag{2.2}$$

These equations, together with Maxwell's Equations,

$$\nabla\cdot\vec{D} = 0 \qquad \nabla\cdot\vec{B} = 0$$

$$\nabla \times \vec{H} = \frac{1}{c}\frac{\partial \vec{D}}{\partial t} \qquad \nabla \times \vec{E} = -\frac{1}{c}\frac{\partial \vec{B}}{\partial t} \tag{2.3}$$

which are valid in any inertial frame, give a full description of wave propagation in the medium. If $\vec{v}$ is a function of y only, the fields can be analyzed into plane wave components with variation

$$f(y)\ \exp[i(k_x x + k_z z - \omega t)] \quad . \tag{2.4}$$

This form for the fields is substituted into equations (2.1), (2.2) and (2.3), eliminating all except the y derivatives. If ε and μ are assumed to be independent of y, then equations (2.1) and (2.2) can be substituted into Maxwell's Equations and all but one component of $\vec{E}$ and $\vec{H}$ may be eliminated. The result is a pair of coupled homogeneous equations for E_z and H_z (Lerche 1974 VII):

$$\frac{d^2H_z}{dy^2}\left[D + c^2k_z^2\omega^{-2}\right] - \frac{c^2k_z^2}{\omega^2}(\ell n\ D)'\frac{dH_z}{dy} + \frac{\omega^2}{c^2}\left[D(D + c^2k_z^2\omega^{-2}) - n^2A^2\right]H_z$$

$$= -i\varepsilon k_z D(A/D)'E_z \tag{2.5}$$

$$\frac{d^2E_z}{dy^2}\left[D + c^2k_z^2\omega^{-2}\right] - \frac{c^2k_z^2}{\omega^2}(\ell n\ D)'\frac{dE_z}{dy} + \frac{\omega^2}{c^2}\left[D(D + c^2k_z^2\omega^{-2}) - n^2A^2\right]E_z$$

$$= i\mu k_z D(A/D)'H_z \tag{2.6}$$

where, $A = ck_x\omega^{-1} + \beta(y)\ [n(y)^2 - 1][1 - n(y)^2\ \beta(y)^2]^{-1}$

$$D = n(y)^2\ [1 - \beta(y)^2][1 - n(y)^2\ \beta(y)^2]^{-1} - c^2k_z^2\omega^{-2}\ ,$$

and the primes indicate differentiation with respect to y. If we divide

the medium up into layers of width Δy in which the velocity, $\beta = \beta(y_n) = v(y_n)/c$, and the index of refraction, $n = n(y_n)$, are constants, then the equations uncouple and take the simpler form

$$[D_n + c^2k_z^2\omega^{-2}] \frac{d^2}{dy^2} [E_z,H_z] + \frac{\omega^2}{c^2} [D_n(D_n + c^2k_z^2\omega^{-2}) - n^2A_n^2][E_z,H_z] = 0 \tag{2.7}$$

These equations have the solutions:

$$H_z(y_n) = \{h_u(y_n) \exp[ik(y_n)y] + h_d(y_n) \exp[-ik(y_n)y]\}$$

$$E_z(y_n) = \{\varepsilon_u(y_n) \exp[ik(y_n)y] + \varepsilon_d(y_n) \exp[-ik(y_n)y]\} \tag{2.8}$$

The temporal variation is $e^{-i\omega t}$, so that the subscripts u and d refer to upgoing and downgoing plane waves with wave vector:

$$k(y_n) = \frac{\omega}{c} \frac{[D_n(D_n + c^2k_z^2\omega^{-2}) - n(y_n)^2A_n^2]^{\frac{1}{2}}}{[D_n + c^2k_z^2\omega^{-2}]^{\frac{1}{2}}} \tag{2.9}$$

The downgoing waves are the reflections of the upgoing waves from the interfaces above. The other components of $\vec{E}$ and $\vec{H}$ can be calculated from E_z and H_z:

$$\begin{aligned}
E_x &= \frac{ic}{\varepsilon\omega D_n} [H_z'(D_n + c^2k_z^2\omega^{-2}) + ik_z\varepsilon A_n E_z] \\
E_y &= D_n^{-1} [\mu H_z A_n + ic^2k_z\omega^{-2}E_z'] \\
H_x &= \frac{-ic}{\mu\omega D_n} [E_z'(D_n + c^2k_z^2\omega^{-2}) - ik_z\mu A_n H_z] \\
H_y &= -D_n^{-1} [\varepsilon A_n E_z = ic^2k_z\omega^{-2}H_z'] \quad .
\end{aligned} \tag{2.10}$$

The complex coefficients $h_u(y_n)$, $h_d(y_n)$, $\varepsilon_u(y_n)$ and $\varepsilon_d(y_n)$ are deter-

mined by the boundary conditions at each interface: that the tangential components of $\vec{E}$ and $\vec{H}$ are continuous. The interfaces are planes of $y = y_n$ = constant, and there are four equations to be satisfied at each:

$$\begin{aligned} H_z(y_n) &= H_z(y_{n-1}) \\ H_x(y_n) &= H_x(y_{n-1}) \\ E_z(y_n) &= E_z(y_{n-1}) \\ E_x(y_n) &= E_x(y_{n-1}) \end{aligned} \tag{2.11}$$

There are N-1 interfaces for N layers, making a total of 4(N-1) equations. There are only 4(N-1) fields to solve for, however, because one is free to specify the incident radiation at the top and bottom of the medium. The method for solving these equations numerically is discussed in §3. Having a complete description of the fields in each layer enables one to follow flux, polarization and ray paths of plane waves through a shearing medium of variable refractive index.

Energy flux and ray paths. The electromagnetic energy flux of the upgoing radiation at height y_n is defined by the time-averaged Poynting vector,

$$\vec{S}_u(y_n) = \frac{c}{8\pi} \mathrm{Re}\{\vec{\varepsilon}_u(y_n) \times \vec{h}_u^{\,*}(y_n)\} \quad . \tag{2.12}$$

In general, the total energy flux in the wave is the electromagnetic energy flux plus the particle energy flux. Ko and Chuang (1977) showed that for a moving, non-absorbing medium having only frequency disper-

sion in its rest frame, the total energy flow is

$$\vec{W} = \vec{S} + U\vec{v} \tag{2.13}$$

where $\vec{S}$ is the time-averaged Poynting flux and $U\vec{v}$ is the particle energy flux associated with the motion. U is the energy density of the wave in the moving medium:

$$U = \frac{1}{16\pi}\,\omega\,\frac{\partial\varepsilon}{\partial\omega'}\,\{\gamma\vec{E}\cdot\vec{E}^{*} - \gamma^{3}\vec{\beta}\cdot[(\vec{E}+\vec{\beta}\times\vec{B})\times\vec{B}^{*} + \vec{E}^{*}\times(\vec{B}-\vec{\beta}\times\vec{E})]\} \tag{2.14}$$

where $\omega' = \gamma(\omega - c\beta k_x)$ is the frequency in the moving frame and $\gamma = (1-\beta^2)^{-\frac{1}{2}}$.

If no spatial dispersion exists in a static medium, $\vec{S}$ is in the same direction as the group velocity and is equal to the total energy flux. If the medium is moving, however, the frequency dispersion may become spatial dispersion in the stationary frame and this is no longer the case.

The ray path of the total power flow in the medium at height y_n is then defined by

$$\frac{dx}{W_x(y_n)} = \frac{dy}{W_y(y_n)} = \frac{dz}{W_z(y_n)} \tag{2.15}$$

The ray paths of the electromagnetic power flow [defined as in eq. (2.15) for $\vec{S}_u(y_n)$] and of the total power flow will not be the same except where $\vec{v} = 0$.

Polarization. The polarization properties of the wave are followed through the medium by calculating the Stokes Parameters of the upgoing electric field, $\vec{\varepsilon}_u(y_n)$, according to the procedure outlined by Chand-

rasekhar (1960). The polarization of the incident radiation is specified through the boundary conditions at $y = 0$; i.e., the relative magnitudes and phases of $\vec{\varepsilon}_u(0)$ and $\vec{h}_u(0)$.

2. Pulse Propagation

We will treat the problem of finite pulse propagation in a shearing medium through the technique of Fourier analysis. A pulse of finite duration can be expressed as a linear superposition of plane waves in the form of a Fourier integral. At each interface in the medium, there will be an incident pulse and a reflected pulse; the field distribution in the layer below the interface will be the sum of upgoing and downgoing pulse electric fields:

$$E_z(y_n,t) = E_{uz}(y_n,t) + E_{dz}(y_n,t)$$

$$= \frac{1}{(2\pi)^{\frac{1}{2}}} \int_{-\infty}^{\infty} \{\varepsilon_u(y_n,\omega)\ \exp[ik(y_n)y] + \varepsilon_d(y_n,\omega)\ \exp(-ik(y_n)y]\}$$

$$\exp[-i\omega t]d\omega \qquad (2.16)$$

$H_z(y_n,t)$ will also have Fourier components $h_u(y_n,\omega)$ and $h_d(y_n,\omega)$ in the n^{th} layer. The components $h_u(y_n,\omega)$, $h_d(y_n,\omega)$, $\varepsilon_u(y_n,\omega)$, and $\varepsilon_d(y_n,\omega)$ are determined by satisfying the boundary conditions for the plane wave component with frequency ω, together with the appropriate boundary conditions for a pulse incident at $y = 0$, at the bottom of the medium:

$$\varepsilon_u(0,\omega) = \frac{1}{(2\pi)^{\frac{1}{2}}} \int_{-\infty}^{\infty} E_{uz}(0,t)e^{i\omega t}\,dt$$

$$h_u(0,\omega) = \frac{1}{(2\pi)^{\frac{1}{2}}} \int_{-\infty}^{\infty} H_{uz}(0,t)e^{i\omega t}\,dt \qquad (2.17)$$

$$h_d(y_N,\omega) = \varepsilon_d(y_N,\omega) = 0$$

For the case we are considering:

$$E_{uz}(0,t) = E_o \exp(-t^2/t_w^2) \exp(-i\omega_o t)$$
$$H_{uz}(0,t) = a\, E_{uz}(0,t) \qquad (2.18)$$

where a and E_o are complex coefficients which determine the polarization of the radiation. We choose a to be real and independent of t, so that the incident pulse is linearly polarized with constant position angle. The Fourier components of E_x, E_y, H_x, and H_y are calculated from $\varepsilon_u(y_n,\omega)$ and $h_u(y_n,\omega)$ according to equation (2.10).

We are interested in the characteristics of the upgoing pulse at each height, which is reconstructed by taking the inverse Fourier transform of the upgoing frequency components (at y_n) times the factor $\exp[ik(y_n)y_n]$ to give the time dependent fields. The electromagnetic energy flux of the upgoing radiation at height y_n is defined by the real part of the complex Poynting vector:

$$\vec{S}_u(y_n,t) = \frac{c}{4\pi} \mathrm{Re}\{\vec{E}_u(y_n,t) \times \vec{H}_u^*(y_n,t)\} \qquad (2.19)$$

We may also define time-dependent Stokes Parameters, $I(y_n,t)$, $Q(y_n,t)$, $U(y_n,t)$ and $V(y_n,t)$ for the electric field $\vec{E}_u(y_n,t)$ so that the polarization properties of the transmitted pulse may be determined. Given functional forms for the variation of $n(y_n)$ and $\beta(y_n)$ through the medium, the propagation of a pulse of polarized radiation is totally specified.

3. Numerical Solution for Field Amplitudes

We use a numerical Fast Fourier Transform to calculate the Fourier

amplitudes $\varepsilon_u(0,\omega)$ and $h_u(0,\omega)$ of the incident pulse (eq. [2.18]) which then become the lower boundary conditions for the field amplitudes at each frequency. In considering only cases where $k_z = 0$, the calculations are greatly simplified since the boundary conditions for E_x and H_x no longer mix the E_z and H_z polarizations.

Since for $k_z = 0$ the boundary conditions for the E_z and H_z polarizations are independent, the two sets of $2(N-1)$ linear equations for the amplitudes of $E_z(y_n)$ and $H_z(y_n)$ in each Fourier mode (cf. eq. [2.11]) may be solved separately. In order to carry out the numerical calculation without having to store and invert large matrices, we write the boundary conditions for H_z at each frequency between layer $(n-1)$ and layer n as: (ω dependence has been suppressed)

$$\begin{vmatrix} h_u(y_n) \\ h_d(y_n) \end{vmatrix} = M_n \begin{vmatrix} h_u(y_{n-1}) \\ h_d(y_{n-1}) \end{vmatrix} \tag{2.20}$$

where

$$M_n = \frac{1}{2} \begin{vmatrix} \left(1 + \frac{k_{n-1}}{k_n}\frac{\varepsilon_n}{\varepsilon_{n-1}}\right) \exp[i(k_{n-1} - k_n)y_n] & \left(1 - \frac{k_{n-1}}{k_n}\frac{\varepsilon_n}{\varepsilon_{n-1}}\right) \exp[-i(k_{n-1} + k_n)y_n] \\ \left(1 - \frac{k_{n-1}}{k_n}\frac{\varepsilon_n}{\varepsilon_{n-1}}\right) \exp[i(k_{n-1} + k_n)y_n] & \left(1 + \frac{k_{n-1}}{k_n}\frac{\varepsilon_n}{\varepsilon_{n-1}}\right) \exp[-i(k_{n-1} - k_n)y_n] \end{vmatrix}$$

There is a similar set of matrices for the boundary conditions of E_z. It follows that:

$$\begin{vmatrix} h_u(y_n) \\ 0 \end{vmatrix} = \prod_{n=2}^{N} M_n \begin{vmatrix} h_u(0) \\ h_d(0) \end{vmatrix} \tag{2.21}$$

Since there is no downgoing wave at the top of the medium, we can solve for $h_d(0)$ and $h_u(y_N)$ from the 2×2 product matrix and the upgoing amplitude at the lower boundary, $h_u(0)$. It is then possible to obtain the amplitudes $h_u(y_n)$ and $h_d(y_n)$ at every level from equation (2.20). The amplitudes $\varepsilon_u(y_N)$ are solved for in the same manner. By this method, we need only store and invert $2(N-1)$ 2×2 matrices rather than two $2(N-1) \times 2(N-1)$ matrices. It is similar in concept to the invariant imbedding technique used to solve for reflection and transmission coefficients in inhomogeneous media (Bellman and Kalaba 1956, Adams and Denman 1966).

Figure 2-1: Model of a plane parallel shearing plasma divided into discrete layers and showing the shearing velocity, $\beta(y_n)$, and the index of refraction, $n(y_n)$, in the n^{th} layer. The plasma is at rest in the regions $y < 0$ and $y > y_N$. A pulse of radiation with a time dependent electric field is incident at the bottom of the shearing region, $y = 0$.

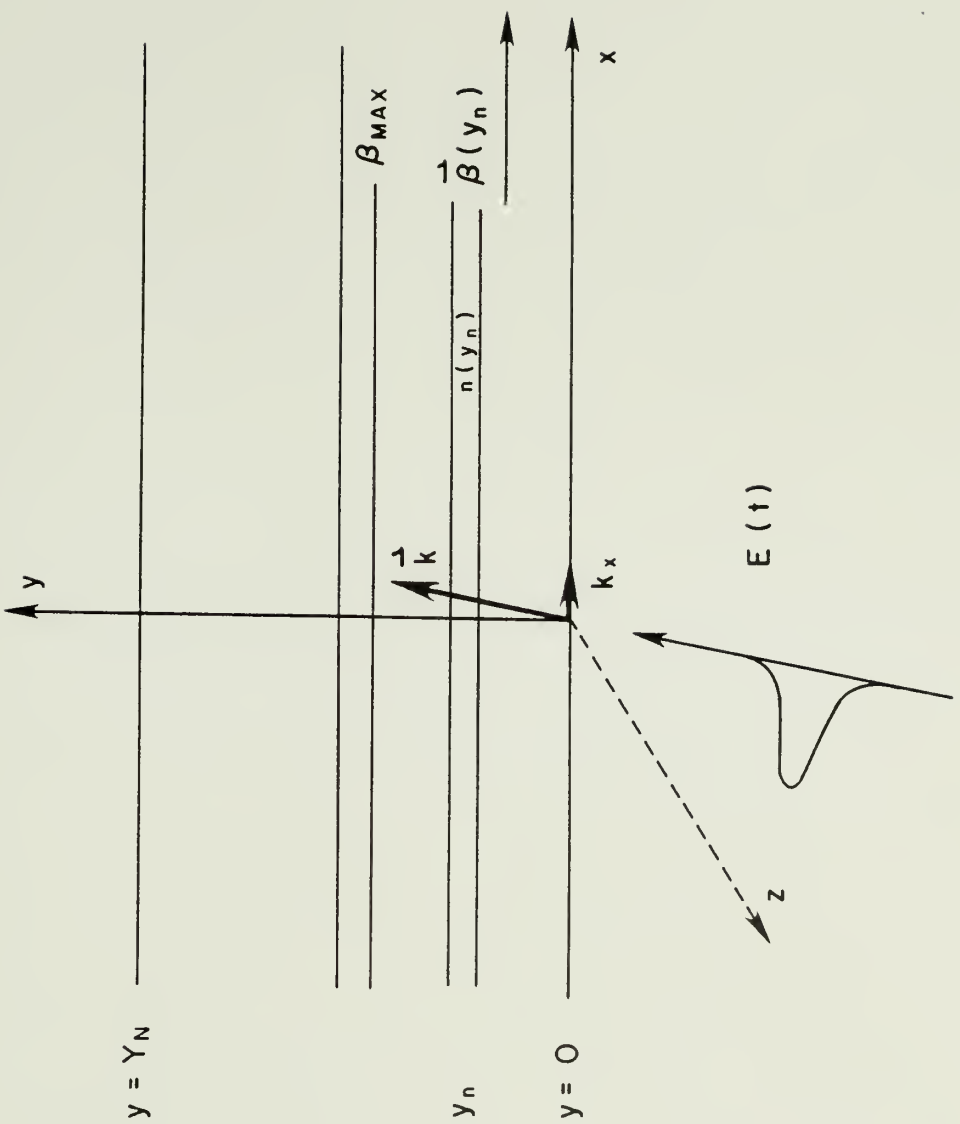
y
x
z
β_{MAX}
$\vec{\beta}(y_n)$
$n(y_n)$
$\vec{k}$
k_x
E (t)
$y = Y_N$
y_n
$y = 0$

CHAPTER III

FIELD-FREE PLASMA

1. Details of the Model

As the simplest approximation to a shearing region of the pulsar magnetosphere, we consider a cold, field-free plasma with a velocity field symmetrically increasing from zero to a maximum value and then decreasing to zero. Certainly, the pulsar's magnetic field will not be negligible, but the physics involved here is basic to an understanding of the more general cases. In the local rest frame of the medium, the plasma is homogeneous, and the index of refraction is given by

$$n^2 = 1 - \omega_p{}^2/\omega'^2 \tag{3.1}$$

where ω_p is the plasma frequency of the medium at rest. The relation between the frequency, ω, measured by observer P and the frequency, ω', measured by the comoving observer is

$$\omega' = \gamma(y)(\omega - c\beta(y)k_x) \tag{3.2}$$

where

$$\gamma(y) = (1 - \beta(y)^2)^{-1/2}$$

In the inertial frame of the radiation, ω is constant, so that ω', and also n varies with height in the medium.

In this model, we consider all of space to be filled with plasma at rest except over the region $0 < y < y_N = 2$, where the plasma is shearing with velocity in the positive x direction (cf. Fig. 2-1). The shearing region is divided into plane parallel layers of width Δy and

we make the simplification that all radiation propagates in the x-y plane with $k_z = 0$.

We choose a velocity profile which can model either light cylinder shearing or emission region shearing. Since there exists no complete solution to the fields and particle dynamics extending across the light cylinder, the functional form for the velocity need only be consistent with the general dynamics. It should be single-peaked, reflecting the velocity variation in the magnetosphere as seen by an observer at rest with respect to the surrounding interstellar medium. The corotation velocity will increase with distance from the star and reach a maximum when shearing begins to occur, thereafter decreasing, eventually to zero, outside the light cylinder. Much less is known about streaming motions in the emission region, but we expect that shearing may result from fluid-like turbulence. In this case, our model shearing region would represent a single turbulent cell. This idea is discussed in greater detail in Chapter VII. In light of these considerations, we choose the velocity profile

$$\gamma(y) = 1 + \gamma_{MAX} \cos[(y-1)\pi/2]$$

which is a maximum at $y = 1$ and symmetric about this point. Unless otherwise specified, $\gamma_{MAX} = 5$ in all calculations.

The layer size was chosen, in every case, to be smaller than the wavelength in the medium. This gives a good approximation to a continuously varying medium and assures that any reflections are from gradients and not from the artificially imposed boundaries. In a few cases, convergence tests were carried out, varying the layer size from $\Delta y = 0.1$

to $\Delta y = .004$ until stable transmission coefficients were achieved. In these cases, $\Delta y/\lambda \lesssim .2$ gave the needed accuracy.

2. Analytic Solutions for Normal Incidence

Before presenting the numerical results on pulse propagation in a field-free plasma, we predict some general behavior of plane waves for the special case of normal incidence. It is shown that the equations for this case take an unusually simple form, allowing us to gain some physical insight from the approximate solutions.

In the model described in §1, the index of refraction (cf. eqs. [3.1] and [3.2]) will vary through the medium due to the fact that each comoving frame measures a different frequency for the wave. Since equation (2.7) was derived for a constant index of refraction, it can only apply to this case over a small enough part of the medium that n does not vary significantly. If we wish to describe the fields analytically throughout the shearing region, we must re-derive the equations, allowing n to be a function of y. For normal incidence, $k_z = k_x = 0$.

Consider the plane medium in §1 with the following relations between the fields in the comoving frame:

$$\begin{aligned} \vec{D}' &= \varepsilon(y)\, \vec{E}' \\ \vec{B}' &= \mu\, \vec{H}' \end{aligned} \tag{3.3}$$

where μ is constant and $\varepsilon(y) = n(y)^2$. The Minkowski formulae relate the fields as seen by the stationary observer:

$$\begin{aligned} \vec{D} + \vec{\beta} \times \vec{H} &= \varepsilon(y)(\vec{E} + \vec{\beta} \times \vec{B}) \\ \vec{B} + \vec{E} \times \vec{\beta} &= \mu(\vec{H} + \vec{D} \times \vec{\beta}) \quad . \end{aligned} \tag{3.4}$$

Following Lerche's derivation for constant ε and μ, we make use of Maxwell's equations with equations (3.4) and assume that $\vec{D}$, $\vec{B}$, $\vec{E}$, and $\vec{H}$ vary as $f(y)\exp(-i\omega t)$. We arrive at two homogeneous differential equations for the z-component of $\vec{E}$ and $\vec{H}$:

$$\frac{d^2E_z}{dy^2} + \frac{\omega^2}{c^2}\gamma^2(n^2 - \beta^2)\,E_z = 0 \tag{3.5}$$

$$\frac{d^2H_z}{dy^2} - \left(\frac{1}{\varepsilon}\frac{\partial\varepsilon}{\partial y}\right)\frac{dH_z}{dy} + \frac{\omega^2}{c^2}\gamma^2(n^2 - \beta^2)\,H_z = 0\ . \tag{3.6}$$

Equation (3.5) is identical to equation (2.7) for E_z with $k_x = 0$, while equation (3.6) contains the extra first order term involving the derivative of $\varepsilon(y)$.

For the field free plasma, $\varepsilon(y) = n(y)^2 = 1 - \omega_p^2/\gamma^2\omega^2$ with $k_x = 0$, and in this particular case,

$$k_y^2 = \frac{\omega^2}{c^2}\gamma^2(n^2 - \beta^2) = \frac{\omega^2}{c^2}n_o^2 \tag{3.7}$$

where $n_o^2 = 1 - \omega_p^2/\omega^2$ is just the index of refraction of a plasma at rest. Therefore, $\vec{k}$ is a constant through the medium. This property of the field free plasma is also true for $k_x \neq 0$, as it can be shown that the expression for k in equation (2.9) is constant for the above n(y). With k constant, the coefficient of the first order term in equation (3.6) can be interpreted as a damping factor. This indicates a fundamental difference in propagation characteristics between the two orthogonal polarizations. Equation (3.5) has the solution for a plane wave:

$$E_z(y) = \varepsilon_u e^{iky} + \varepsilon_d e^{-iky} \tag{3.8}$$

which holds throughout the medium, along with the solutions for the other components:

$$H_x(y) = \frac{-ic}{\mu\omega}\frac{dE_z}{dy}, \quad H_y(y) = \frac{-\beta(n^2-1)}{\mu(1-\beta^2)}E_z(y) \quad . \tag{3.9}$$

An analytic solution exists to equation (3.6) if we take $(\partial\varepsilon/\partial y)/\varepsilon = A$, where A is not a function of y, but may be a function of ω. We find:

$$H_z(y) = e^{Ay/2}[h_u e^{iky} + h_d e^{-iky}] \tag{3.10}$$

$$E_x(y) = \frac{ic}{\varepsilon\omega}\frac{dH_z}{dy}, \quad E_y(y) = \frac{\beta(n^2-1)}{\varepsilon(1-\beta^2)}H_z(y) \quad . \tag{3.11}$$

If A is real, this is the solution of a damped or exponentially growing plane wave, depending on whether A is negative or positive. Unfortunately, the plasma is a dispersive medium where $\varepsilon = \varepsilon(\omega,y)$ and A being constant with y requires the velocity field to be different for each value of ω, which is an unphysical situation. Equation (3.10), therefore, only holds for y distances over which A is slowly varying. In different parts of the medium, A will have a different value, and the damping of the wave will depend on how fast ε is changing with y, as well as on ω. Furthermore, the solution for H_z is not symmetric for a symmetric velocity field, as is the solution for E_z. Consequently, transmitted waves with $\vec{E} \parallel \vec{v}$ will be attenuated while those with $\vec{E} \perp \vec{v}$ will not. We see that a shearing plasma is a birefringent medium, with the modes polarized parallel and perpendicular to the plane of shearing behaving quite differently.

Due to the dependence of H_y and E_y in equations (3.9) and (3.11) on β which increases and decreases through the medium, the ray path of

the electromagnetic energy flux, which follows the Poynting vector, changes direction while the wave vector does not. The ray path of the total energy in a cold plasma, as we will show here for the case of normal incidence, does follow the wave vector and therefore does not change its direction. Using equations (2.12), (2.13) and (2.14) from Chapter II, we calculate the total energy flux in the wave from the Poynting flux and the particle energy flux. A cold field-free plasma is an example of a medium having only frequency dispersion and we consider the x component of $\vec{W}$, using equations (3.9) through (3.11). Since $\vec{v}$ is purely in the x direction, this is the only direction in which $\vec{W}$ and $\vec{S}$ are not equal. We have

$$S_x = \frac{c}{8\pi}\left[E_y H_z^* - E_z H_y^*\right] = -\frac{\beta c}{8\pi}\frac{\omega_p^2}{\omega^2}\left[|E_z|^2 + |H_z|^2\right] \qquad (3.12)$$

$$U = \frac{1}{8\pi}\frac{\omega_p^2}{\omega^2}\left\{\frac{1}{\gamma^2}|E_x|^2 + \left(\frac{1}{\gamma^2} + \beta^2\right)\left(|E_y|^2 + |E_z|^2\right)\right.$$

$$\left. - \frac{\beta}{\gamma^2}\left(E_y^* B_z + E_y B_z^*\right) + \frac{\beta^2}{\gamma^2}|B_z|^2\right\} = \frac{1}{8\pi}\frac{\omega_p^2}{\omega^2}\left[|E_z|^2 + |H_z|^2\right]. \qquad (3.13)$$

Therefore, $W_x = S_x + U\beta c = 0$ and the particle energy flux exactly balances the electromagnetic energy flux in the direction of the motion. The ray path of the total power flow has only a y component and therefore follows the wave vector. The component of $\vec{S}_u$ in the direction of $\vec{k}$ then represents the total upgoing energy flux, and we use this result in the numerical calculations.

It is evident from this solution that waves in a shearing plasma behave differently from waves in a shearing non-dispersive medium of

constant refractive index. The field-free plasma is a special case in that the wave vector remains constant and the ray path does not bend, as in the general cases Lerche studied. Waves polarized perpendicular to the plane of shearing are able to pass through completely uninfluenced by the motion of the medium, while the orthogonal polarization is significantly affected.

3. Properties of the Transmitted Pulse

Normal incidence. We consider first the case where $k_x = 0$ and examine the behavior of the transmission coefficient as a function of frequency for plane waves in the E_z and H_z polarization. The transmission coefficient is defined by

$$T(\omega) = \frac{|S_u(y = 2,\omega)|}{|S_u(y = 0,\omega)|} \tag{3.14}$$

where $S_u(y,\omega)$ is the Poynting flux for the upgoing radiation, as defined by equation (2.12). At $y = 2$, the medium is at rest, so that $S_u(y = 2,\omega)$ represents the total transmitted energy at frequency ω.

We find that the shearing plasma is indeed birefringent, as predicted by the analytic results of §2. Waves in the E_z polarization suffer no attenuation for $\omega > \omega_p$ and we will refer to this as the ordinary mode. Waves in the H_z polarization, which we refer to as the extraordinary mode, show an interesting effect for frequencies $\omega \gtrsim \omega_p$. Figure 3-1 shows the behavior of the transmission coefficient for the extraordinary mode near the plasma frequency. $T(\omega)$ exhibits a series of sharp resonances due to successive reflections in the shearing region. These reflections occur when the index of refraction changes

significantly in a distance comparable to the wavelength in the medium. The exact locations of the reflection producing gradients in refractive index depend on the velocity profile. This model shearing region, in which the velocity systematically increases and then decreases, provides two such gradients. Since partial reflection will occur at each gradient, parts of the wave traversing different distances are able to interfere with one another. At frequencies where $k \tilde{\sim} m\pi/y_N$ (m is an integer), constructive interference takes place for the upgoing waves and the transmission coefficient is unity. Notice that the resonances in Figure 3-1 become weaker and broader with increasing frequency; they eventually disappear at wavelengths too small to be affected by the velocity gradients. The resonance spacing, $\Delta k = \pi/y_N$, also increases with frequency. Using the result that $k = n_o\omega/c$ is constant with y (cf. §2), we have

$$\frac{\Delta\omega}{c} = \frac{\pi n_o}{y_N} = \frac{\pi}{y_N}(1 - \omega_p^2/\omega^2)^{1/2} \qquad (3.15)$$

which is in agreement with the numerically determined resonance spacings.

Similar behavior occurs in optics, where gradients in the index of refraction caused by spatial variations in the properties of media can produce reflections. These gradients most often take the form of sharp boundaries, and similar interference phenomena will take place in thin films or slabs of dielectric material.

An exact analogy, however, is found in the one dimensional potential well problem of quantum mechanics (see e.g. Merzbacher 1970). Resonances show up in the transmission coefficient for particles of energy E greater than the well depth and look very similar to the re-

sonance peaks in Figure 3-1. The shape of the well can vary, but the potential, analogous to the index of refraction, must change significantly on the order of the particle's wavelength. The potential can also be thought of as an effective plasma frequency, $\omega_p' = \omega_p/\gamma$, allowing the possibility of "bound states" with frequencies below ω_p existing inside the shearing region.

The condition under which sharp resonances occur is the same as the condition under which the geometrical optics approximation breaks down:

$$\frac{\lambda_o}{2\pi}\left|\frac{dn/dy}{n^2}\right| \gtrsim 1 \tag{3.16}$$

(Ginzburg 1970) where $\lambda_o = 2\pi c/\omega$ is the free space wavelength. With equations (3.1) and (3.2) for $k_x = 0$, this condition becomes

$$\left(\frac{\omega^2}{c^2}\gamma^2 - \frac{\omega_p^2}{c^2}\right)^{3/2} \frac{c^2}{\omega_p^2} \lesssim \frac{d\gamma}{dy} \tag{3.17}$$

where we have used $dn/dy = (dn/d\gamma)(d\gamma/dy)$. Resonances therefore occur when $\omega \sim \omega_p$ or when the velocity changes rapidly. Since we have chosen a smoothly varying velocity profile, the resonance effect is restricted to frequencies close to ω_p. However, if one invokes a velocity profile with steeper gradients, the effect may be present over a much larger frequency range. This aspect of the model will be discussed in more detail in Chapter V.

Calculations of the time dependent Poynting flux of transmitted pulses with ω_o near ω_p reveal the birefringent behavior. Figure 3-2 shows ordinary (O) and extraordinary (X) mode upgoing pulse envelopes

at several heights in the medium, including the incident pulse at $y = 0$ and the transmitted pulse at $y = 2$. The O mode propagates through the shearing plasma as if the medium were at rest and the pulse center moves at the expected group velocity, $v_g = c(1 - \omega_p^2/\omega_o^2)^{1/2}$. The pulse is dispersed because ω_o is near ω_p but the transmission coefficient for the integrated pulse energy is 1.0. There is, consequently, no reflected pulse. The X mode pulse breaks up into a string of quasi-periodic pulses, due to the successive reflections in the shearing region. There is also a series of reflected pulses, not shown in the figure, which exit at $y = 0$. The transmission and reflection coefficients for the total energy add up to 1.0, indicating that no absorption takes place.

The period of the time structure is the inverse of the resonance spacing in frequency, so that

$$P = \frac{1}{\Delta\omega} = \frac{y_N}{\pi c}(1 - \omega_p^2/\omega^2)^{-1/2} \quad . \tag{3.18}$$

The period P, therefore, is frequency dependent and decreases as ω_o/ω_p increases. As ω_o becomes large (and as the group velocity in the plasma approaches c), P approaches the asymptotic value $y_N/\pi c$ (Figure 3-3). A requirement for this time structure to show up in the transmitted pulse is that the incident pulse width, t_w, be small enough for the frequency spectrum to include at least two resonance peaks. In fact, the number of components in the transmitted pulse is equal to the number of strong resonances present in its spectrum.

For an incident pulse of arbitrary linear polarization, the birefringence of the shearing plasma causes interesting time-dependent polarization effects. From the Stokes Parameters of the transmitted

pulse, we have calculated the position angle, $\psi(t)$ and degree of circular polarization $d_V(t)$:

$$\psi(t) = 0.5 \tan^{-1} [U(t)/Q(t)] \tag{3.19}$$

$$d_V(t) = V(t)/I(t) \tag{3.20}$$

In this model, $\psi = 0°$ is the orientation of the X mode electric field, E_X, and $\psi = 90°$ is the orientation of the O mode electric field, E_O.

Figure 3-4 shows $\psi(t)$ and $d_V(t)$ for a transmitted pulse envelope when the incident pulse is 100% linearly polarized with an arbitrary but constant position angle. The position angle of the transmitted pulse envelope is not constant, but changes from one mode to the other on the edge of the first component. This component is a mixture of O and X modes while the other components are purely X mode. Rotations of position angle are therefore caused by changes in the relative magnitudes of E_O and E_X, establishing a correlation between the position angle and intensity changes. Changes in position angle will be expected to occur on the edges of components, where E_X is rapidly increasing or decreasing. When E_X is a minimum, i.e. between components, the position angle will flip to the O mode, if present in that part of the pulse. Large degrees of circular polarization (up to 90%) are found to be present in the transmitted pulse and it is highly variable on the time scale of the intensity fluctuations. Changes in sense of circular polarization, as the one in Figure 3-4, seem to be coincident with the rapid position angle changes. If the circular polarization arises from phase differences between E_X and E_O, then this phenomenon can be understood if the phase and magnitude changes of E_X are coincident.

That is, the zero crossings of phase occur near the minima in the magnitude.

It is evident that these time dependent polarization effects occur only when the transmitted pulse contains comparable amounts of each mode. If $E_X >> E_o$, the periodic intensity modulations will be present but the position angle will be constant in the direction of E_X. If $E_0 >> E_X$, the periodic modulations will be too weak to detect and the position angle will be constant in the direction of E_0. The requirement for polarization changes to be present is that $|E_0|/|E_X| \sim T^{1/2}$ in the incident pulse, where T is the transmission coefficient for the extraordinary mode. We see that the presence of periodic time structure is a necessary but not sufficient condition for the presence of polarization fluctuations.

Oblique incidence. We now consider radiation incident at arbitrary angles to the shearing velocity ($k_x \neq 0$). The O and X modes still propagate independently with much the same characteristics as the normally incident modes. The y component of the wave vector is still a constant through the medium and equal to

$$k_y^2 = \frac{\omega^2}{c^2} n_o^2 - k_x^2 \qquad (3.21)$$

Because a wave entering the medium at this angle can be viewed as a normally incident wave to another inertial observer, the wave vector must be constant for all k_x. When $|k_x c/\omega| = |\cos\theta| \geq n_o$, k_y is imaginary and waves at these angles will not propagate. This is because the waves in the plasma actually propagate at angles defined by $\cos\theta' = \cos\theta/n_o$.

Resonances appear in the transmission coefficient, $T(\omega)$, of the X mode, but their spacing is now

$$\frac{\Delta\omega}{c} = \frac{\pi}{y_N} (n_o^2 - \cos^2\theta)^{1/2} \quad , \tag{3.22}$$

which is smaller, due to the larger effective size of the shearing region. The strength of the resonances, as measured by the depth of the minima in $T(\omega)$, also varies with angle of incidence. This is plotted in Figure 3-5 for several different frequencies, showing the trend from stronger resonances at negative angles of incidence to weaker resonances at positive angles of incidence. When $\cos\theta < 0$, the wave propagates against the direction of shear and therefore sees larger effective velocity gradients. As was shown in equation (3.16), larger velocity gradients lead to stronger reflections and resonance effects (other parameters being equal). When $\cos\theta > 0$, the wave propagates in the direction of shear and sees smaller effective velocity gradients.

At a given frequency, spatial interference fringes are present in the transmitted intensity. In Figure 3-6, the transmission coefficient is plotted as a function of angle of incidence, $\cos\theta'$, for a frequency near ω_p. The fringes have spacing

$$\Delta(\cos\theta') \sim \tan\theta' \frac{\lambda}{y_N} \tag{3.23}$$

where $\lambda = 2\pi c/n_o\omega$ is the wavelength in the medium. The spacing is infinite at $\theta' = \pi/2$, normal incidence, and becomes very small as $\theta' \to 0$, tending to the constant value λ/y_N. The asymmetry about $\theta' = 0$ does not result from the asymmetry in propagation; the location of the fringe peaks shifts with frequency and only at certain frequencies are

they symmetric about $\theta' = 0$.

The behavior of pulses at different angles of incidence is shown in Figure 3-7. In this case, the pulses with $\cos\theta = \pm .10$ propagate at 33.7° to the normal. The period of the time structure in the $|\cos\theta| = .10$ pulses is longer than that in the $\cos\theta = 0$ pulse due to the difference in resonance spacings (cf. equation [3.22]). The period grows large at grazing angles of incidence ($\cos\theta \to n_o$) but does not vary too much at other angles, as illustrated in Figure 3-8. The pulses at oblique angles are also more dispersed owing to the larger distance they travel through the medium. The presence of three components for $\cos\theta = -.10$ and only two for $\cos\theta = +.10$ is a result of stronger resonances in the frequency spectrum of the transmitted pulse at the negative angle. Temporal changes in the polarization are, in general, more pronounced for oblique incidence. For incident pulses having the same initial position angle, there is a systematic rotation of position angle with angle of incidence in the first component of the transmitted pulse. This occurs because the X mode undergoes more attenuation at negative incident angles, while the O mode is unattenuated at all angles.

Figure 3-1: Transmission coefficient versus frequency for a range of values of ω/c near the plasma frequency, $\omega_p/c = 300$.

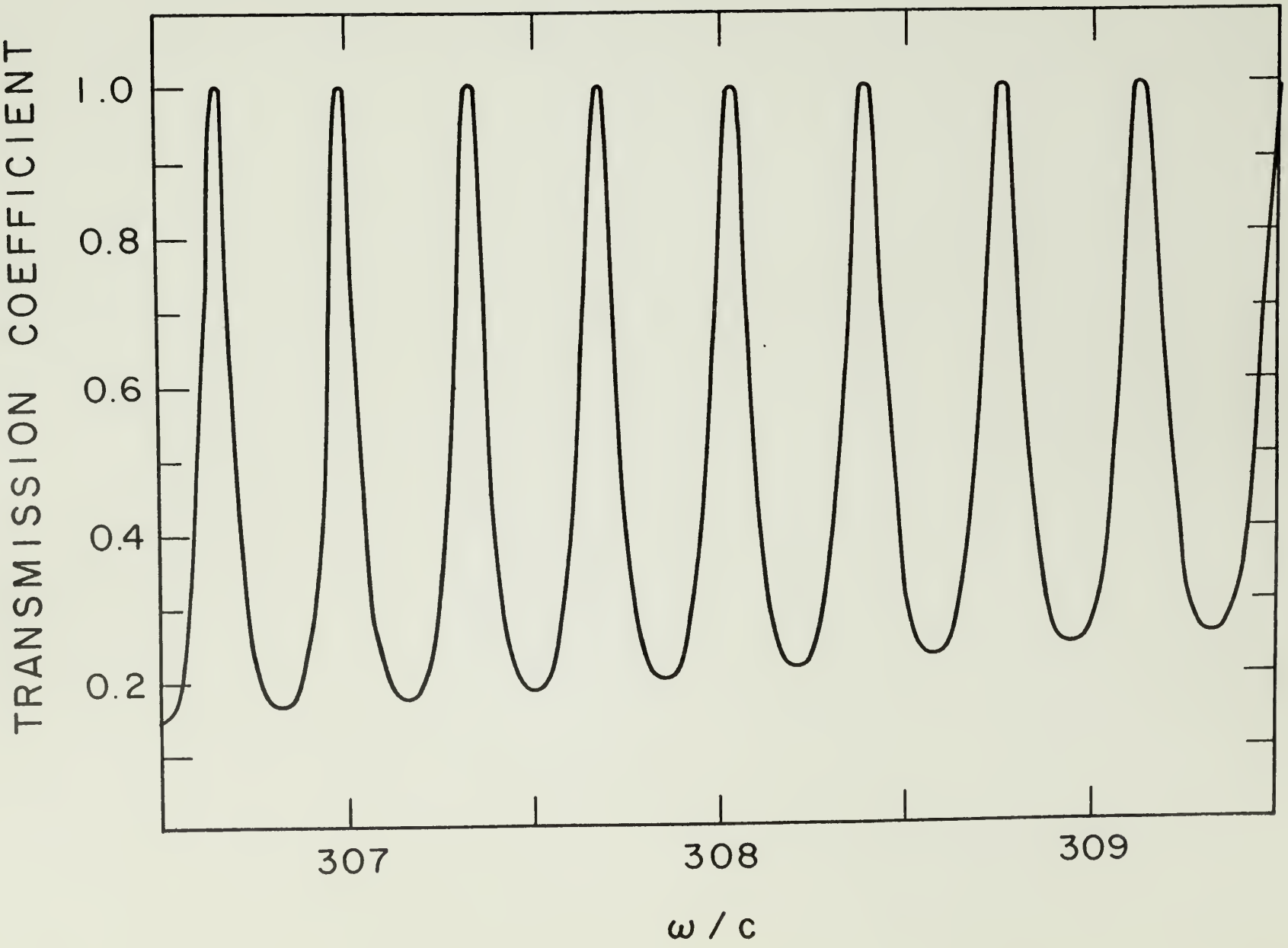
TRANSMISSION COEFFICIENT
1.0
0.8
0.6
0.4
0.2
307
308
309
ω / c

Figure 3-2: Ordinary and extraordinary mode pulse envelopes at frequency $\omega_o/c = 1003$, shown at several heights in the shearing region with plasma frequency $\omega_p/c = 10^3$. The normally incident pulses at $y = 0$ have a width $ct_w = 0.5$ and travel in the positive y direction. a) The O mode is unaffected by the motion of the medium and propagates with the expected group velocity and dispersion of a stationary plasma. b) The X mode is highly dispersed and attenuated due to multiple reflections in the shearing region. The transmission coefficient is 0.066.

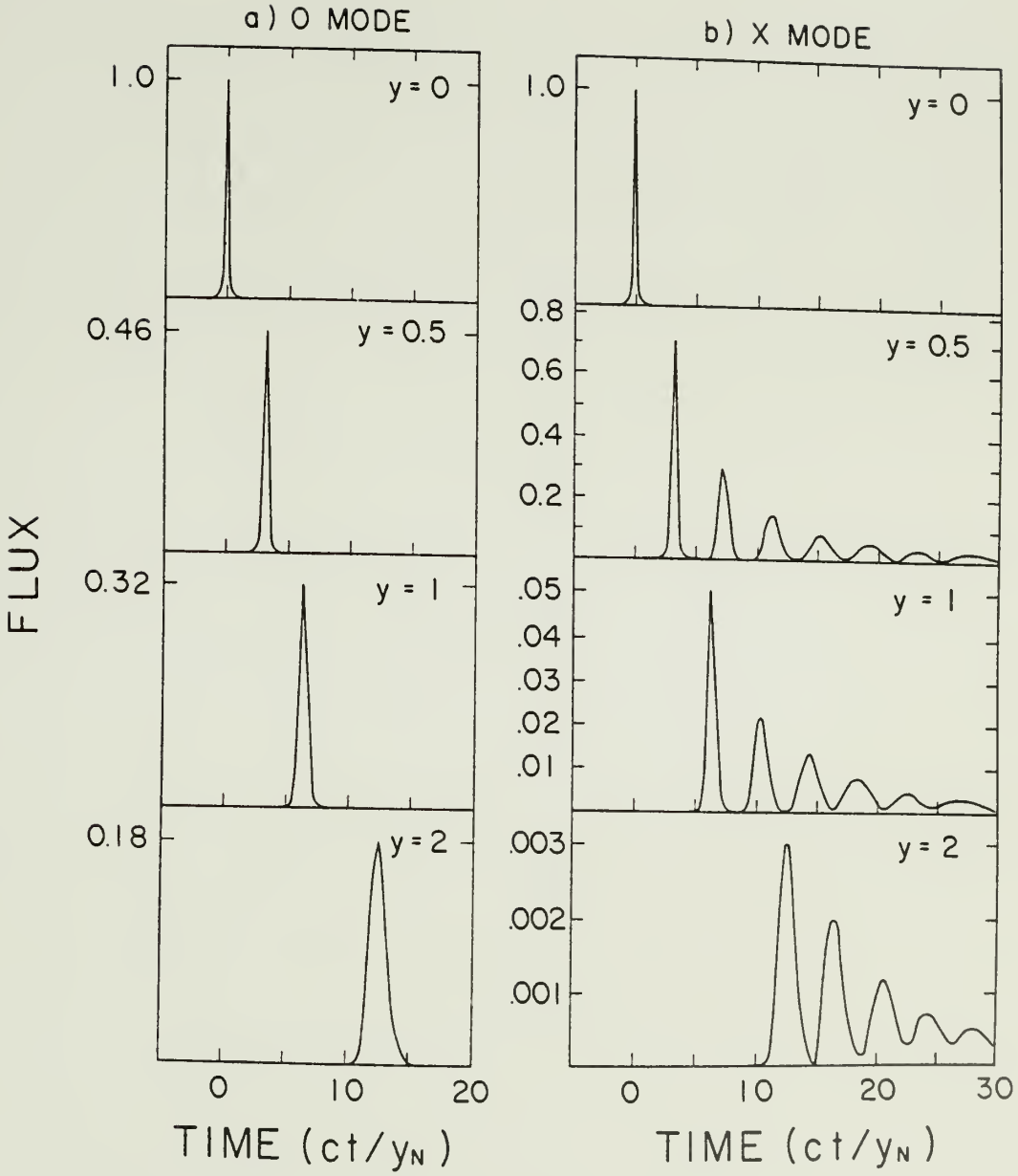
a) O MODE
b) X MODE
FLUX
1.0
0.46
0.32
0.18
y = 0
y = 0.5
y = 1
y = 2
0.8
0.6
0.4
0.2
.05
.04
.03
.02
.01
.003
.002
.001
0
10
20
30
TIME (ct/y_N)

Figure 3-3: Period of transmitted pulse time structure versus frequency from equation (3.18).

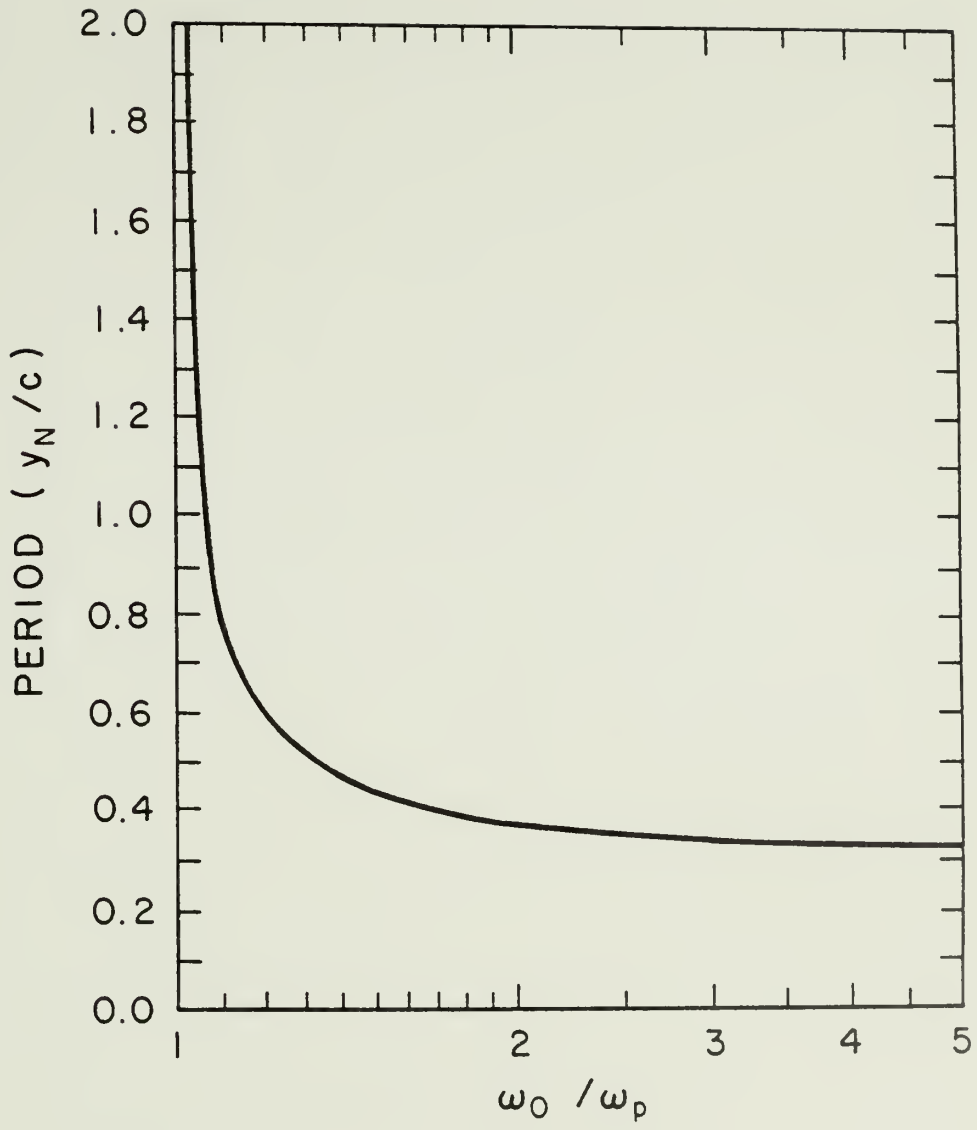
2.0
1.8
1.6
1.4
1.2
1.0
0.8
0.6
0.4
0.2
0.0
PERIOD (y_N/c)
1
2
3
4
5
ω_0/ω_p

Figure 3-4: Position angle and degree of circular polarization of a transmitted pulse envelope at $y = 2$ for $\omega_p/c = 10^4$. Incident pulse parameters are

$$\omega_o/c = 10{,}005$$

$$ct_w = 0.5$$

$$E_o/E_X = 0.1$$

$$k_x = 0.$$

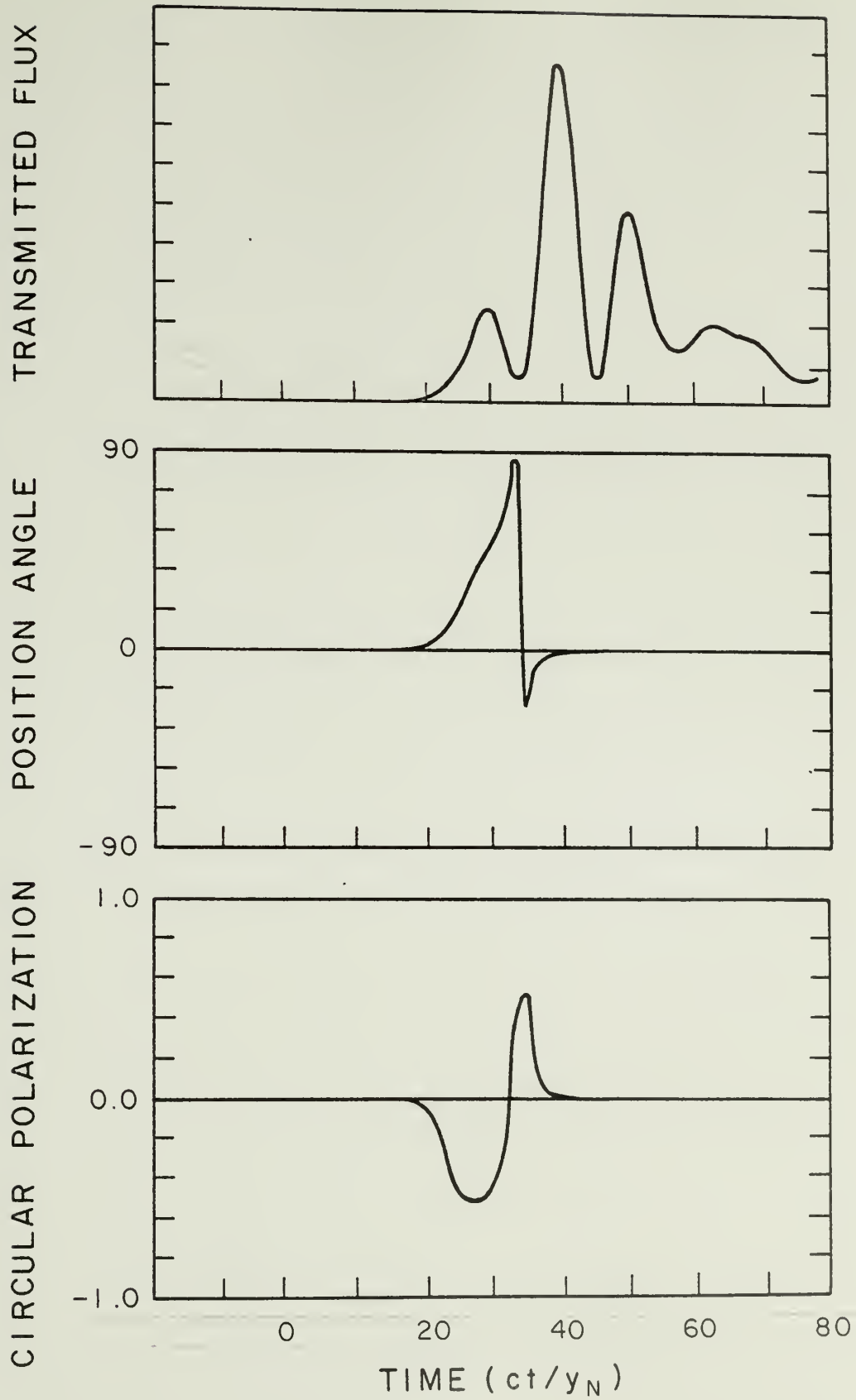
TRANSMITTED FLUX
POSITION ANGLE
90
0
-90
CIRCULAR POLARIZATION
1.0
0.0
-1.0
0
20
40
60
80
TIME (ct/y_N)

Figure 3-5: Transmission coefficient minima versus angle of incidence for $\omega_p/c = 300$ and different values of ω/c.

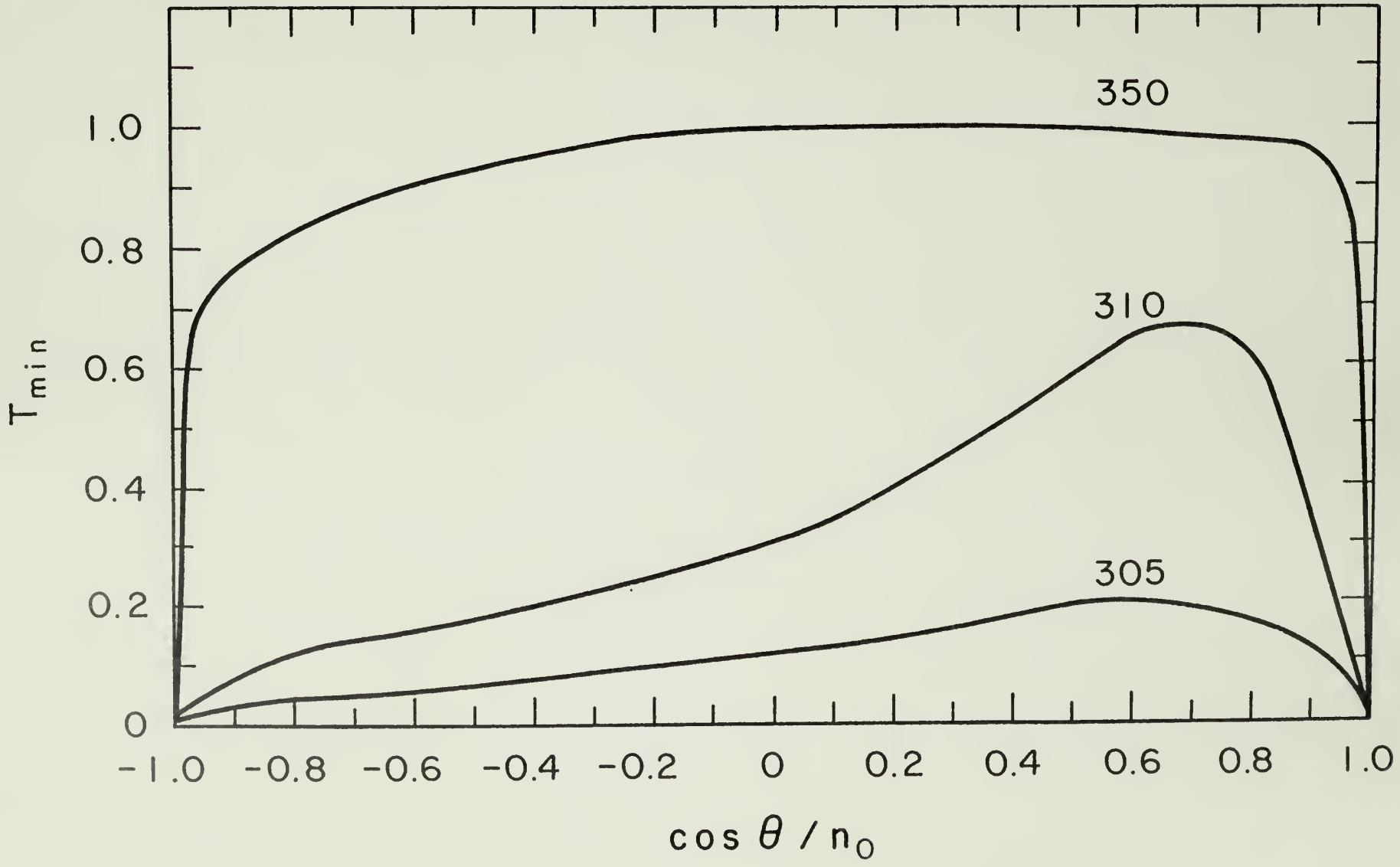
350
310
305
1.0
0.8
0.6
0.4
0.2
0
T_{min}
-1.0
-0.8
-0.6
-0.4
-0.2
0
0.2
0.4
0.6
0.8
1.0
$\cos\theta / n_0$

Figure 3-6: Transmission coefficient versus angle of incidence, showing spatial fringes, for $\omega_p/c = 300$ and $\omega/c = 305$.

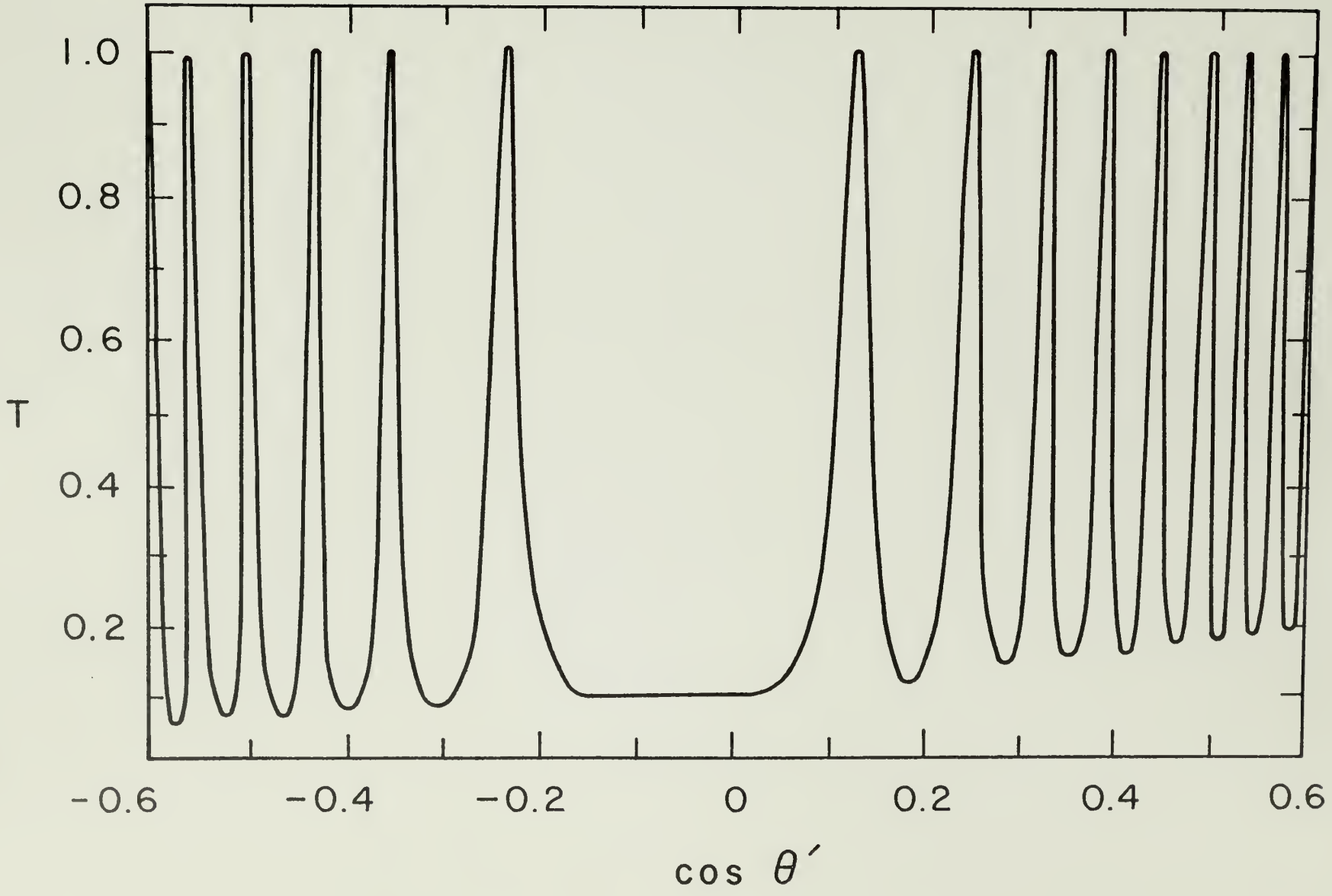
1.0
0.8
0.6
0.4
0.2
T
-0.6
-0.4
-0.2
0
0.2
0.4
0.6
cos θ′

Figure 3-7: X mode transmitted pulse envelopes and polarization for $\cos\theta = k_x c/\omega = -0.1, 0, 0.1$ and

$$\omega_p/c = 300$$

$$\omega_o/c = 305$$

$$ct_w = 0.5$$

$$E_o/E_X = 0.2$$

Fluxes are normalized to the peak flux of the incident pulse.

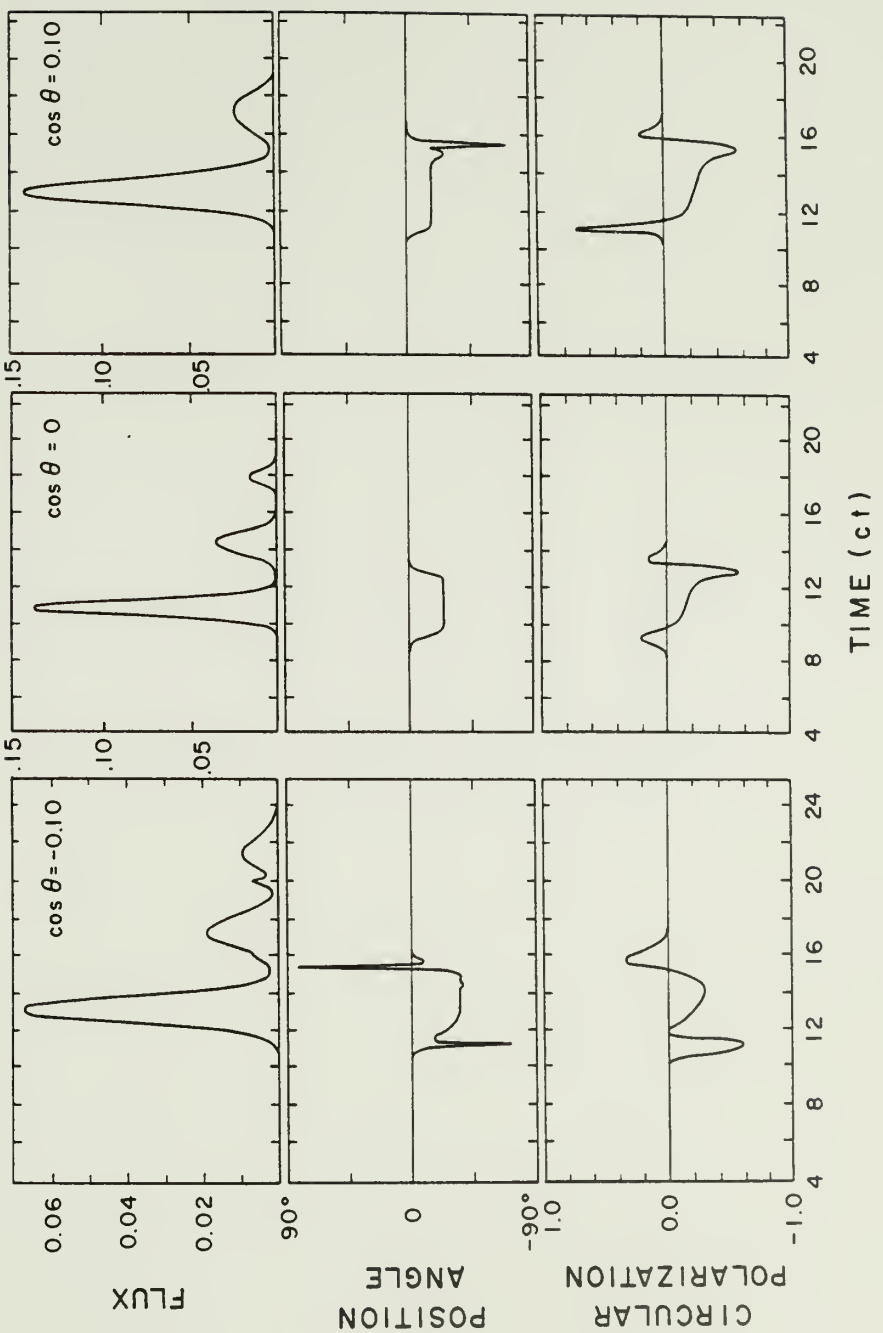
cos θ = -0.10
cos θ = 0
cos θ = 0.10
FLUX
POSITION ANGLE
CIRCULAR POLARIZATION
TIME (ct)

Figure 3-8: Period of transmitted pulse time structure versus angle of incidence from

$$P = P_o(1 - \cos^2\theta/n_o^2)^{-1/2} \quad .$$

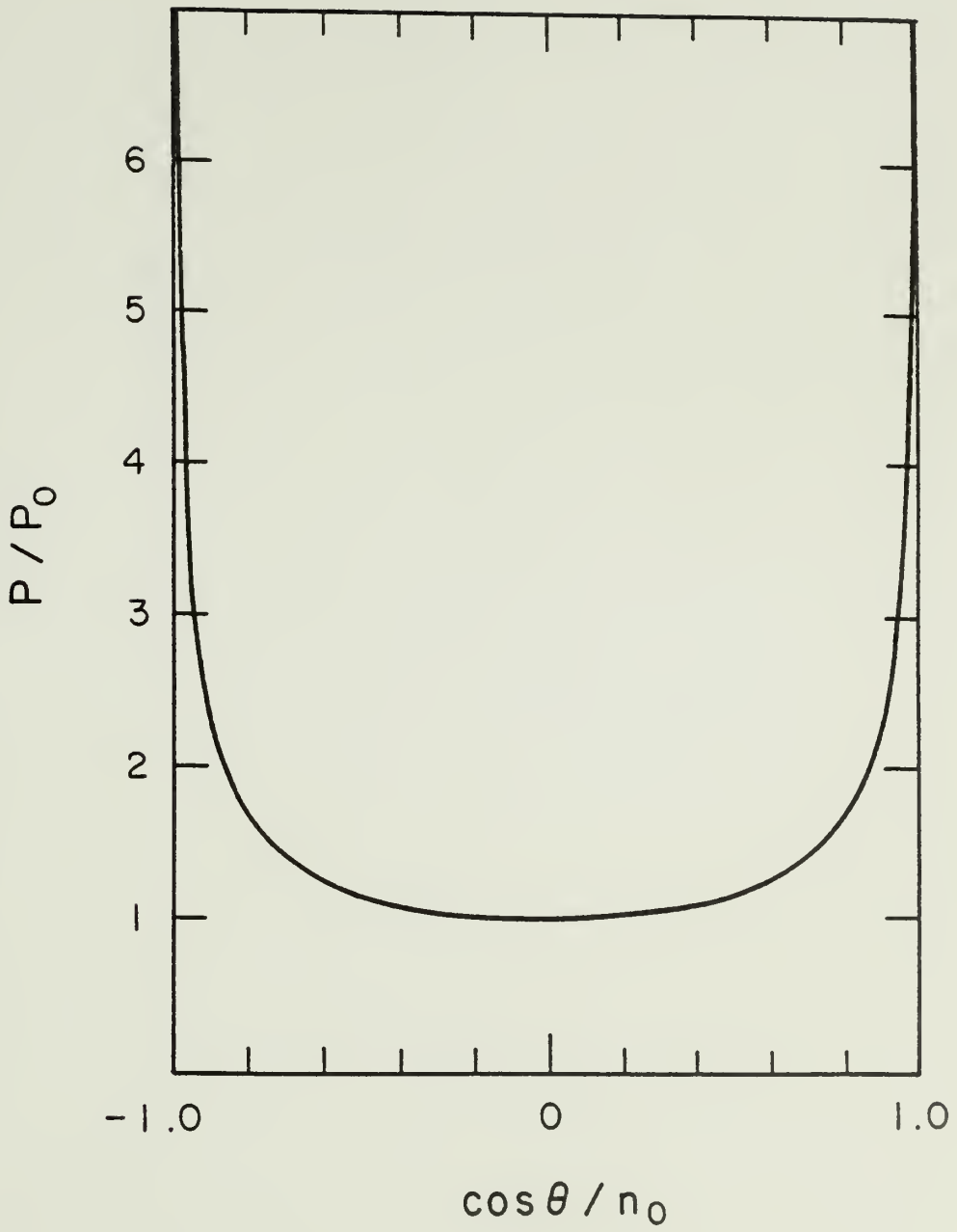
6
5
4
3
2
1
P / P0
-1.0
0
1.0
cos θ / n0

CHAPTER IV

SHEARING PLASMA IN A MAGNETIC FIELD

In any realistic model for propagation of radiation in a pulsar magnetosphere, magnetic field effects cannot be ignored, since field strengths of at least a few gauss are expected as far out as the light cylinder. Up to this point, we have neglected the effects of a magnetic field on the shearing plasma in order to understand the basic physics of wave and pulse propagation in a simple manner. The field-free plasma is isotropic in its rest frame (i.e., ε is a scalar quantity) but anisotropic in the stationary observer's frame due to the shearing motion. In the presence of a magnetic field, ε is a Hermitian matrix, so that the plasma is anisotropic even in its rest frame. It is well known that even a weak field can have an effect on the properties of a stationary plasma. In this chapter, we study the propagation of radiation in a shearing plasma in the presence of a magnetic field. The propagation modes of waves in the medium will no longer be linearly polarized and constant. A derivation of the equations for the fields in an anisotropic medium is therefore required to determine the propagation modes and boundary conditions in the stationary observer's frame.

In this model, we consider a magnetic field parallel to the direction of the shearing velocity. This case is the simplest because the Lorentz transformation between stationary and moving frames leaves the magnetic field unchanged, and produces no electric field. It is also perhaps the most realistic for reasons which will be discussed in Chapter VII.

1. Propagation Modes and Boundary Conditions

As before, we consider a cold, collisionless electron plasma and neglect ion motions. We take $\vec{B}_{ext} = B_o \hat{x}$, so that the external magnetic field is constant, uniform and parallel to the shearing velocity. In the frame of a comoving observer, the radiation fields will have the constitutive relations, $\vec{D}' = \varepsilon \cdot \vec{E}'$ and $\vec{B}' = \vec{H}'$, where ε is the dielectric tensor and has the form,

$$\varepsilon = \begin{pmatrix} \varepsilon_0 & 0 & 0 \\ 0 & \varepsilon_1 & -i\varepsilon_2 \\ 0 & i\varepsilon_2 & \varepsilon_1 \end{pmatrix} \tag{4.1}$$

where $\varepsilon_0 = 1 - \alpha^2$,

$$\varepsilon_1 = 1 - \frac{\alpha^2}{1 - Y^2} \quad , \qquad \varepsilon_2 = \frac{\alpha^2 Y}{1 - Y^2} \quad ,$$

and $\alpha = \omega_p/\omega' \quad , \quad Y = \omega_B/\omega' \ ,$

$$\omega_B = \frac{eB_o}{mc} \quad .$$

The frequency in the comoving frame, ω', is related to the frequency in the stationary frame, ω, by equation (3.2). Since $\vec{B}_{ext}$ in this model is parallel to $\vec{\beta}$, $B_o' = B_o$ in the expression for the gyrofrequency ω_B. The relations between the fields measured by a stationary observer are then given by

$$\begin{aligned} \vec{D} + \vec{\beta} \times \vec{H} &= \varepsilon \cdot (\vec{E} + \vec{\beta} \times \vec{B}) \\ \vec{B} - \vec{\beta} \times \vec{E} &= \vec{H} - \vec{\beta} \times \vec{D} \quad . \end{aligned} \tag{4.2}$$

We again assume for simplicity that $k_z = 0$ and that the radiation fields

are described by the dependence,

$$f(y)\ \exp(-i\omega t + ik_x x) \quad .$$

If equations (4.2) are substituted into Maxwell's equations, and all field components except E_z and H_z are eliminated, we obtain the coupled equations,

$$(P^2 - \varepsilon_1 Q^2)H_z - \frac{\varepsilon_1}{\varepsilon_0}\frac{c^2}{\omega^2}(1-\beta^2)\frac{\partial^2 H_z}{\partial y^2} = -i\varepsilon_2 PQE_z \tag{4.3}$$

$$P[(P^2 - \varepsilon_1 Q^2)E_z - \frac{c^2}{\omega^2}(1-\beta^2)\frac{\partial^2 E_z}{\partial y^2}] = i\varepsilon_2 Q^3 H_z +$$

$$\frac{i\varepsilon_2}{\varepsilon_0} Q \frac{c^2}{\omega^2}(1-\beta^2)\frac{\partial^2 H_z}{\partial y^2} \tag{4.4}$$

where $P = \frac{k_x c}{\omega} - \beta$, $\quad Q = 1 - \beta\frac{k_x c}{\omega}$.

In the presence of the magnetic field, the E_z and H_z polarizations are not independent propagation modes. The orthogonal propagation modes in the medium are defined as a function of β, and are linear combinations of E_z and H_z. Note that for the field free case, $\varepsilon_2 = 0$ and $\varepsilon_1 = \varepsilon_0$, uncoupling the equations and reducing them to the forms derived in Chapter II. We also have, for the other components of $\vec{E}$ and $\vec{H}$,

$$E_x = \frac{ic}{\varepsilon_0\omega}\frac{\partial H_z}{\partial y} \quad , \quad H_x = \frac{-ic}{\omega}\frac{\partial E_z}{\partial y} \quad , \tag{4.5}$$

$$E_y = \frac{\gamma^2}{\varepsilon_1}[(P + \beta\varepsilon_1 Q)H_z + i\varepsilon_2 QE_z] \quad , \tag{4.6}$$

$$H_y = \gamma^2[(\beta\frac{\varepsilon_2^2}{\varepsilon_1}Q - P - \beta\varepsilon_1 Q)E_z - \frac{i\varepsilon_2}{\varepsilon_1}\beta PH_z] \quad . \tag{4.7}$$

We wish to determine the independent propagation modes for each

value of β, i.e., for each layer in the medium. If equation (4.3) is used to solve for E_z in terms of H_z, then that expression may be substituted into equation (4.4) to give a fourth order equation for H_z:

$$\frac{c^4}{\omega^4}(1-\beta^2)^2\frac{\varepsilon_1}{\varepsilon_0}\frac{\partial^4 H_z}{\partial y^4} - \frac{c^2}{\omega^2}(1-\beta^2)\left[(P^2-\varepsilon_1 Q^2)\left(\frac{\varepsilon_1}{\varepsilon_0}+1\right)\right.$$

$$\left.+\frac{\varepsilon_2^2}{\varepsilon_1}Q^2\right]\frac{\partial^2 H_z}{\partial y^2} + \left[(P^2-\varepsilon_1 Q^2)^2 - \varepsilon_2^2 Q^4\right]H_z = 0 \qquad (4.8)$$

In each layer, where β, ε_0, ε_1 and ε_2 are constants, all the coefficients are independent of y, so we can assume a solution for H_z of the form,

$$H_z(y_n) = h_u e^{ik_n y} + h_d e^{-ik_n y} \quad . \qquad (4.9)$$

Then by substitution of this expression for H_z into equation (4.8), we obtain a quadratic equation for k_n^2. Two solutions exist for the y component of the wave vector, which are

$$(k_n^{\pm})^2 = \gamma^2\frac{\omega^2}{c^2}\frac{1}{2}\left\{F_n \pm \left\{F_n^2 - 4\frac{\varepsilon_0}{\varepsilon_1}\left[(P_n^2-\varepsilon_1 Q_n^2)^2\right.\right.\right.$$

$$\left.\left.\left.-\varepsilon_2^2 Q_n^4\right]\right\}^{1/2}\right\} \qquad (4.10)$$

where $F_n = (\varepsilon_1 Q_n^2 - P_n^2)\left(1+\frac{\varepsilon_0}{\varepsilon_1}\right) - \frac{\varepsilon_2^2}{\varepsilon_1}Q_n^2$.

There are, consequently, two propagation modes in each layer, which have the above dispersion relations. The polarization of these modes can be found by substituting the solution for H_z into equation (4.3) and solving for E_z:

$$E_z(y_n) = \frac{i}{\varepsilon_2 Q_n P_n}\left[(P_n^2-\varepsilon_1 Q_n^2) + \frac{\varepsilon_1}{\varepsilon_0}\frac{c^2}{\omega^2}\frac{(k_n^{\pm})^2}{\gamma^2}\right]H_z(y_n)$$

$$= iR_n^{\pm} H_z(y_n) \qquad (4.11)$$

These elliptically polarized propagation modes, which we have labeled + and -, involve different combinations of E_z and H_z in each layer. As a result of the Lorentz transformation on the x component of the wave vector between stationary and moving frames,

$$k_x' = \gamma(k_x - \frac{\omega}{c}\beta) \quad , \tag{4.12}$$

each comoving observer will measure a different angle between $\vec{k}'$ and $\vec{B}'_{ext} = \vec{B}_{ext}$, even when $k_x = 0$. They will therefore determine propagation modes corresponding to these angles and to the frequency, ω', in the moving frame. Thus, the propagation of a plane wave through a shearing magneto-plasma is characterized by continually changing, elliptical modes.

This solution reduces to the correct form in several limits. As $\vec{B}_{ext} \longrightarrow 0$ and $k_x = 0$,

$$(k^{\pm})^2 \longrightarrow \frac{\omega^2}{c^2}\varepsilon_0 \quad , \qquad R^{\pm} \longrightarrow \mp 1 \quad ,$$

which agrees with our solution for the field-free plasma, since two circularly polarized modes with equal, constant wave vectors are equivalent to two linearly polarized modes. In the limit $\beta \to 0$ and $k_x = 0$,

$$(k^{+})^2 \longrightarrow \frac{\omega^2}{c^2}\varepsilon_0 \quad ,$$

$$(k^{-})^2 \longrightarrow \frac{\omega^2}{c^2}(\varepsilon_1 - \frac{\varepsilon_2^2}{\varepsilon_1}) = \frac{\omega^2}{c^2}[1 - \frac{(1-\alpha^2)\alpha^2}{1-\alpha^2-Y^2}] \quad ,$$

$$R^{+} \longrightarrow 0 \quad , \qquad R^{-} \longrightarrow \infty \quad ,$$

which are just the linear ordinary (+) and extraordinary (-) modes for propagation transverse to $\vec{B}_{ext}$.

The boundary conditions are still those given by equations (2.11), but we must now use all four equations simultaneously to solve for the four amplitudes of the + and - modes in each layer. If the tangential fields are written in terms of these amplitudes, then using equations (4.5), (4.9), (4.11), we have

$$H_z(y_n) = h_u^+ e^{ik_n^+ y} + h_u^- e^{ik_n^- y} + h_d^+ e^{-ik_n^+ y} + h_d^- e^{-ik_n^- y}$$

$$E_z(y_n) = iR_n^+(h_u^+ e^{ik_n^+ y} + h_d^+ e^{-ik_n^+ y}) +$$

$$iR_n^-(h_u^- e^{ik_n^- y} + h_d^- e^{-ik_n^- y})$$

$$E_x(y_n) = -\frac{c}{\varepsilon_0 \omega}[k_n^+(h_u^+ e^{ik_n^+ y} - h_d^+ e^{-ik_n^+ y}) +$$

$$k_n^-(h_u^- e^{ik_n^- y} - h_d^- e^{-ik_n^- y})]$$

$$H_x(y_n) = \frac{c}{\omega}[ik_n^+ R_n^+(h_u^+ e^{ik_n^+ y} - h_d^+ e^{-ik_n^+ y}) +$$

$$ik_n^- R_n^-(h_u^- e^{ik_n^- y} - h_d^- e^{-ik_n^- y})] \quad . \qquad (4.13)$$

At $y = 0$, the incident Fourier amplitudes are $h_u(0)$ and $\varepsilon_u(0)$ from equation (2.17), so that

$$h_u(0) = h_o^+ + h_o^-$$

$$\varepsilon_u(0) = iR_1^+ h_o^+ + iR_1^- h_o^- \quad .$$

Solving for h_o^+ and h_o^-, we have

$$h_o^+ = \frac{R_1^+ h_u(0) + i\varepsilon_u(0)}{R_1^- - R_1^+} \quad , \quad h_o^- = -\frac{[\, i\varepsilon_u(0) + R_1^+ h_u(0)]}{R_1^- - R_1^+} \tag{4.14}$$

Using equations (4.13), the boundary conditions on the tangential fields at $y = y_n$ may then be written in the form

$$\begin{pmatrix} h_u^+(y_n) \\ h_u^-(y_n) \\ h_d^+(y_n) \\ h_d^-(y_n) \end{pmatrix} = A_n^{-1} C_{n-1} \begin{pmatrix} h_u^+(y_{n-1}) \\ h_u^-(y_{n-1}) \\ h_d^+(y_{n-1}) \\ h_d^-(y_{n-1}) \end{pmatrix} \tag{4.15}$$

where A_n is the 4x4 matrix of the coefficients of the mode amplitudes in layer n, and C_{n-1} is the matrix of the coefficients in layer n-1, all evaluated at $y = y_n$. We can use the same method outlined in §II 3 to solve for the amplitudes by writing

$$\begin{pmatrix} h_u^+(y_N) \\ h_u^-(y_N) \\ 0 \\ 0 \end{pmatrix} = \prod_{n=2}^{N} A_n^{-1} C_{n-1} \begin{pmatrix} h_o^+ \\ h_o^- \\ h_d^+(0) \\ h_d^-(0) \end{pmatrix}$$

a set of four equations from which we obtain the transmitted and reflected amplitudes at the top and bottom of the medium. Amplitudes for the other layers may then be calculated in steps, using equation (4.15).

All upgoing field components may be obtained from the amplitudes $h_u^+(y_n)$ and $h_u^-(y_n)$ using equations (4.13), (4.6), and (4.7). In the case of pulse propagation, the inverse Fourier transform of the upgoing fields gives $\vec{E}_u(y_n,t)$ and $\vec{H}_u(y_n,t)$, from which the flux and polarization are calculated.

Due to the anisotropy of the dielectric tensor, the expression

given in Chapter II for the energy density in the wave (cf. equation [2.14]) must now be written,

$$U = \frac{1}{16\pi}\left[\gamma\omega\left(E_i \frac{\partial\varepsilon_{ij}}{\partial\omega'} E_j^*\right) - \gamma^2\omega\beta_i \frac{\partial\varepsilon_{ij}}{\partial\omega'}\left\{(\vec{E} + \vec{\beta} \times \vec{B}) \times \vec{B}^* + \vec{E}^* \times (\vec{B} - \vec{\beta} \times \vec{E})\right\}_j\right] . \tag{4.16}$$

If we substitute for the components of ε_{ij}, and write U in terms of the components of $\vec{E}$ and $\vec{H}$,

$$U = \frac{1}{8\pi}\gamma\alpha^2\frac{\omega}{\omega'}\left\{|E_x|^2 + \frac{1}{(1-Y^2)^2}\left(|E_y|^2 + |E_z|^2\right) - \frac{i}{2}\frac{Y(3-Y^2)}{(1-Y^2)^2}\left(E_y E_z^* - E_z E_y^*\right) - \beta^2\left[|E_y|^2 - \gamma^2|E_z|^2 - \gamma^2 Q^2|H_z|^2 + \frac{Q}{\beta}\left(E_y H_z^* + E_y^* H_z\right)\right]\right\} .$$

This form is used to calculate the particle energy flux contribution to the total energy flux in the moving layers. The particle energy flux is zero where the medium is at rest, since none of the components of ε_{ij} explicitly depend on $\vec{k}'$, i.e., the medium is not spatially dispersive in its rest frame.[1]

2. Results for Plane Wave Propagation

We first examine the behavior of plane waves propagating through the medium, both as a function of magnetic field strength and frequency. The velocity profile used in these calculations is the same symmetric function of y defined in Chapter III. Due to the orientation of the

[1] See Ginzburg 1970, p. 7 and p. 320 for more details on spatial dispersion and particle energy flux.

external field along the shearing velocity, normally incident waves will initially propagate transverse to the field. At the bottom of the medium, where $\beta = 0$, the propagation modes are linearly polarized with their electric vectors parallel (ordinary) and perpendicular (extraordinary) to $\vec{B}_{ext}$. The ordinary mode, the limiting case of the + mode when $\beta \to 0$, is uninfluenced by $\vec{B}_{ext}$ and propagates above the plasma cutoff at ω_p as in a field-free plasma. The extraordinary mode, the limiting case of the - mode, is affected by the upper hybrid resonance at

$$\omega_1 = (\omega_B^2 + \omega_p^2)^{1/2} \quad , \tag{4.17}$$

where the wave vector k_1^- is infinite, and the cyclotron cutoffs at

$$\omega_{2,3} = \pm \frac{\omega_B}{2} + (\frac{\omega_B^2}{4} + \omega_p^2)^{1/2} \quad . \tag{4.18}$$

In a warm plasma, the wave vector does not actually become infinite, because collisions or thermal motions can result in absorption or mode conversion at the resonance.[2] The region between ω_1 and ω_2, then, is really a stopband in which the wave does not propagate. Since all plasmas have a finite temperature, the cold plasma approximation does not accurately describe the wave behavior at resonances. However, it is a good approximation to the behavior of waves in a nearly cold plasma in the regions above or below the resonance.

As the wave moves into layers of high shearing velocity, there are

---

[2] It has been shown that part of the extraordinary wave energy in a warm plasma can be carried away from the resonance by the excitation of longitudinal plasma waves. This conversion of electromagnetic waves to plasma waves can take place in the absence of collisions (Ginzburg 1970, Tang 1970).

two effects in the comoving frame which are responsible for most of the propagation characteristics. The Lorentz transformation on the wave vector (cf. equation [4.12]) changes its apparent angle to the field, thus changing the propagation modes. In addition, the frequency in the moving frame (cf. equation [3.2]) increases with γ, changing the ratios ω'/ω_p and ω'/ω_B and, thus, the index of refraction. From the point of view of the stationary observer, the wave encounters a variable effective plasma frequency and gyrofrequency. Although the equations derived in §1 enable us to perform the calculations in the stationary (lab) frame, we will discuss in the following paragraphs the physics of wave propagation from the point of view of the comoving observer.

In the presence of the magnetic field, wave propagation in the shearing plasma exhibits a number of interesting features. There are, in fact, too many cases to allow a detailed consideration of each. We will therefore concentrate our discussion on situations where the wave frequency, ω, is near ω_p. We find that the propagation characteristics are markedly different in two regimes: $\omega_B > \omega_p$ (strong field) and $\omega_B < \omega_p$ (weak field).

Propagation in the weak field regime is illustrated in Figure 4-1, which shows the numerically calculated magnitudes of the wave vectors of the + and - modes as a function of y. The waves are normally incident, and curves are plotted for several different values of $\omega_B/\omega_p < 1$, with the ratio ω_p/ω remaining constant. Since β, shown on the upper axis, is a symmetric function of y, the curves are all symmetric about $y = 1.0$. As ω_B/ω_p decreases, both k^+ and k^- converge to the constant value $\frac{\omega}{c} n_o = \frac{\omega}{c} \sqrt{\epsilon_o}$. This agrees with the limit already established for

the field-free case in the previous section. It is also evident that, as ω_B approaches ω_p, neither k^+ nor k^- diverge far from this value at high velocity. At $\beta = 0$, however, k^- varies with ω_B/ω_p because the cyclotron cutoff, ω_2, is located just above ω_p. As ω_B increases, ω_2 moves closer to ω, affecting the - mode propagation. If the wave frequency is initially above both ω_p and ω_2, then it remains above them in all comoving frames since ω' increases with β.

Propagation in the strong field regime is illustrated in Figure 4-2, which shows the magnitudes of k^+ and k^- as a function of y for different values of $\omega_B/\omega_p > 1$. In this regime, the upper hybrid resonance is above ω and may affect - mode propagation as $\beta \to 1$. For large values of ω_B/ω_p, ω_1 is located at so high a frequency above ω that the effect on k^-, even at high velocities, is negligible. As ω_B/ω_p decreases, ω_1 moves down into the range of $\omega' = \gamma\omega$, increasing the dependence of k^- on β. For a given γ_{MAX} and ω, there is a critical value of ω_B/ω_p such that $\omega_1/\omega = \gamma_{MAX}$, below which the - mode encounters the resonance and $k^- \to \infty$. The critical curve corresponding to this value, where $k^- = \infty$ only at the point $y = 1.0$, is shown in Figure 4-2 and labeled $\omega_B/\omega_p = 6.3$ ($\gamma_{MAX} = 6$). As previously mentioned, an infinite wave vector is unphysical and indicates that absorption or mode conversion will take place at this frequency. For given values of ω_B, ω_p and γ_{MAX}, then, there is a high frequency cutoff at $\omega_c = \omega_1/\gamma_{MAX}$, above which the wave suffers strong absorption. It is not an absolute cutoff, however, because there is propagation above the cyclotron cutoff ω_2, so that ω_c really defines the lower end of an absorption band stretching to ω_2/γ_{MAX}. Figure 4-3 shows the behavior of k^- for a fixed value of ω_p/ω as ω_B/ω_p is decreased below

the critical value. The wave encounters the resonance at lower and lower values of $\gamma = \gamma_R$, where

$$\gamma_R = \omega_1/\omega = (\omega_B^2/\omega^2 + \omega_p^2/\omega^2)^{1/2} \quad .$$

At a low enough value of ω_B/ω_p, it passes through the stop-band, where k^- is imaginary, into a region where it is again able to propagate (k^- is real). By the time the wave reaches this region, though, it may be somewhat attenuated.

Returning to Figure 4-2, it is evident that the k^+ curves depend on the value of ω_B/ω_p to a much lesser extent. All curves have the value $\frac{\omega}{c} n_o^+$ at $y = 0$, but approach ω/c as β increases. In the limit $\omega_B/\omega_p >> 1$, $k^+ \rightarrow k^- \rightarrow \omega/c$ at high velocities, and both modes propagate with phase velocity $\sim c$. This is in striking contrast to the limit $\omega_B/\omega_p << 1$, where both modes have constant wave vectors and propagate at a phase velocity greater than c.

The wave vectors of the modes at oblique angles of incidence in the strong field regime are shown in Figure 4-4. Plotted here is the magnitude of the total wave vector,

$$|k_T^{\pm}| = (k^{\pm 2} + k_x^2)^{1/2} \quad .$$

At angles inclined to the normal, the propagation modes at $y = 0$ are no longer transverse, linearly polarized modes, since $\vec{k}_T \cdot \vec{B}_{ext} \neq 0$. It is evident that k_T^- has a greater dependence on β at negative angles of incidence. This trend results from the increase in ω' with negative k_x at a given β (cf. equation [3.2]), allowing the upper hybrid resonance to have a greater effect on the - mode. For large negative k_x, the wave

will eventually run into the resonance and suffer strong absorption. For positive angles of incidence, ω' may actually decrease with increasing β, as in the case $k_x c/\omega = .80$, where ω' dips below ω_p in a region between $y = 0$ and $y = .1$, causing the y component of k_T^+ to become imaginary. It is interesting that the case $k_x \sim \omega/c$, propagation along the field, simulates the case $\omega_B/\omega_p >> 1$ for normal incidence. Both insure that $\omega' << \omega_1$ throughout the medium.

As might be expected, the polarization properties of plane waves transmitted through the shearing plasma are considerably changed by the presence of a magnetic field. It was clear from the equations derived in §1 that no two orthogonal polarization modes propagate through the medium independently. Even though E_z and H_z define the linear propagation modes at $\beta = 0$ for normal incidence, the modes in the moving layers are elliptical and mix the two polarizations. Figure 4-5 shows an example of how the total energy flux in a wave, initially polarized in the x direction, divides itself between + and - modes through the medium. At $y = 0$, all of the energy resides in the + mode, since the wave's electric vector points in the direction of the external field. The magnitude of the upgoing total energy flux in the + mode, $|W^+|$, is therefore normalized to 1.0 at $y = 0$ and the energy flux in the - mode, $|W^-|$, equals 0. As β increases, some of the wave energy begins to propagate in the - mode, and as $\beta \to 1$, the energy is almost equally divided between the modes. Meanwhile, the mode polarizations have changed from linear to elliptical to nearly circular. It appears to the comoving observers that the wave propagates almost antiparallel to the field as $\beta \to 1$, and so resolves itself into left and right handed circular modes of equal amplitude.

As β decreases for $y > 1.0$, the energy in the modes stays almost constant, even when they become linearly polarized again near $y = 2$. Because the radiation propagates in nearly circular modes over a certain distance in the plasma, there is some Faraday rotation and the emergent position angle may be different from the incident position angle. Therefore, the transmitted radiation may contain both modes, even though the incident radiation contained only one. Figure 4-6 shows a case where significant reflections occur and the wave does not divide its energy equally among the + and - modes.

Since, in general, the wave propagates in elliptical modes having different indices of refraction over most of the shearing region, one would expect both Faraday rotation and net circular polarization. Figure 4-7 shows the polarization changes which occur for the upgoing wave of Figure 4-6a as it moves through the medium. The position angle in this case rotates through about 6π radians at a variable rate, depending on the extent to which the modes are circularly polarized. Net circular polarization also appears and oscillates in synchronization with the position angle rotation. It varies between extreme values as the position angle rotates through $\pi/2$ radians. This is the general polarization behavior one would expect in the case of orthogonal elliptical modes of unequal amplitude travelling at different phase velocities. If the wave is initially polarized at 90° to the wave in Figure 4-7 (i.e., in the z-direction), the net position angle rotation is the same, but the circular polarization is produced in the opposite sense. Two incident orthogonal linear polarizations emerge from the shearing region with position angle separated by 90° and equal degrees but opposite

signs of circular polarization. Therefore, orthogonality is preserved in wave propagation through the shearing magneto-plasma.

The frequency dependence of the transmission coefficient depends to a large extent on the magnetic field strength, as a result of the propagation characteristics we have already discussed. As in the field-free case, resonances appear in the transmission coefficient just above the plasma frequency for waves polarized along the x-axis. Now, resonances also appear just above the cyclotron cutoff and below the upper hybrid resonance for waves polarized along the z-axis. There is a major difference in the resonance behavior between the weak and strong field regimes and it occurs in the frequency dependence of the resonance spacings. When $\omega_p > \omega_B$, the spacing changes with frequency, having the same dependence as the field-free case (cf. equation [3.15]). When $\omega_B >> \omega_p$, the resonance spacing is frequency independent for both polarizations. As far as we have been able to ascertain from our numerical calculations, this is a general result which holds regardless of the specific values of ω_p or ω_B.

It was found that when $\beta \gtrsim .80$, $k^+ \sim k^- \sim \omega/c$ in the strong field case. Since β is this large over most of the shearing region, then the resonance spacing $\Delta\omega/c$ will be

$$\frac{\Delta\omega}{c} \sim \Delta k^- \sim \Delta k^+ = \frac{\pi}{y_N} \quad ,$$

which is independent of frequency. Figure 4-8 shows the transmission coefficient for the E_x polarization just above ω_p and for the E_z polarization in the vicinity of ω_1 and ω_2 in the strong field case. In both frequency bands, the resonance spacing is constant and equal to $\pi/y_N = 1.5708$. The resonance peaks above the plasma and cyclotron cutoffs be-

come weaker with increasing frequency, for the same reasons already discussed in some detail in Chapter III. The region between ω_1 and ω_2 is the stop-band for - mode propagation, so that these frequencies are highly attenuated in the first few layers. At frequencies just below ω_1, k^- has a y dependence similar to the $\omega_B/\omega_p = 2$ curve in Figure 4-3. The waves propagate freely at $\beta = 0$ but pass through an absorption layer into a region where they again propagate freely. If the absorption layer is narrow enough, as is the case here, the waves are partially transmitted into the region where k^- is real and then partially transmitted at the second absorption layer (a mirror image of the first). This situation is responsible for the resonances which appear just below ω_1, because the partially transmitted and reflected waves are able to mutually interfere. Since the absorption layers are located very near $y = 0$ and $y = y_N$, the resonance spacing will also be constant and equal to π/y_N.

In the weak field regime, k^+ and k^- tend to the constant value $\frac{\omega}{c} n_o^+$ in the limit $\omega_p >> \omega_B$, and even when $\omega_p \gtrsim \omega_B$, the wave vectors are never far from this value in the high velocity regions. Consequently, the resonance spacing will depend on the frequency as if ω_B were zero. We see, then, that the field-free shearing plasma is just a special case of the shearing plasma in a weak magnetic field. The presence of the field, however, does introduce some interesting variations on the field-free case, primarily due to polarization effects. Figure 4-9 shows transmission coefficients for both polarizations just above $\omega_2 \sim \omega_p$ as well as the position angle and circular polarization of the transmitted waves at each frequency. The resonances generally grow weaker with in-

creasing frequency, but are modulated by an oscillating envelope with an increasing period. The resonances die out much more quickly in the E_z polarization, but the modulation persists as a steady oscillation. The position angle sweeps in frequency at a generally decreasing rate, with superimposed fluctuations synchronized with the resonances. Since the rate of position angle sweep at a given frequency is the same for both polarizations, they remain orthogonal. The circular polarization of the transmitted waves oscillate in frequency, also with superimposed fluctuations, reaching positive maxima when the position angle equals 90° and negative maxima when the position angle is zero. Note that the sign of circular polarization is opposite for the two polarizations at any given frequency.

These effects occur noticeably when $\omega_B \gtrsim 10^{-2}\ \omega_p$ and become stronger as ω_B approaches ω_p. The position angle sweep is caused by Faraday rotation over the distance y_N, which increases as the average values of k^+ and k^- diverge. In fact, the change in position angle of a wave is directly proportional to $(k^+ - k^-)$, which decreases both as ω increases above ω_B and as ω_B decreases below ω_p. The circular polarization, as pointed out earlier, arises from phase changes and the ellipticity of the modes. The modulation of the resonances can then be completely explained in terms of Faraday rotation. A wave polarized in the x direction initially has a position angle equal to 0. After undergoing a net rotation in the shearing region, the radiation propagates in nearly linear modes at the gradient near y_N with amplitudes depending on the orientation of the position angle. If the change in position angle ($\Delta\psi$) over the distance y_N is $m\pi$, where $m = 0,1,2,\ldots$, then all radiation is

polarized in the x direction and the reflection at the second gradient is large. The resonances at these frequencies are relatively strong. If $\Delta\psi = (2m+1)\pi/2$, then all radiation is polarized in the z direction, which undergoes much less reflection at the gradient. Therefore, the resonances at these frequencies are suppressed. For a wave polarized initially in the z direction, the situation is similar. Above the E_z resonance band, almost all the radiation is transmitted at the first gradient, and if $\Delta\psi = m\pi$, all radiation is polarized in the z direction at the second gradient and is transmitted. At these frequencies, $T = 1.0$. If $\Delta\psi = (2m+1)\pi/2$, all radiation is polarized in the x direction at y_N and the reflection is large, producing a minimum in the transmission coefficient.

It should be pointed out that these effects due to Faraday rotation are valid only in the case of an electron plasma, and where ion motions can be neglected. In an electron-positron plasma, for instance, Faraday rotation may be negligible or even zero, if the numbers of electrons and positrons are equal. Because of their equal masses and opposite charges, their motions in the field tend to cancel each other.

The various effects of the magnetic field on plane wave propagation which have been discussed in this section are summarized in Figure 4-10. It shows, schematically, the behavior of the transmission coefficient for waves initially polarized along the x and z directions over the entire range of interesting frequencies. The lower electron cyclotron cutoff, ω_3, is the lower limit for all propagation in the E_z polarization. Absorption bands are present between ω_1 and ω_2 and for both polarizations between ω_1/γ_{MAX} and ω_2/γ_{MAX}. Resonances from multiple reflections occur

for both E_x and E_z and can appear, in the strong field regime, in frequency bands separated by many orders of magnitude.

3. Pulse Propagation

Numerical results for pulse propagation through the shearing region at frequencies near ω_p further confirm the differences found between the weak and strong field regimes. As mentioned before, the period of the time structure in the transmitted pulse is equal to the inverse of the resonance spacing in the frequency spectrum. It follows that the period is frequency independent in the strong field regime and frequency dependent in the weak field regime.

Figure 4-11 shows a transmitted pulse, and its polarization when a weak field is present. The incident pulse in this case was linearly polarized in the x direction. Figure 4-9a includes the frequency range covered by the incident pulse spectrum, and it is clear by comparison that the period of the components in the transmitted pulse is the inverse of the resonance spacing around $\omega/c = 308$. From the time delay of the pulse ($ct > 2$), it is evident that its velocity in the medium is significantly below c. The time dependence of the polarization is more difficult to interpret, but a periodicity exists which is apparently equal to the component period. The position angle changes sharply on the edges of the components and undergoes slower sweeps over their duration. The circular polarization oscillates, rotating steadily through the components and changing sign rapidly between them.

An example of pulse propagation in the presence of a strong field is shown in Figure 4-12. The incident pulse was linearly polarized with

an arbitrary position angle, so that both + and - modes were initially present. The transmitted radiation is composed of three periodic pulses polarized in the x direction ($\psi = 0°$) and one pulse polarized in the z direction ($\psi = 90°$). The incident pulse has been resolved into E_x and E_z polarizations, which each propagate in + and - modes but undergo negligible Faraday rotation. Their identities are therefore preserved in the transmitted pulse. The period of the E_x pulses is around the predicted value $y_N/\pi = .64$. The E_z pulse apparently travels slower in the medium because it arrives at $y = 2$ after the second E_x pulse, which has undergone two reflections. Evidently, the transmission characteristics for E_x and E_z polarizations seen in plane wave propagation are operating in pulse propagation. The two polarizations separate out of an initial mixture, even through energy is continually being transferred between them in the shearing region. Our choice of a magnetic field parallel to the shearing velocity no doubt emphasizes the propagation differences between the E_x and E_z polarizations. If the field were oriented at an arbitrary angle to the velocity, the propagation would surely be more complex, but the shearing would tend to resolve the radiation into these orthogonal linear modes.

In summary, we have found that the presence of a magnetic field can drastically alter the propagation characteristics of waves and pulses in shearing media. The existence of more than one cutoff frequency allows the resonance effect of Chapter III to appear in both polarizations and in different frequency ranges. Transmission is also affected by the presence of absorption bands. If the field is relatively weak, the medium behaves much like the field-free plasma, which is the limit-

ing case. If the field is strong, the wave vector becomes a function of the velocity in such a way that resonance spacings are frequency independent. More complex polarization changes occur and they are largest as the gyrofrequency approaches the plasma frequency. Most notable is the conversion of linear to circular polarization and Faraday rotation of the position angle.

The complexity of wave and pulse propagation in a shearing, anisotropic medium makes the consideration of other magnetic field orientations difficult. A field in the z direction would allow E_z and E_x to be independent modes of propagation throughout the medium, but, as previously mentioned, this situation is complicated by the variation of B_o or B_o'. However, we suspect that the case studied here has the most relevance to the geometries likely to exist in the pulsar magnetosphere.

Figure 4-1: Plus and minus mode wave vectors versus y (and β) at normal incidence for different values of $\omega_B/\omega_p < 1$. The quantity, $\omega_p/\omega = 0.8$, is fixed.

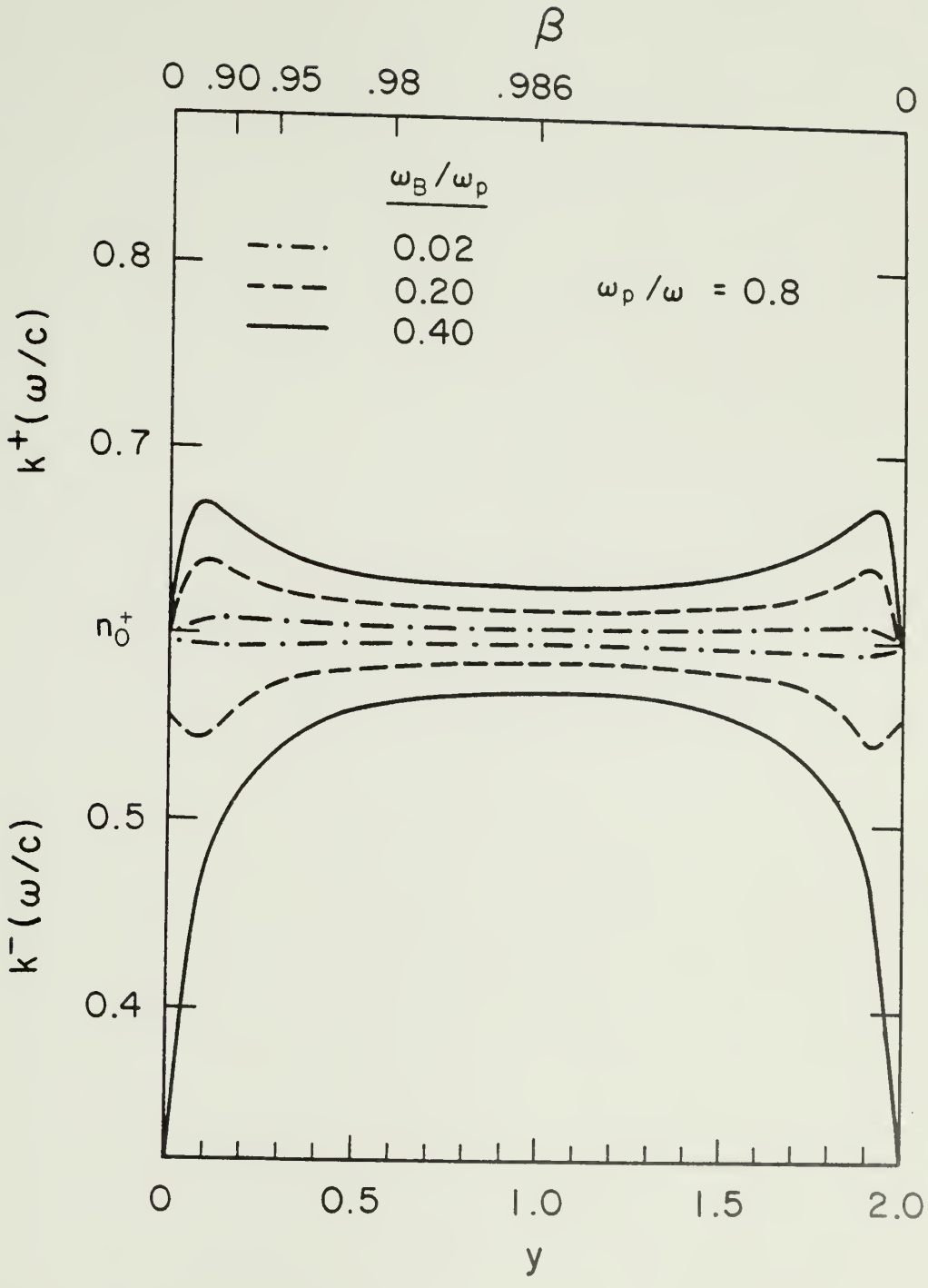
β
0 .90 .95 .98 .986 0
ω_B/ω_p
0.02
0.20
0.40
ω_p/ω = 0.8
k⁺(ω/c)
k⁻(ω/c)
n₀⁺
0.8
0.7
0.5
0.4
0 0.5 1.0 1.5 2.0
y

Figure 4-2: Plus and minus mode wave vectors versus y (and β) at normal incidence for different values of $\omega_B/\omega_p > 1$. The quantity, $\omega_p/\omega = 0.96$, is fixed.

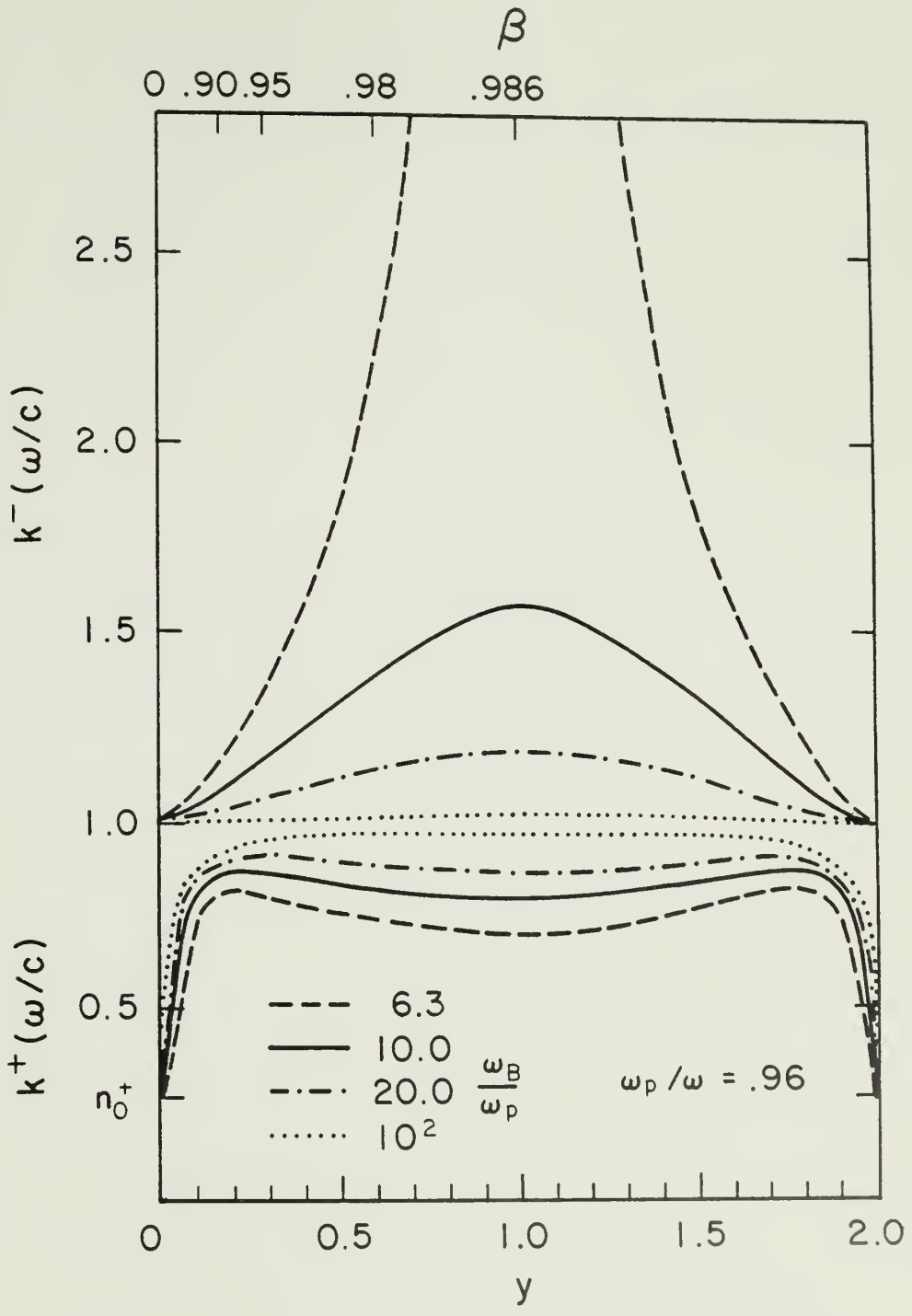
β
0 .90 .95 .98 .986
2.5
2.0
1.5
1.0
0.5
n_0^+
$k^-(\omega/c)$
$k^+(\omega/c)$
6.3
10.0
20.0
10^2
$\frac{\omega_B}{\omega_p}$
$\omega_p/\omega = .96$
0
0.5
1.0
1.5
2.0
y

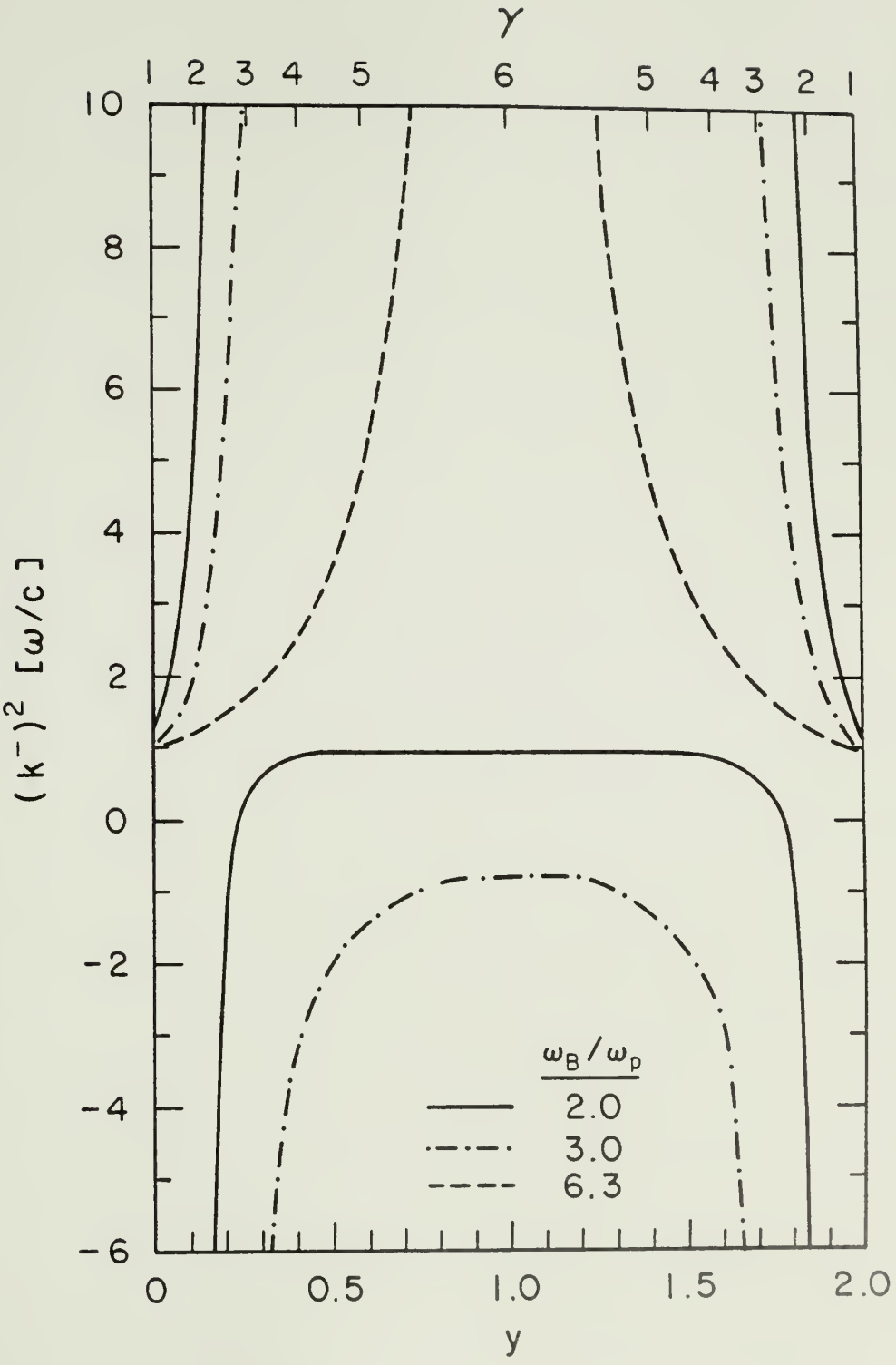
γ
1 2 3 4 5 6 5 4 3 2 1
10
8
6
4
2
0
-2
-4
-6
$(k^-)^2$ [ω/c]
0
0.5
1.0
1.5
2.0
y
ω_B/ω_p
2.0
3.0
6.3

Figure 4-4: Plus and minus mode wave vectors versus y (and β) for different angles of incidence, with $\omega_p/\omega = .96$ and $\omega_B/\omega_p = 20$. Curves are labeled with values of $k_x c/\omega$.

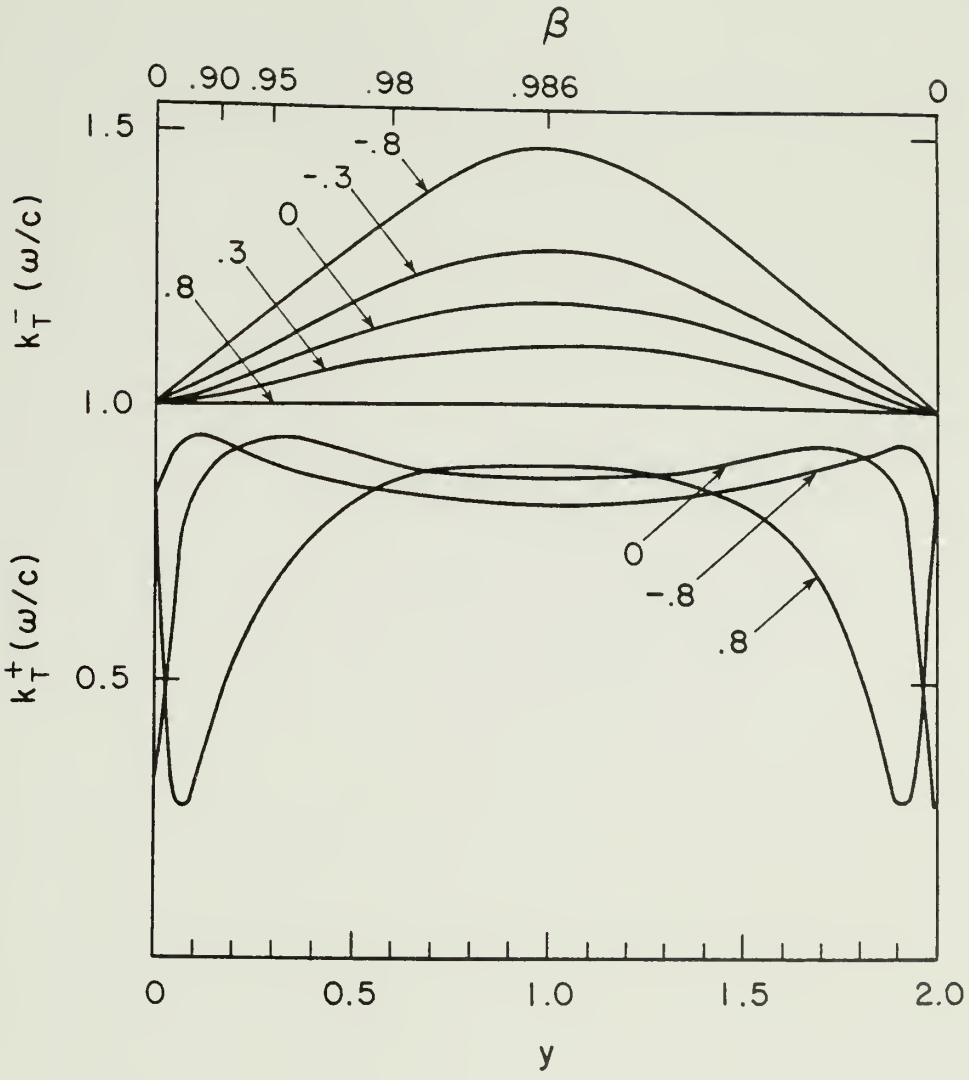
β
0 .90 .95 .98 .986 0
1.5
1.0
0.5
k_T^- (ω/c)
k_T^+ (ω/c)
-.8
-.3
0
.3
.8
0
-.8
.8
0 0.5 1.0 1.5 2.0
y

Figure 4-5: Total energy flux in upgoing plus and minus modes versus y for

$$\omega_p/c = 100$$

$$\omega_B/c = 200$$

$$\omega/c = 10^3$$

$$k_x = 0 \quad .$$

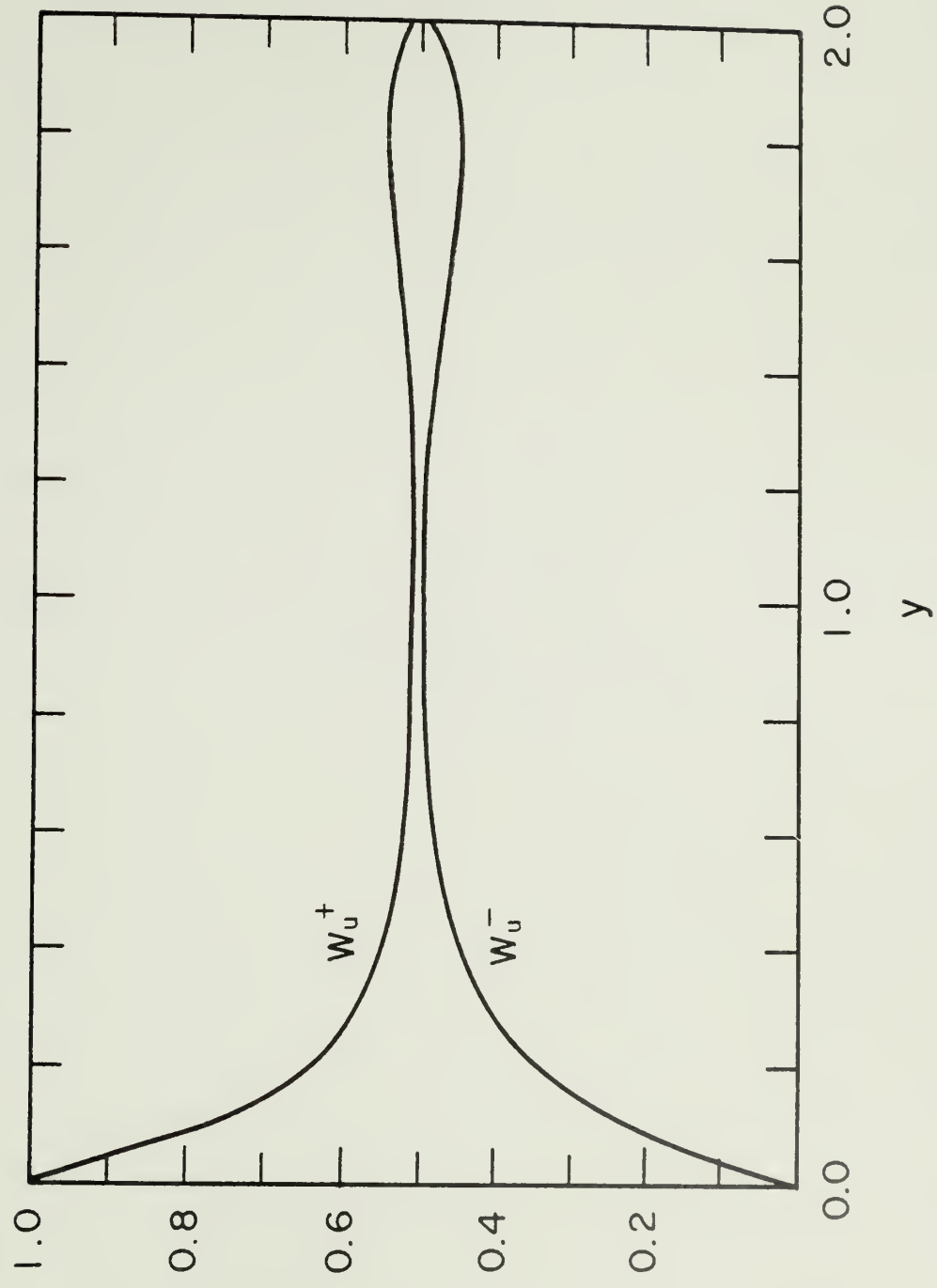
1.0
0.8
0.6
0.4
0.2
0.0
1.0
2.0
y
W_u^+
W_u^-

Figure 4-6: Total energy flux versus y for

$$\omega_p/c = 50$$

$$\omega_B/c = 10^3$$

$$\omega/c = 52$$

$$k_x = 0$$

and two initial linear polarizations:

a) E_x b) E_z .

Upgoing fluxes, $W_u^{\pm}$, are shown for each mode. Downgoing flux, W_d, is the sum of downgoing fluxes in each mode.

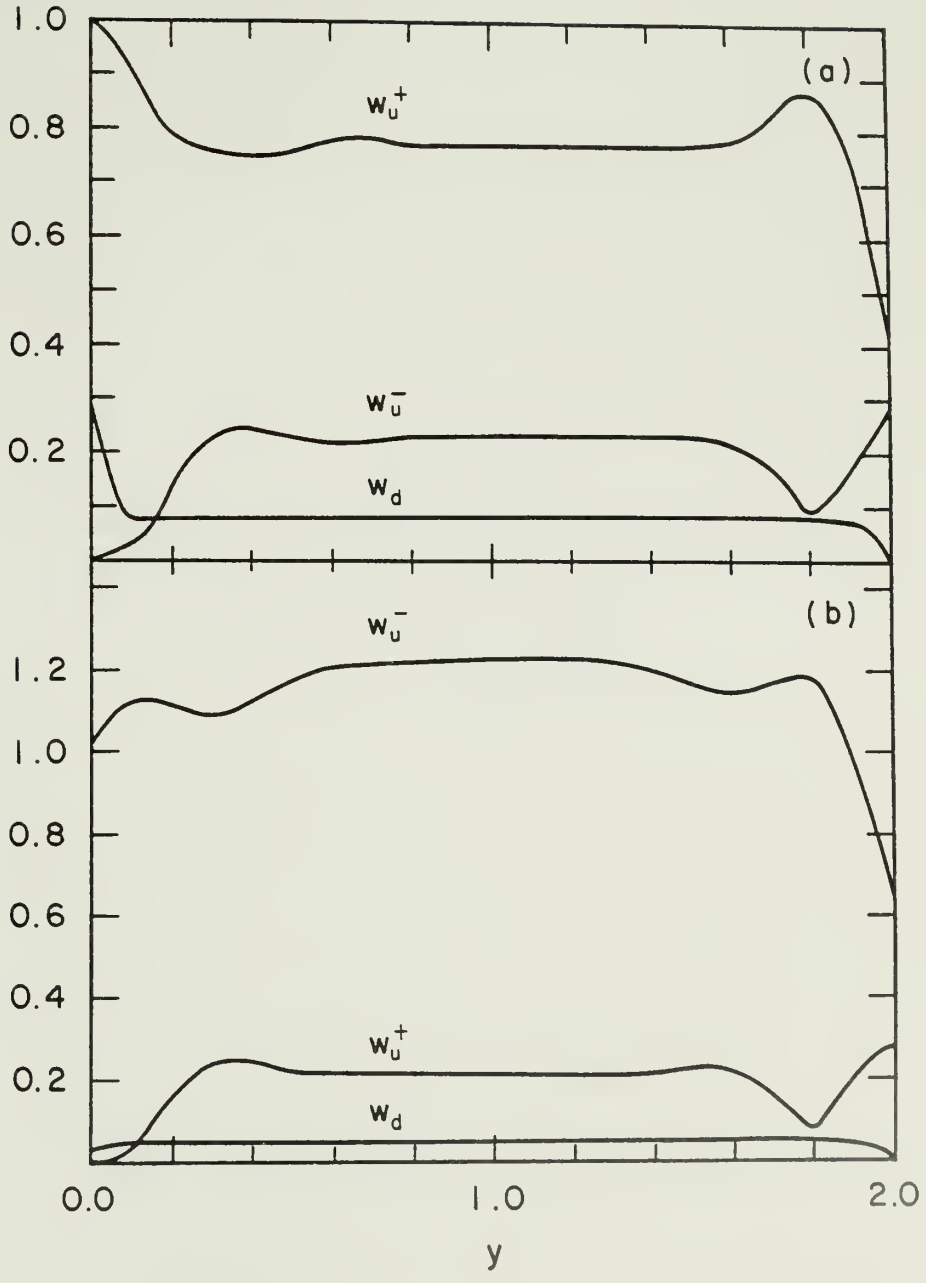
1.0
0.8
0.6
0.4
0.2
(a)
w_u^+
w_u^-
w_d
(b)
w_u^-
1.2
1.0
0.8
0.6
0.4
0.2
w_u^+
w_d
0.0
1.0
2.0
y

Figure 4-7: Circular polarization and position angle versus y for the wave of Figure 4-6a.

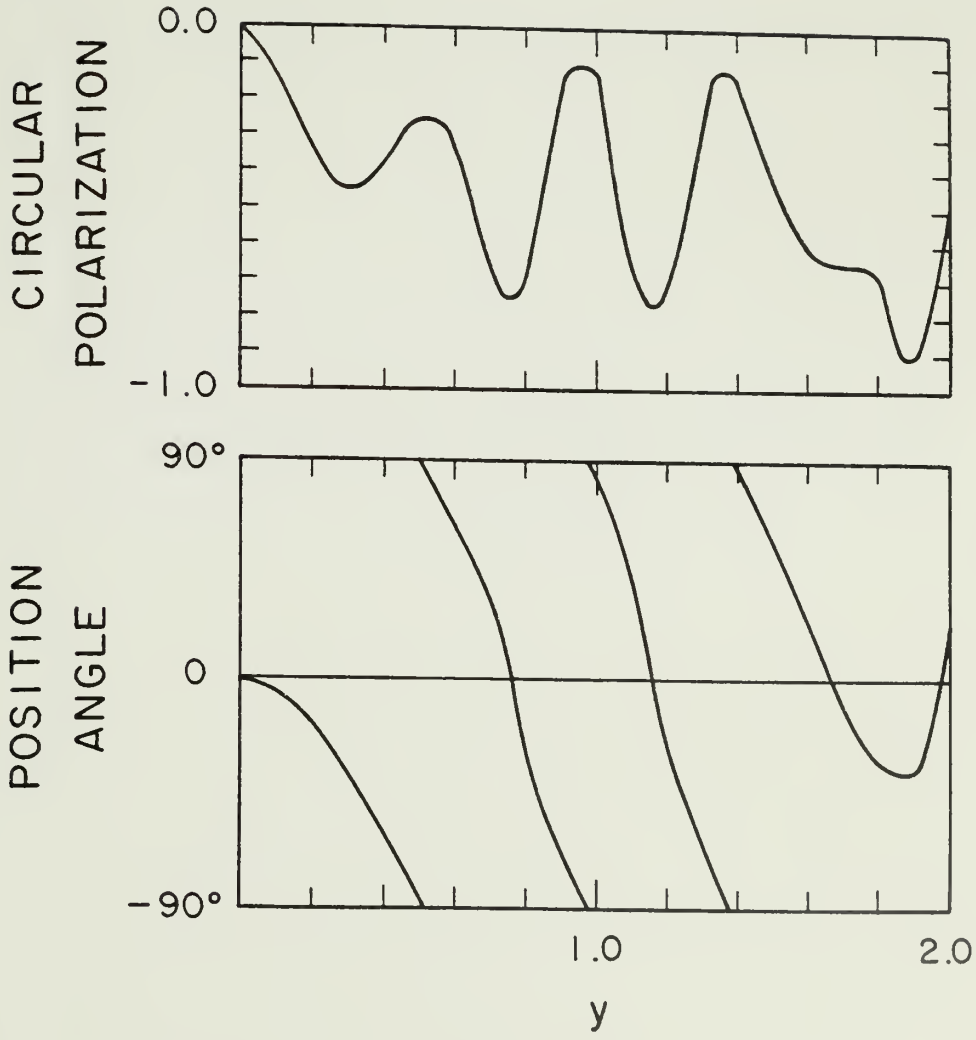
CIRCULAR POLARIZATION
0.0
-1.0
POSITION ANGLE
90°
0
-90°
1.0
2.0
y

Figure 4-8: Transmission coefficient versus frequency in the strong field regime with $\omega_p/c = 300$, $\omega_B/c = 10^4$, $k_x = 0$.

a) E_x polarization, shown in the range $\omega \sim \omega_p$.

b) E_z polarization, shown in the range $\omega \sim \omega_B$, including the upper hybrid resonance ω_1/c and the electron cyclotron cutoff ω_2/c.

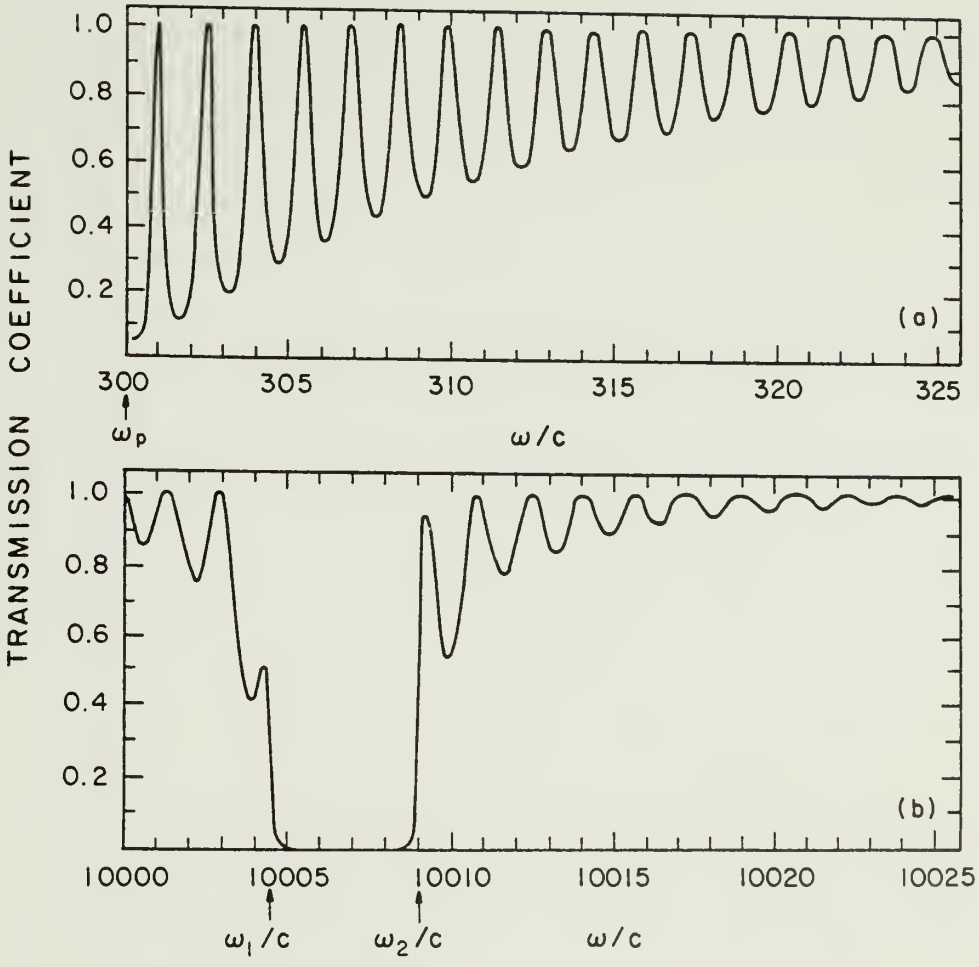
TRANSMISSION COEFFICIENT
1.0
0.8
0.6
0.4
0.2
(a)
300
305
310
315
320
325
ω_p
ω/c
1.0
0.8
0.6
0.4
0.2
(b)
10000
10005
10010
10015
10020
10025
ω_1/c
ω_2/c
ω/c

Figure 4-9: Transmission coefficient and wave polarization versus frequency in the weak field regime with $\omega_p/c = 300$, $\omega_B/c = 10$, $k_x = 0$, shown in the range above the electron cyclotron cutoff $\omega_2/c = 305$.

a) E_x polarization

b) E_z polarization

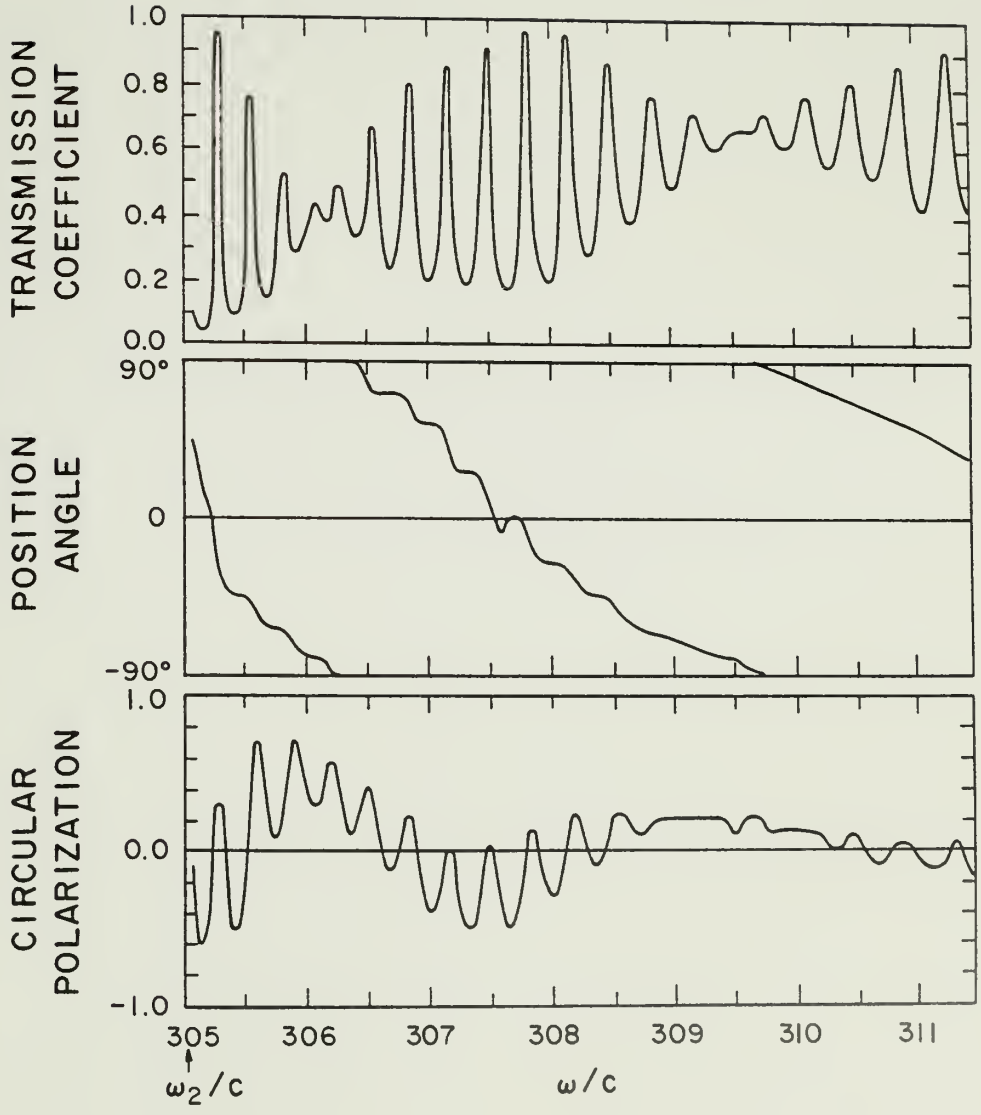
TRANSMISSION COEFFICIENT
1.0
0.8
0.6
0.4
0.2
0.0
POSITION ANGLE
90°
0
-90°
CIRCULAR POLARIZATION
1.0
0.0
-1.0
305
306
307
308
309
310
311
ω2/c
ω/c

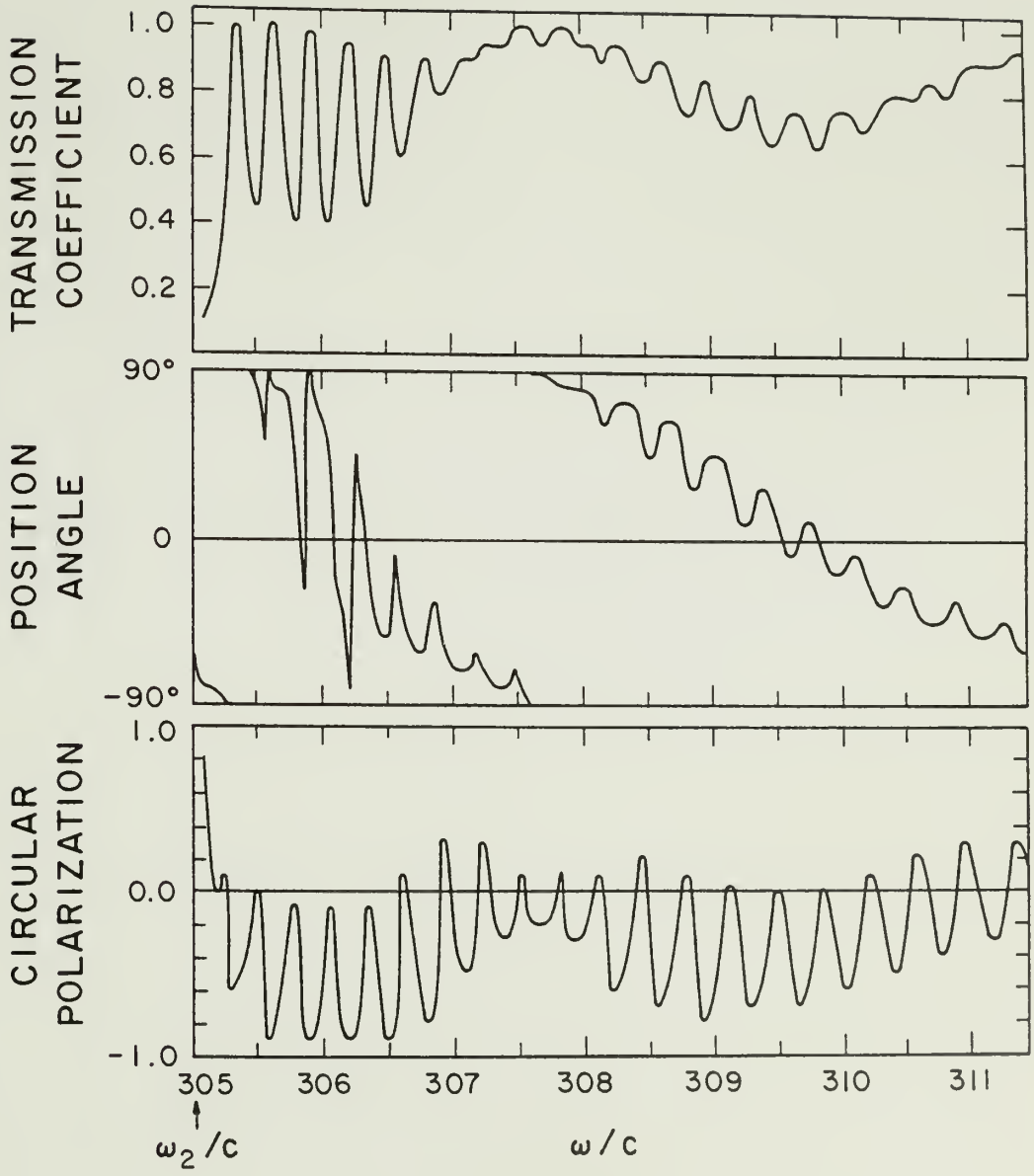
TRANSMISSION COEFFICIENT
1.0
0.8
0.6
0.4
0.2
POSITION ANGLE
90°
0
-90°
CIRCULAR POLARIZATION
1.0
0.0
-1.0
305
306
307
308
309
310
311
ω_2/c
ω/c

Figure 4-10: Schematic transmission characteristics of the E_x and E_z polarization modes with frequency for the two regimes $\omega_B/\omega_p > 1$ (top) and $\omega_B/\omega_p < 1$ (bottom). Diagonal lines indicate regions where waves do not propagate ($T = 0$), light vertical lines indicate regions where resonances appear in the transmission coefficient, and blank areas are regions where $T = 1$.

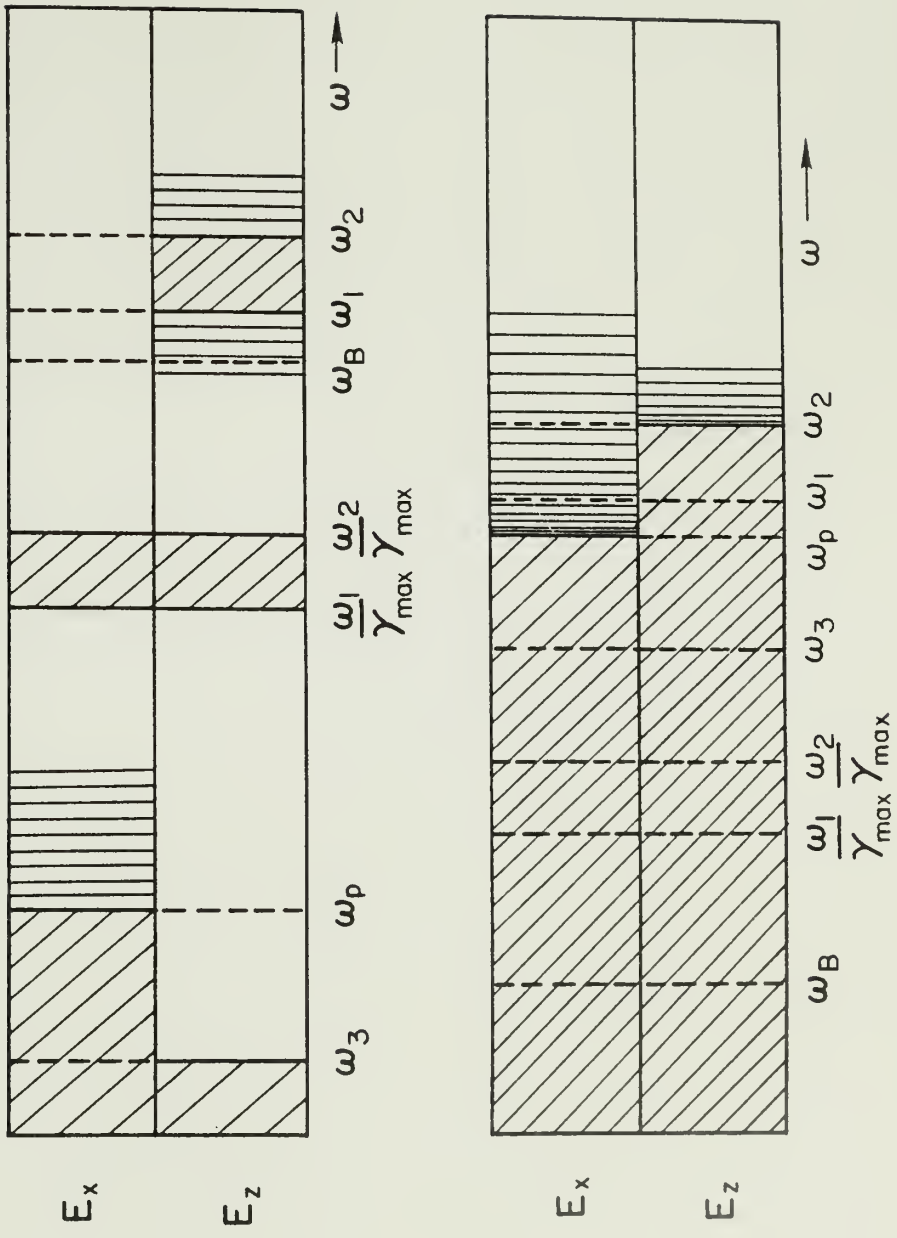
E_x
E_z
ω_3
ω_p
$\frac{\omega_1}{\gamma_{max}}$ $\frac{\omega_2}{\gamma_{max}}$
ω_B ω_1 ω_2
ω
E_x
E_z
ω_B
$\frac{\omega_1}{\gamma_{max}}$ $\frac{\omega_2}{\gamma_{max}}$
ω_3 ω_p ω_1 ω_2
ω

Figure 4-11: Transmitted pulse envelope and polarization for an incident pulse with

$$\omega_p/c = 300$$

$$\omega_B/c = 10$$

$$\omega_o/c = 308$$

$$ct_w = 0.50$$

$$k_x = 0$$

$$E_x = 0 \quad .$$

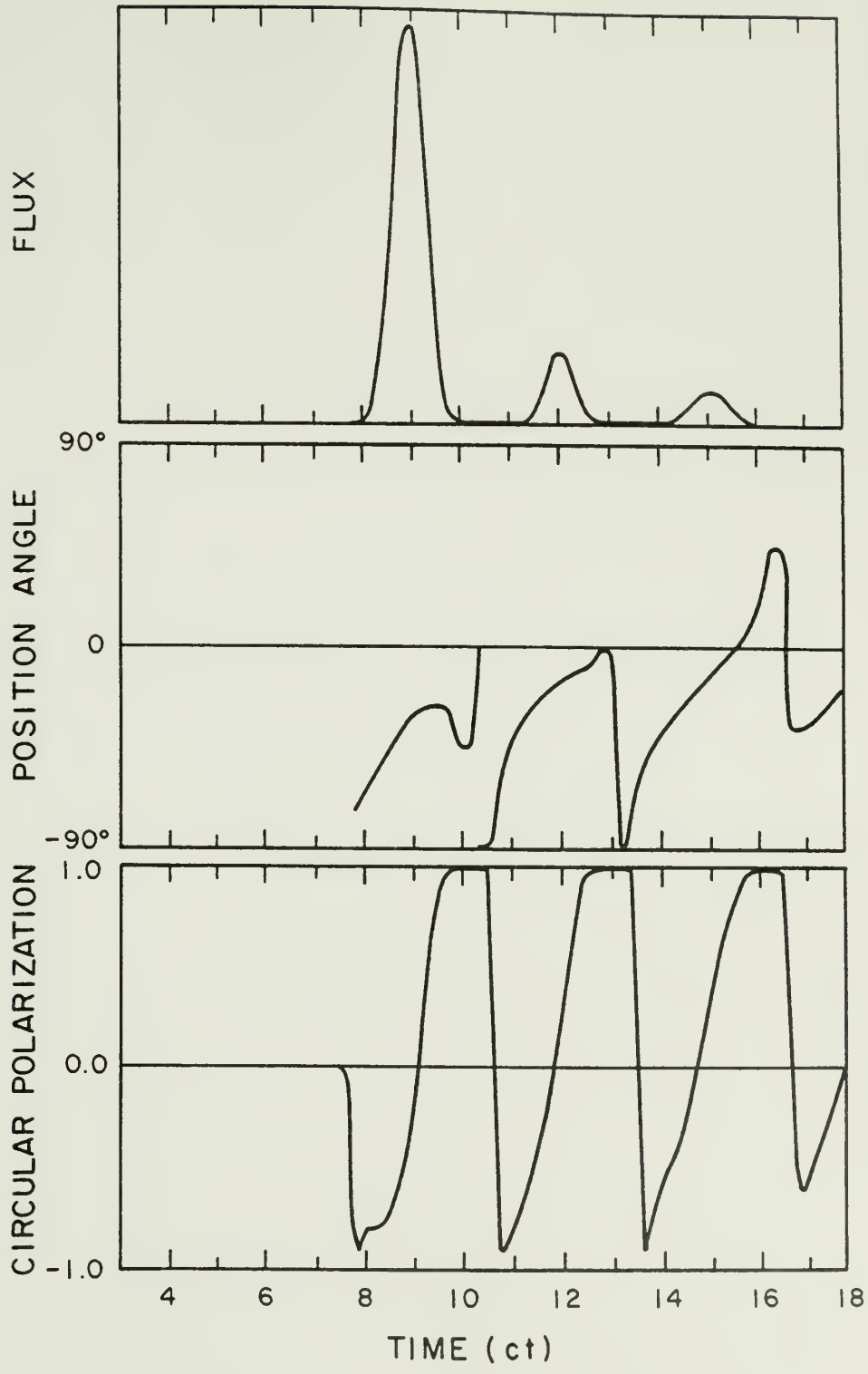
FLUX
90°
0
-90°
POSITION ANGLE
1.0
0.0
-1.0
CIRCULAR POLARIZATION
4
6
8
10
12
14
16
18
TIME (ct)

Figure 4-12: Transmitted pulse envelope and polarization for an incident pulse with

$$\omega_p/c = 300$$

$$\omega_B/c = 2000$$

$$\omega/c = 302$$

$$ct_w = 0.10$$

$$k_x = 0$$

$$E_z/E_x = 0.6 \ .$$

The 180° transition in position angle is not physical, but a consequence of the wrap-around ambiguity of the arc tangent function.

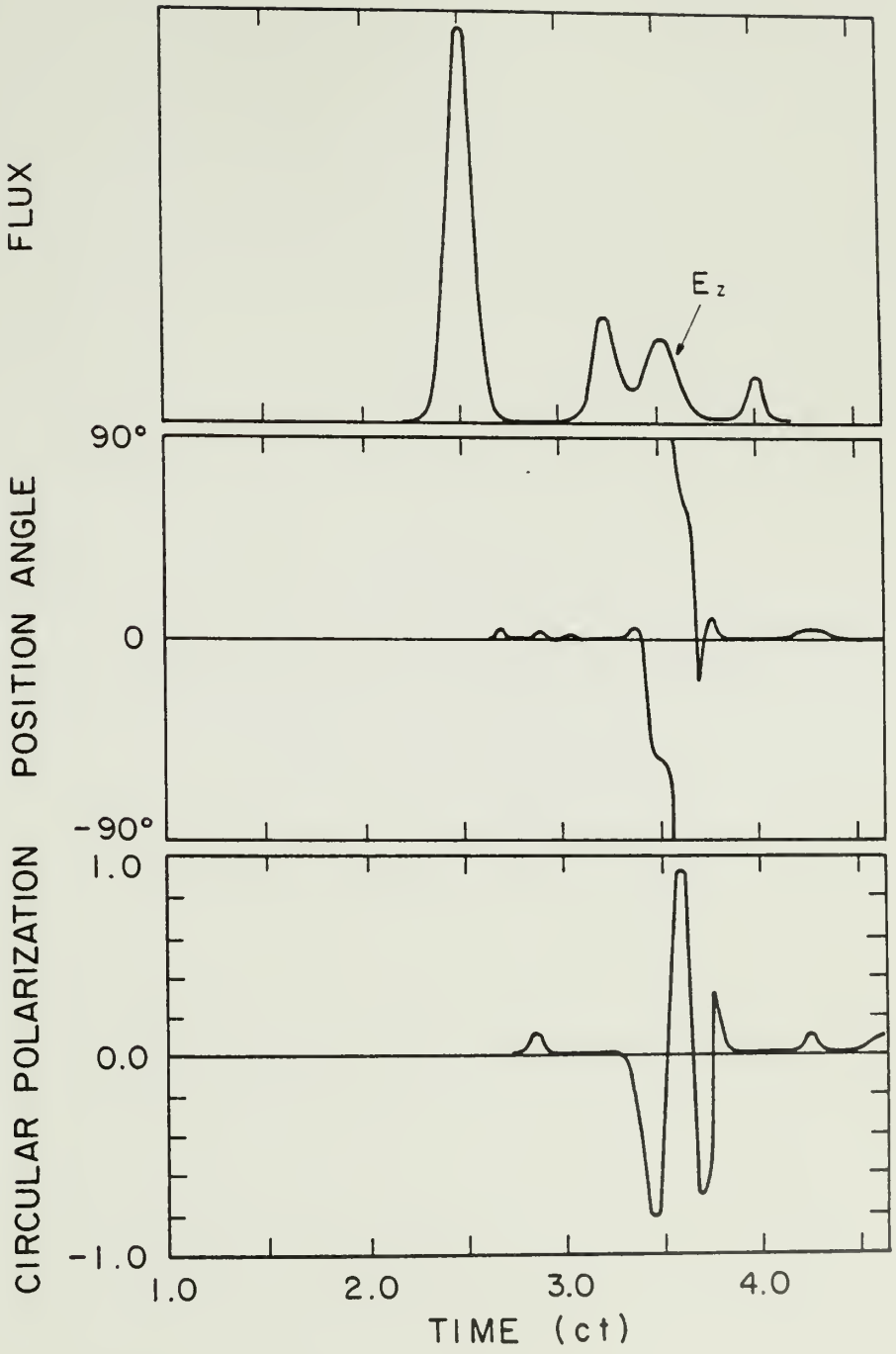
FLUX
E_z
90°
0
-90°
POSITION ANGLE
1.0
0.0
-1.0
CIRCULAR POLARIZATION
1.0
2.0
3.0
4.0
TIME (ct)

C H A P T E R V

TURBULENT SHEARING

One of the results presented in Chapter III was the condition under which the resonance effect would occur in the extraordinary mode transmission coefficient. Equation (3.17) restricted the effect to very small frequency ranges above the plasma frequency for smoothly varying velocity profiles. If the structure of the shear allowed the presence of steeper velocity gradients, then resonances could actually occur over a larger frequency range. If the shear were to become turbulent, very large gradients in velocity would be expected. We therefore consider the propagation of radiation in a turbulent shearing plasma to determine if fluid-like turbulence can produce a broadband resonance effect. The model used in these calculations is identical to that of Chapter III with the exception of the velocity profile, which is described in the first section.

1. Model of a Turbulent Velocity Field

Most turbulent flows are statistically stationary with respect to time, meaning that the velocity components at a fixed point are stationary random functions of the time (Townsend 1976). In describing turbulence mathematically, it is convenient to divide the motion into a mean flow and stochastic fluctuations about the mean. In a frame moving uniformly at the mean flow velocity, the mean of the fluctuations remains zero because kinetic energy cannot be transferred from random fluctuations to bulk motions. Rather, the energy contained in

the random motions is dissipated in the smallest eddies, so that the maintainence of a turbulent flow requires a constant energy source.

We model the turbulent velocity profile, $\beta_T(y_n)$, as the sum of two components: $\beta_o(y_n)$, a smooth, symmetric velocity field and $\beta_R(y_n)$ representing the random fluctuations around the mean flow. These velocity components are added at each level in the medium according to the relativistic velocity addition formula:

$$\beta_T(y_n) = \frac{\beta_o + \beta_R}{1 + \beta_o\beta_R} \tag{5.1}$$

Both β_o and β_R have components only in the x-direction. $\beta_R(y_n)$ can be well described as correlated Gaussian noise with zero mean and a variance indicating the degree of turbulence (Adams and Denman 1966). The spatial correlation function models the distribution of eddy sizes, with the correlation length L_o indicating the average size of the eddies in the flow. For the mean profile $\beta_o(y_n)$, we take the velocity field,

$$\beta_o(y_n) = \beta_{MAX} \cos[(y-1)\,\pi/2] \tag{5.2}$$

The fluctuations $\beta_R(y_n)$ in each realization are determined by generating 512 random numbers with a rectangular distribution between 0 and 1. This distribution is converted to a normal distribution with zero mean and variance σ_v, having the probability function[1]

---

[1]For more details on the conversion of rectangular probability distributions to normal distributions, see Adams and Denman 1966 or Box and Muller 1958.

$$P[\beta_R(y_n),\ \beta_R(y_{n+1})] = \frac{1}{2\pi} \exp[-(\beta_R(y_n)/2\sigma_v)^2] \times$$

$$\exp[-(\beta_R(y_{n+1})/2\sigma_v)^2] \qquad (5.3)$$

The choice of a Gaussian distribution for β_R unfortunately allows the possibility of $|\beta_R| \geq 1$, in violation of special relativity. In the calculations that follow, σ_v is small enough to give a negligible probability of this happening. Nevertheless, we must cut off the distribution by checking the value of each β_R calculated and discarding those with $|\beta_R| \geq 1$. Since the number of layers, $N = 500$, and 512 values of β_R are calculated for each realization, the small number of violations does not exceed this difference. We then correlate this noise over a scale length L_o by convolving the series of numbers with a spatial correlation function,

$$\Phi(y) = \exp[-\pi y^2/L_o^2] \quad . \qquad (5.4)$$

Finally, we set $\beta_R(y_N) = \beta_R(0) = 0$ so that the velocity is zero at the boundaries of the medium. Three parameters then determine the turbulent velocity field: β_{MAX} is the maximum of the mean profile, σ_v is the standard deviation of the turbulent velocity from the mean velocity, and L_o is the mean length over which the motions of the medium are correlated.

2. Broadband Propagation Effects

Having specified the form for the turbulent motion of the medium, we now examine the effect of this motion on the X mode transmission coefficient at normal incidence over a broad range of frequencies. In Figures 5-1, 5-2 and 5-3 the transmission coefficient is plotted as a function of frequency for turbulent media having $\omega_p/c = 300$. The

velocity fields are realizations of motions having an increasing degree of turbulence, as determined by the parameters σ_v and L_o. Figure 5-1 shows $T(\omega)$ vs. ω/c for the limiting case of no turbulence ($\sigma_v = 0$) and for a small degree of turbulence ($\sigma_v = .02$), both cases having $\beta_{MAX} = 0.9$. With no turbulence, the resonances are weak and die out very quickly due to the small gradients of the smooth velocity profile, $\beta_o(y_n)$. With some turbulence present, however, the resonances are stronger just above ω_p and persist out to higher frequencies. In Figure 5-2, with an increased degree of turbulence and a decreased correlation length, strong resonances are present at even higher frequencies. Unlike the strictly periodic resonances in Figure 3-1, these are quasi-periodic and much more irregular. Furthermore, there seems to be a modulation in the strength of the resonances which occurs over different frequency intervals. Over a given band of frequencies, there is also a variation in resonance strength and spacing from one realization to another. The <u>average</u> resonance spacing, though, increases with frequency approximately according to equation (3.15), with the peaks generally becoming broader and weaker.

Multiple reflections are similarly responsible for the resonance behavior of waves in the turbulent medium but there are now gradients in velocity appearing at random locations. The gradients tend to be largest at the edges of the shearing region, where β_o is increasing or decreasing fastest and where the relative degree of turbulence, σ_v/β_o is greatest. Consequently, these are the dominant reflection producing gradients, but their exact location and strength are variable in time. For a particular frequency, therefore, a spectrum of resonance spacings is possible with

$$\frac{\pi n_o}{y_N} \lesssim \frac{\Delta\omega}{c} \lesssim \frac{\pi n_o}{L_o}$$

The smallest spacings are most probable, since the gradients at $y = 0$ and $y = y_N$ are largest. The largest possible spacing would result from multiple reflections occurring within the smallest turbulent cell whose size is roughly L_o.

Increasing the degree of turbulence while decreasing the correlation length results in larger and larger resonance bandwidths, i.e. the frequency range above ω_p over which resonance behavior is present. Figure 5-3 shows $T(\omega)$ for a highly turbulent medium, illustrating the strong resonances which can occur at frequencies twice the plasma frequency. The dominant spacing in this bandwidth is close to the asymptotic value π/y_N, since $n_o \sim 1$, and is effectively frequency independent.

A high degree of turbulence is not necessary to produce a large resonance bandwidth if the turbulence exists on a scale comparable to or smaller than the wavelength of the radiation. We have investigated different combinations of σ_v and L_o and the "empirical" results are shown in Figure 5-4. The frequency at which resonances disappear, ω_{MAX} ($T = 1$ for $\omega > \omega_{MAX}$), is plotted against the degree of turbulence for different values of L_o. The resonance bandwidth, $(\omega_{MAX} - \omega_p)$, increases monotonically with increasing σ_v and also with decreasing L_o. Although our spatial resolution Δy prevents us from considering smaller values of L_o, it is clear that large bandwidths are possible for moderate degrees of turbulence by choosing a small enough correlation length. In fact, ω_{MAX} increases more rapidly for decreasing L_o than for increasing σ_v.

We can estimate the size of the velocity gradients which are present for given values of L_o and σ_v:

$$\frac{d\gamma}{dy} = \frac{d\gamma}{d\beta}\frac{d\beta}{dy} = \frac{d\beta}{dy}\frac{\beta}{(1-\beta^2)^{3/2}} \sim \frac{\sigma_v}{L_o}\beta\gamma^3 \tag{5.5}$$

If we substitute this expression for $d\gamma/dy$ into equation (3.17), we have

$$\left(\frac{\sigma_v}{L_o}\right)^{2/3}\beta^{2/3}\gamma^2 \gtrsim \left(\frac{\omega^2}{c^2}\gamma^2 - \frac{\omega_p^2}{c^2}\right)\left(\frac{c}{\omega_p}\right)^{4/3} \tag{5.6}$$

If $\gamma \sim 1$, then a rough equality should hold for $\omega = \omega_{MAX}$:

$$\left(\frac{\omega_{MAX}}{c} - \frac{\omega_p}{c}\right) \sim \left(\frac{\sigma_v}{L_o}\right)^{2/3}\beta^{2/3}\left(\frac{\omega_p}{c}\right)^{1/3} \tag{5.7}$$

The curves in Figure 5-4 for ω_{MAX}/c vs. σ_v do have this predicted dependence, so that the resonance behavior in these turbulent media must result from reflections at velocity gradients as described by equations (3.17) and (5.5). In all of the calculations described thus far, $\gamma < 10$, so that equation (5.7) should give a reasonably good representation of the dependence of bandwidth on turbulence parameters. If $\gamma >> 1$, equation (5.6) gives approximately,

$$\frac{\omega_{MAX}}{\omega_p} \sim \left(\frac{\sigma_v}{L_o}\right)^{1/3}\left(\frac{c}{\omega_p}\right)^{1/3} . \tag{5.8}$$

This would seem to indicate that for highly relativistic shear flows, larger degrees of turbulence are required to produce the same bandwidths.

The propagation of pulses in a turbulent shearing plasma also shows broadband effects, as might be expected from the behavior of the

transmission coefficient. Figure 5-5 shows transmitted pulse envelopes for three realizations of turbulent shearing (the transmission coefficient for the first realization was plotted in Figure 5-2). Also shown are the normalized autocorrelation functions (acf) for each pulse, defined by

$$r(\tau) = \frac{\sum_j S(y = 2, t_j)\, S(y = 2, \tau - t_j)}{\sum_j S(y = 2, t_j)^2} \tag{5.9}$$

where $S(y = 2, t_j)$ is the Poynting vector for the transmitted radiation. There are several noticeable differences in the transmitted pulses when turbulence is present in the medium. First of all, this high a frequency would show no obvious propagation effects in the turbulence free model. Second, only one periodicity would be present, while the pulses in Figure 5-5 exhibit periodicities smaller than the predicted $cP = y_N/\pi n_o = 1.08$. This is due to the different resonance spacings which are present in the frequency spectrum of the pulses. Third, a variation in the periodicities from one pulse to the next is evident, especially in the acfs. The first break in each acf indicates the component width and the bumps indicate periodicities or harmonics of periodicities. If an average acf were computed for many realizations of this degree of turbulence, these features would tend to weaken because of the variation of period from one realization to another.

All results discussed so far in this chapter have involved the effects of turbulence in the field-free plasma model. We now consider briefly the effects of turbulence in the model of Chapter IV which includes a magnetic field. Figure 5-6 shows the intensity and polariza-

tion of a pulse transmitted through a turbulent shearing magneto-plasma. The parameters are the same as those of Figure 4-11 except for the velocity field. This particular realization has more closely spaced quasi-periodic peaks, although there is a suggestion of a larger period equal to the one in Figure 4-11. Comparing the polarization of the pulse in each figure, the fluctuations in position angle and circular polarization in Figure 5-6 are much more irregular, though still correlated with the intensity fluctuations. The presence of more than two gradients in the turbulent medium serves to randomize the polarization state of the transmitted radiation, when it results from the combination of Faraday rotation, phase delays and birefringence due to shearing described in §IV 2. In addition, the polarization state seems to be more constant through each pulse component and this is also the case for other realizations.

We have shown that the propagation effects found in Chapter III can be present over relatively large frequency ranges, provided that a physical mechanism is available to produce steep velocity gradients in the shearing medium. The effects appear both in the frequency dependence of the transmission coefficient and in the transmitted pulse structure. We see that the presence of a stochastic process introduces an irregularity and unpredictability into the structure of the transmitted radiation. In the case of a turbulent medium, the propagation process itself becomes unpredictable. We will discuss the possibility of turbulent shearing in pulsar magnetospheres in Chapter VII.

Figure 5-1: Transmission coefficient versus frequency for a turbulent shearing plasma with

$$\omega_p/c = 300$$

$$\beta_{MAX} = 0.9$$

$$\sigma_v = .02$$

$$L_o = .01$$

The limiting case $\sigma_v = 0$ is shown for comparison.

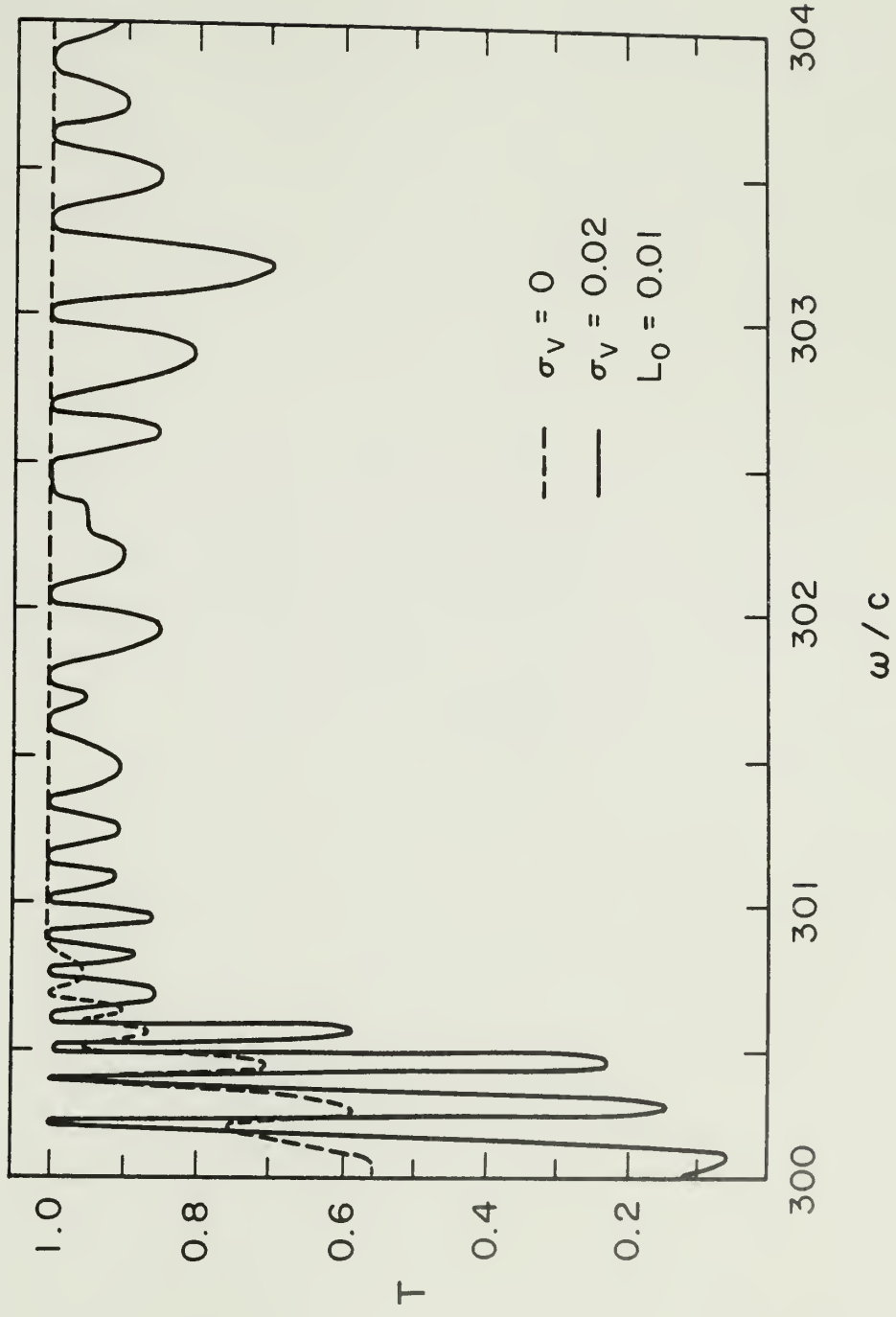
1.0
0.8
0.6
0.4
0.2
T
300
301
302
303
304
ω / c
σv = 0
σv = 0.02
L0 = 0.01

Figure 5-2: Transmission coefficient versus frequency for a turbulent shearing plasma with

$$\omega_p/c = 300$$

$$\beta_{MAX} = 0.8$$

$$\sigma_v = 0.1$$

$$L_o = .005$$

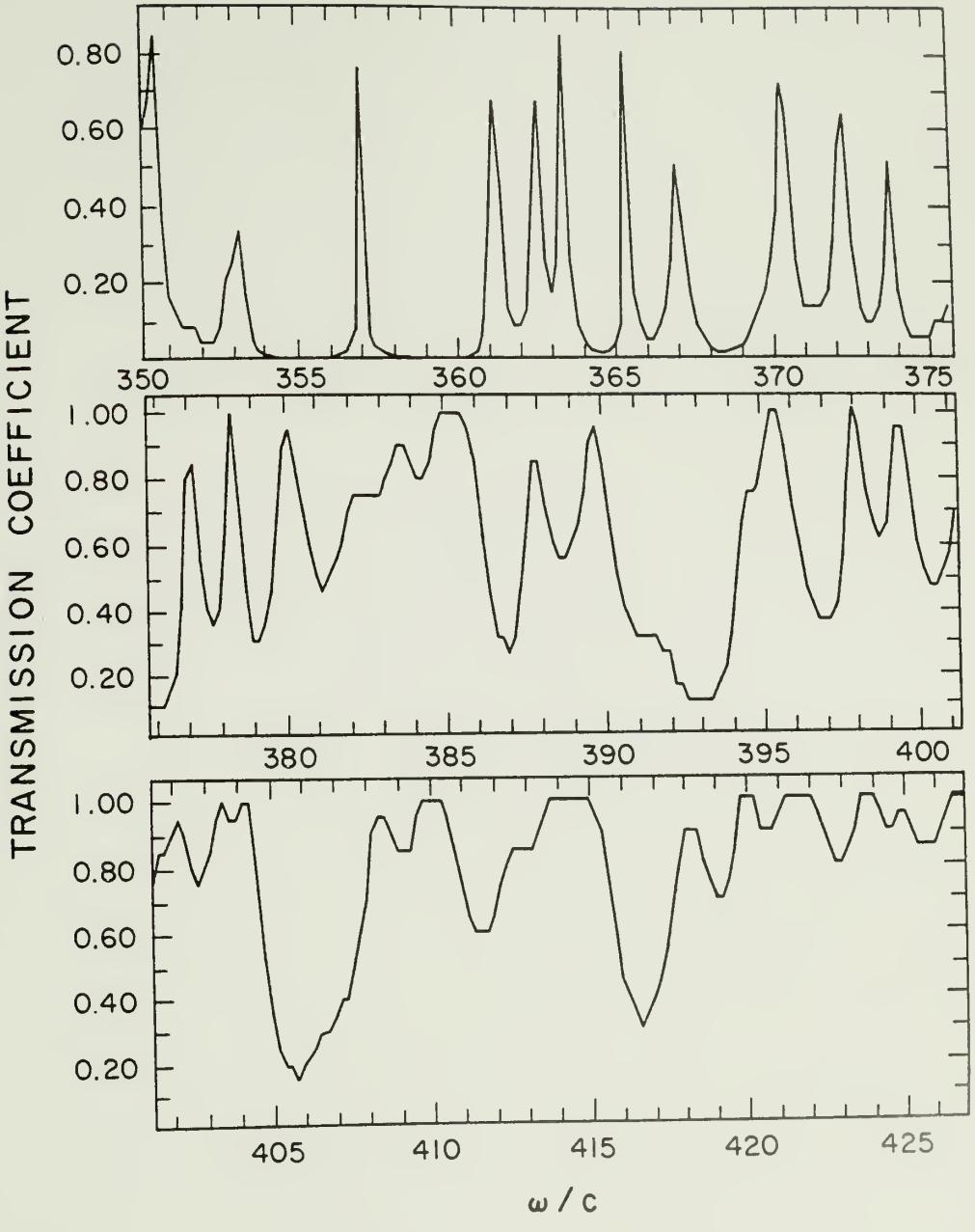
TRANSMISSION COEFFICIENT
0.80
0.60
0.40
0.20
350
355
360
365
370
375
1.00
0.80
0.60
0.40
0.20
380
385
390
395
400
1.00
0.80
0.60
0.40
0.20
405
410
415
420
425
ω / c

Figure 5-3: Transmission coefficient versus frequency for a turbulent shearing plasma with

$$\omega_p/c = 300$$

$$\beta_{MAX} = 0.99$$

$$\sigma_v = 0.3$$

$$L_o = .002$$

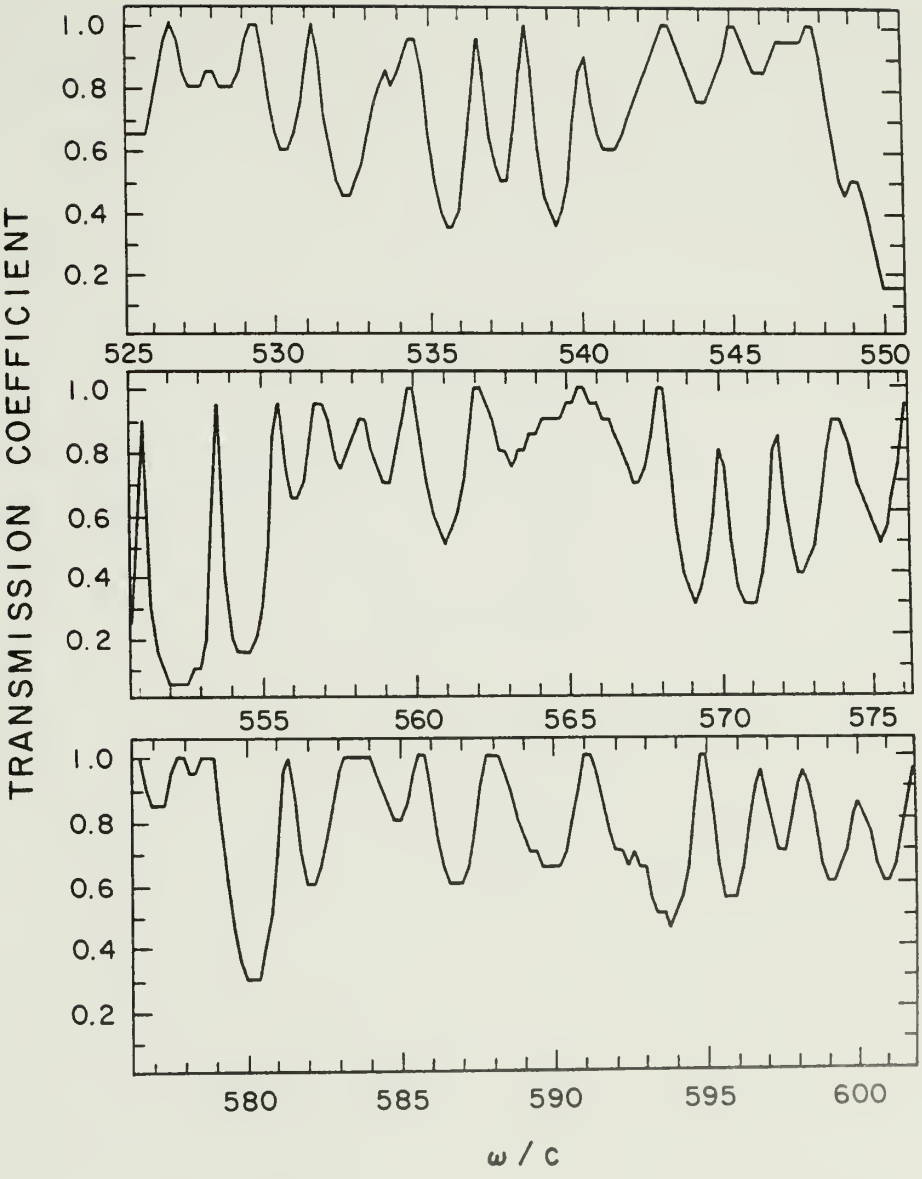
TRANSMISSION COEFFICIENT
1.0
0.8
0.6
0.4
0.2
525
530
535
540
545
550
555
560
565
570
575
580
585
590
595
600
ω / c

Figure 5-4: Resonance bandwidth versus degree of turbulence for different values of the correlation length, L_o, and $\omega_p/c = 300$. The curves are insensitive to the value of β_{MAX} for the range of parameters studied.

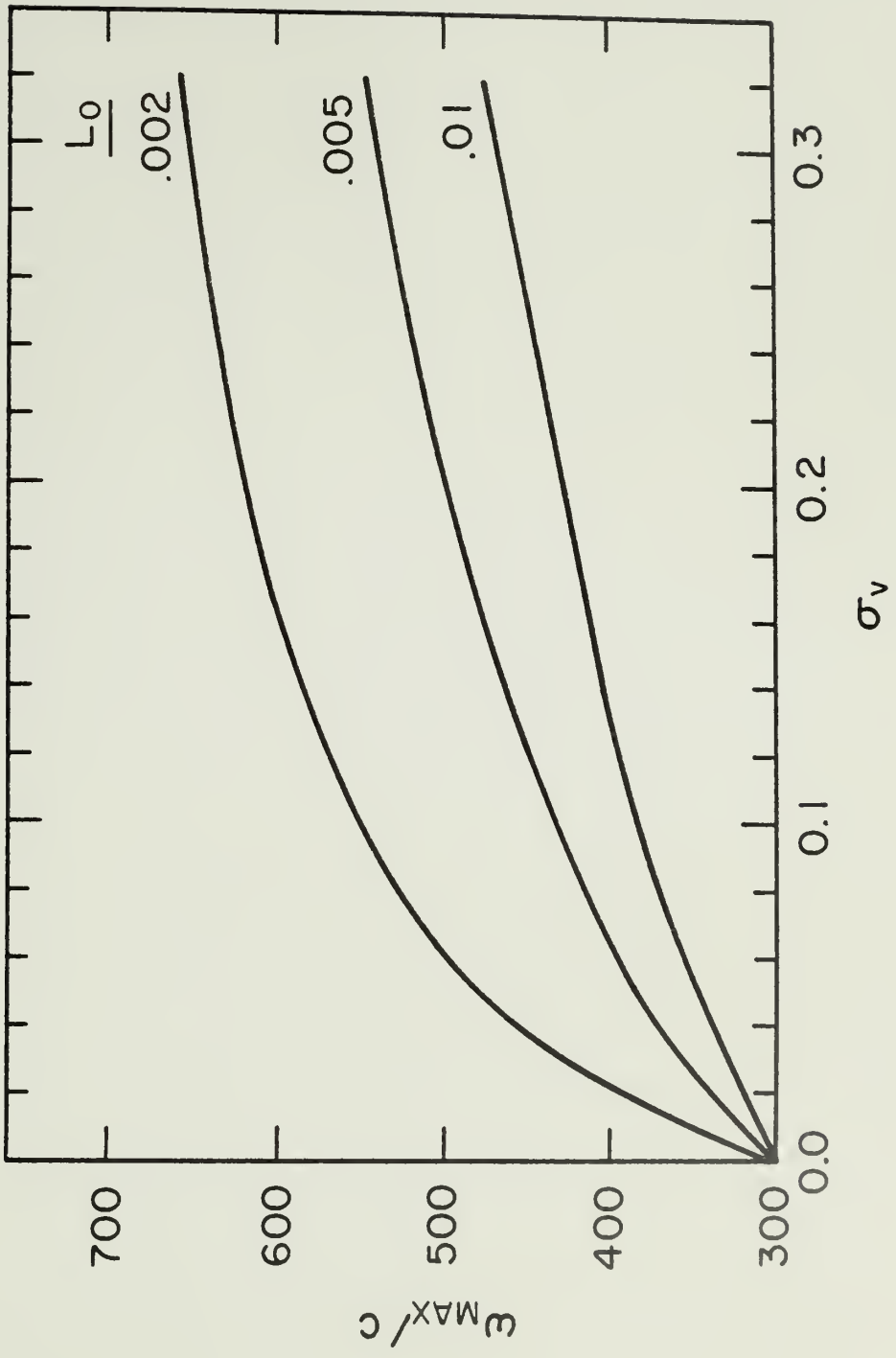
700
600
500
400
300
ε_{MAX}/c
0.0
0.1
0.2
0.3
σ_v
$\frac{L_0}{}$
.002
.005
.01

Figure 5-5: Transmitted pulses and their autocorrelation functions for three realizations of a turbulent shearing plasma with

$\omega_p/c = 300$ $\beta_{MAX} = 0.8$

$\omega_B/c = 0$ $\sigma_v = 0.1$

$\omega_o/c = 372$ $L_o = .005$

$ct_w = 0.05$

Fluxes are normalized to the peak flux of the incident pulse.

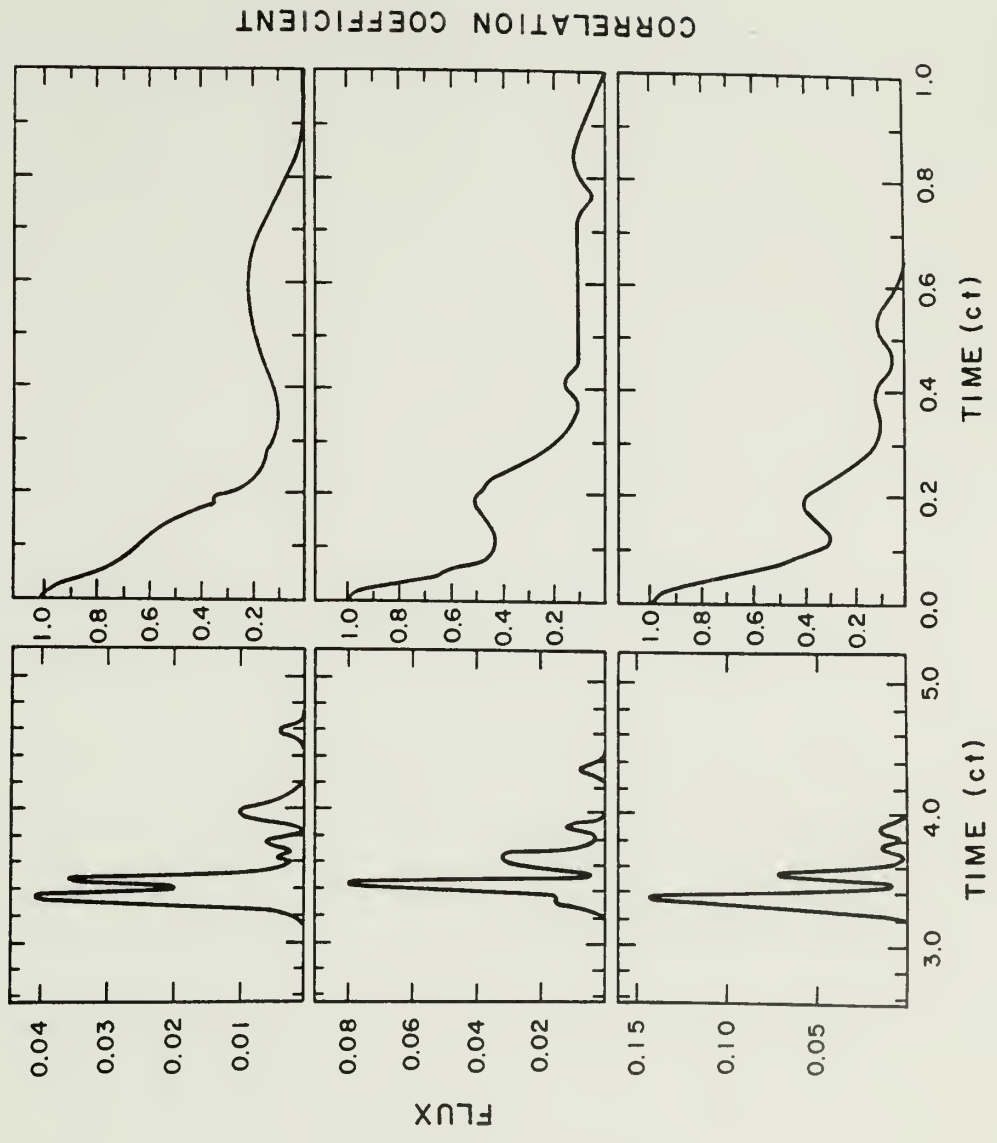
CORRELATION COEFFICIENT
FLUX
TIME (ct)
TIME (ct)

Figure 5-6: Transmitted pulse and polarization for a turbulent shearing magneto-plasma with

$\omega_p/c = 300$ $\quad\quad$ $\beta_{MAX} = 0.8$

$\omega_B/c = 10$ $\quad\quad$ $\sigma_v = 0.3$

$\omega_o/c = 308$ $\quad\quad$ $L_o = .02$

$ct_w = 0.5$

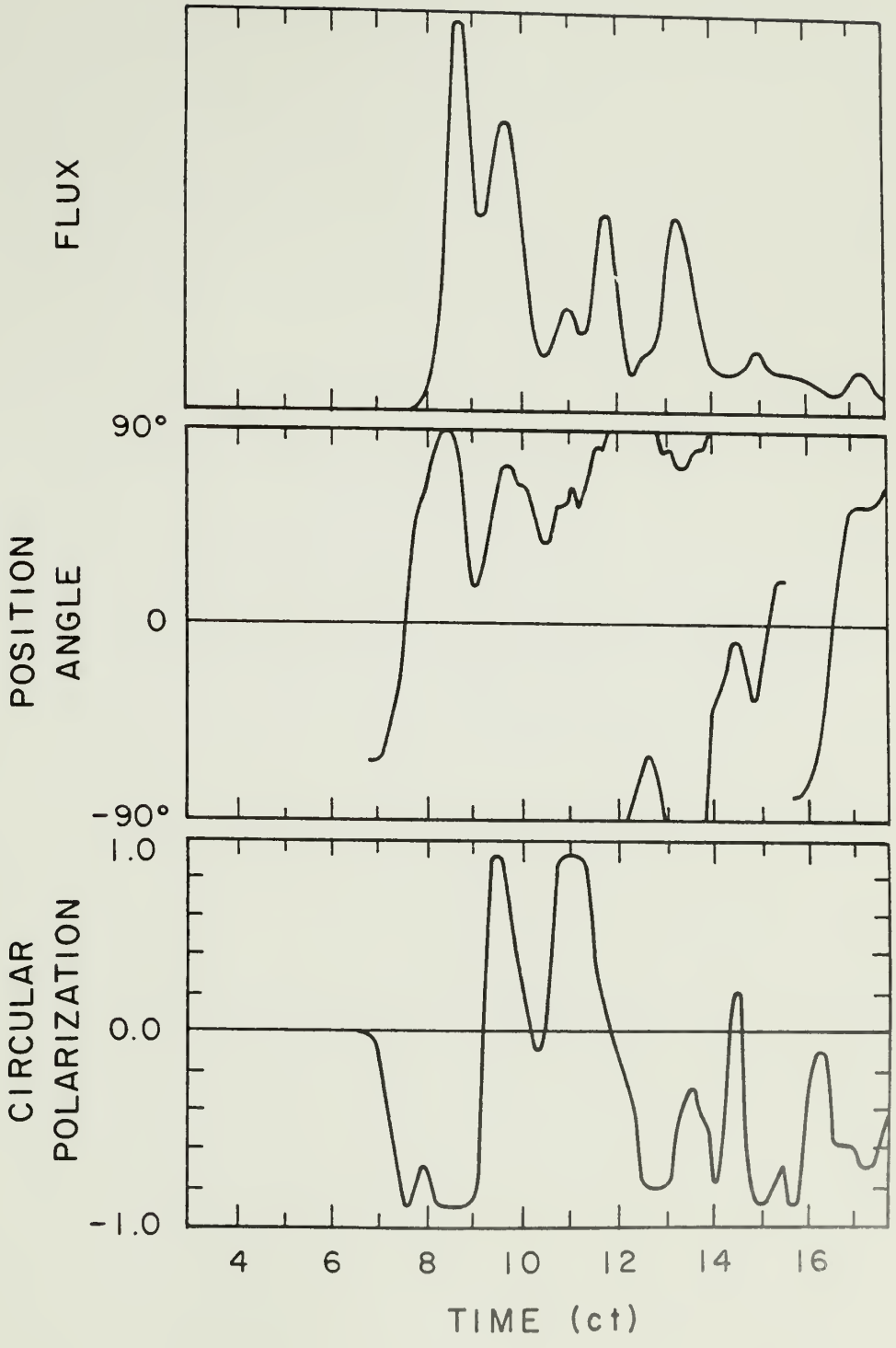
FLUX
90°
POSITION ANGLE
0
-90°
1.0
CIRCULAR POLARIZATION
0.0
-1.0
4
6
8
10
12
14
16
TIME (ct)

CHAPTER VI

AMPLITUDE MODULATED NOISE

In the previous chapters, we have considered a highly simplified form for the radiation incident on the shearing region: a Gaussian modulated plane wave. Pulsar radiation seems to be best described as a stochastic process, producing noisy signals very unlike modulated plane waves. As a more physically realistic model of the emitted pulsar signal, we consider Gaussian modulated shot noise as the incident pulse and investigate its propagation properties.

In this model, the frequency components of the pulse have random phases and modulated random amplitudes. The electric field of the pulse now takes the form

$$E_z(0,t) = E_o \exp(-t^2/t_w^2) n(t) \tag{6.1}$$

where n(t) is complex shot noise with a band limited spectrum:

$$n(t) = \sum_j c(t_j)\, h(t-t_j)\, e^{-i\omega_o t} \tag{6.2}$$

The function h(t) is the shape of the shot pulses and determines the spectrum of the noise. Each $c(t_j)$ is a random number giving the amplitude of a shot pulse. We determine n(t) for each incident pulse by generating a series of random numbers for $\tilde{c}(\omega_j)$ between -1 and +1 in frequency space, $\tilde{c}(\omega_j)$ being the Fourier transform of $c(t_j)$. The spectrum is then band limited with the function

$$\tilde{h}(\omega) = \begin{cases} 1 & \omega_o - \frac{\omega_N}{2} \leq \omega \leq \omega_o + \frac{\omega_N}{2} \\ 0 & \text{otherwise} \end{cases}$$

which is the Fourier transform of h(t). The product of $\tilde{h}(\omega)$ and $\tilde{c}(\omega)$,

$$\tilde{n}(\omega) = \tilde{h}(\omega)\ \tilde{c}(\omega)$$

is then the Fourier transform of n(t). The noise spectrum, $\tilde{n}(\omega)$, has a bandwidth ω_N centered on frequency ω_o. By virtue of having a unique series of random numbers, each incident pulse is a different realization of the random process which generates the amplitudes and phases contained in $c(t_j)$.

We investigate the propagation of this type of modulated noise through the shearing field-free plasma described in Chapter III. To determine the structural characteristics of the transmitted pulses, we study both the variation in appearance and the average statistical properties of many realizations. Single realizations of transmitted pulses are smoothed, simulating a lower time resolution in order to show up large scale features which would otherwise be washed out by the noise. The pulse is smoothed over a certain time scale by convolving it with a rectangle function of that width. The effective time resolution is then equal to the width of the smoothing function. The average statistical properties of the transmitted pulse realizations can be obtained from the average autocorrelation function (acf) of the intensity. This is computed by summing the individual, normalized acfs (defined by equation [5.9]) of many unsmoothed pulses.

We first consider the propagation of normally incident X mode pulses of narrow band noise with $\omega_N << \omega_o$ and $\omega_o \sim \omega_p$. Figure 6-1 shows smoothed transmitted pulses for several different realizations of n(t). The details of each realization are quite different, showing a much more irreg-

ular structure than the transmitted pulses in the modulated plane wave model. Figure 6-1a clearly shows peaks similar to the corresponding plane wave case in Figure 3-4 and with the same period, while in other realizations this structure is not so apparent. The noisiness of the incident radiation seems to cause a variation in the appearance of different transmitted pulses. The average acf of 30 realizations, plotted in Figure 6-2, indicates that in spite of these variations, a common time structure is present. The feature at zero lag is the decorrelation time of the noise, equal to the inverse of the noise bandwidth, ω_N. If the transmitted pulse were made up of pure noise, this would be the only feature and the acf would be flat at all other lags. Other features that appear in Figure 6-2 suggest that the same propagation effects are present in every realization. The shoulder on the zero lag spike indicates the width of the peaks and the enhancements at roughly equal intervals indicate a fundamental period and harmonics. Average acfs computed for independent sets of the same number of realizations are almost identical.

The effect of broadband noise with $\omega_N \lesssim \omega_o$ on the pulse propagation characteristics is next considered. When $\omega_o \sim \omega_p$, the pulse is dispersed so severely that any time structure is smeared out and hence undetectable. At frequencies higher above the plasma frequency, there is much less dispersion, but the propagation effects due to the shearing are no longer strong enough to change the pulse structure according to the model of Chapter III. We therefore study the propagation of a broadband noise pulse in the turbulent shearing model of Chapter V, where propagation effects may be seen high above the plasma frequency.

Figure 6-3 shows the results of calculations for two noise realiza-

tions with the first two turbulent velocity profiles of Figure 5-5. There are now two independent random processes determining the structure of the transmitted pulse and, consequently, the variations from one realization to another are more extreme. The noise-like radiation can change the relative amplitudes of the peaks in the transmitted pulse although the dominant period of each realization is determined by the turbulence structure. This is verified by comparing the individual acfs of identical realizations with (Figure 6-3) and without (Figure 5-5) noise.

Another effect of the noise, in particular broadband noise, is to greatly increase the spectral range of the incident pulse. The incident pulses in Figure 6-3 are ten times wider than the incident pulses in Figure 5-5 and therefore would have 1/10 the spectral range if modulating a narrow band signal. This frequency range, $\sim 1/\pi t_w$, would be smaller than a resonance spacing and no periodic structure could then show up in the transmitted pulse. An incident pulse of this width modulating a broadband signal would have a frequency spectrum determined by the signal or noise spectrum, which can be much greater than the resonance spacing. In this case, the transmitted pulse shows periodic time structure superimposed on a broad envelope of width t_w because the period $P < t_w$.

In the radiation model presented here, the transmitted pulses are shot noise modulated by quasi-periodic intensity variations which are independent of the noise process. Different realizations show the modulations to varying extent, but the common propagation characteristics show up clearly in the average acf of many single realizations. In

connection with an earlier result, we find that the presence of a broad band noise signal relaxes the requirement (cf. § III 3) that the incident pulse envelope be narrower than $1/\pi\Delta\omega$ to produce periodic time structure in the transmitted pulse.

Figure 6-1: Transmitted pulses in the field-free model for three realizations of incident Gaussian modulated shot noise with

$$\omega_p/c = 10^4$$

$$\omega_o/c = 10{,}005$$

$$ct_w = 0.5$$

$$\omega_N/c \simeq 10$$

The pulses are smoothed to a resolution of 1.0.

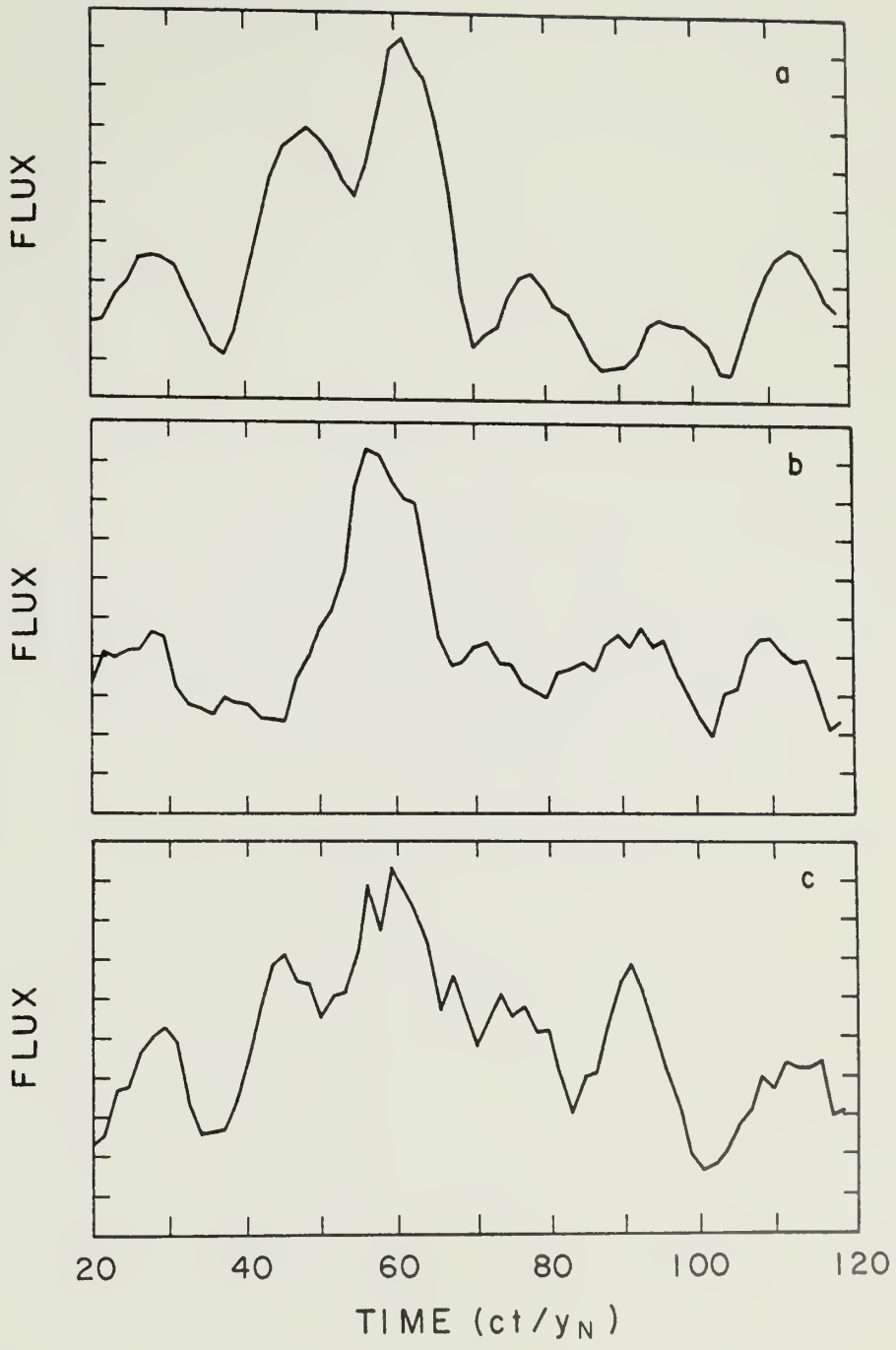
a
b
c
FLUX
FLUX
FLUX
20
40
60
80
100
120
TIME (ct/y$_N$)

Figure 6-2: Average autocorrelation function for 30 transmitted pulse realizations having the parameters of Figure 6-1.

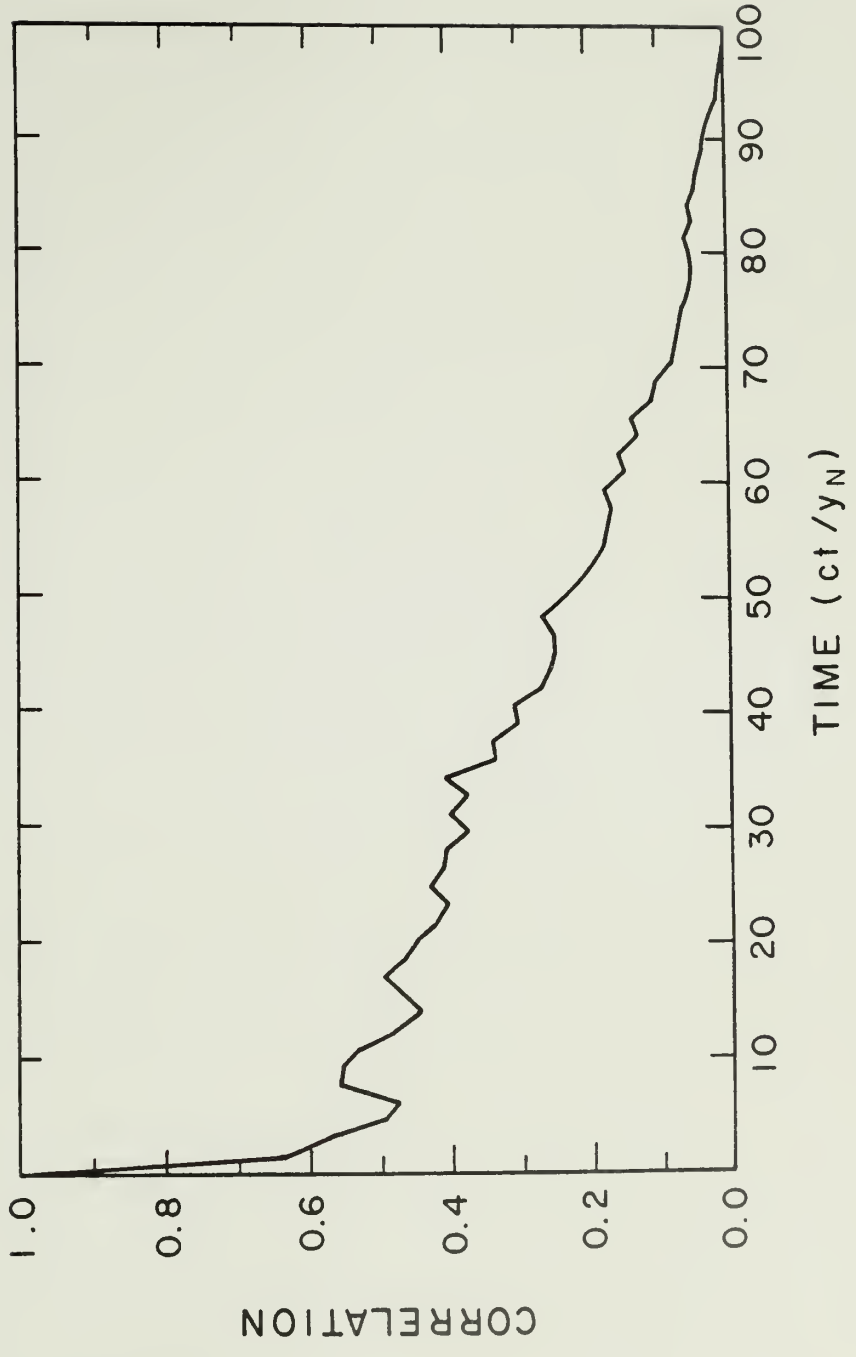
CORRELATION
1.0
0.8
0.6
0.4
0.2
0.0
10
20
30
40
50
60
70
80
90
100
TIME (ct / y_N)

Figure 6-3: Transmitted pulses and their autocorrelation functions for two realizations of Gaussian modulated shot noise with

$$\omega_p/c = 300$$

$$\omega_o/c = 372$$

$$ct_w = 0.5$$

$$\omega_N/c \simeq 50$$

incident on realizations of a turbulent shearing plasma with the parameters of Figure 5-5. The pulses are smoothed to a resolution of 0.1, and their fluxes are normalized to the peak flux of the incident pulse.

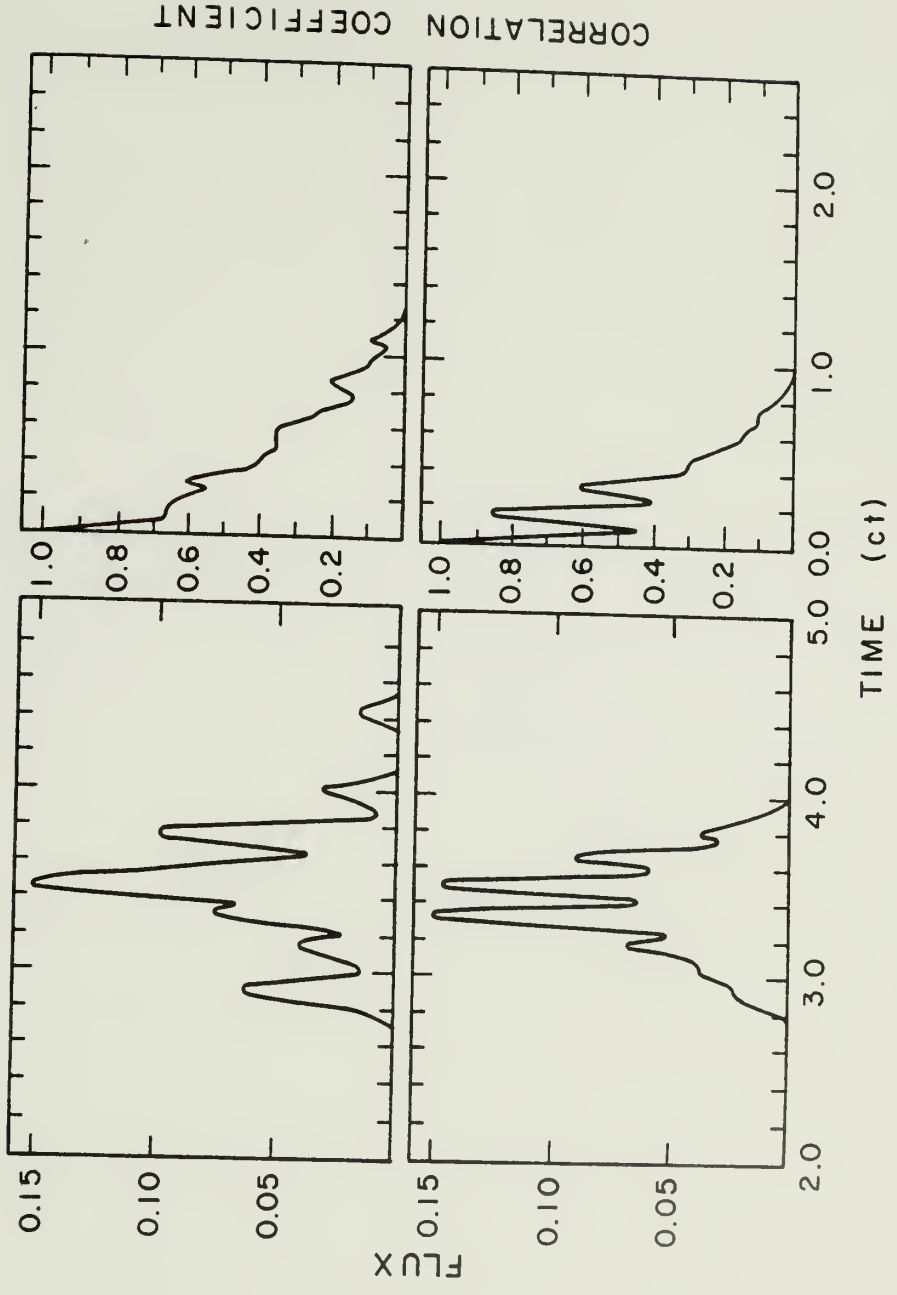
CORRELATION COEFFICIENT
1.0
0.8
0.6
0.4
0.2
0.0
1.0
2.0
FLUX
0.15
0.10
0.05
2.0
3.0
4.0
5.0
TIME (ct)

CHAPTER VII

SHEARING IN THE PULSAR MAGNETOSPHERE

While regions of relativistic velocity shear very likely exist in a pulsar magnetosphere, given the rapid rotation and high particle densities, the details of their location and geometry are somewhat speculative. Velocity shearing most certainly occurs near the speed of light cylinder, and even in the corotation zone, waves propagating out of the magnetosphere travel through moving plasma with increasing linear velocities. We also suggested that shearing could occur closer to the star as a result of particle streaming in flux tubes along the magnetic field. In this chapter, we examine the different kinds of velocity shear that are possible within present pulsar models and then evaluate the relevance of our calculations to propagation in the magnetosphere.

Corotation shearing could involve the entire magnetosphere, since the corotation zone extends from the stellar surface to near the light cylinder. The velocity in this zone, $v = \Omega r$, increases linearly with distance from the star. Corotation breaks down where the particle energy density equals the magnetic field energy density, at the Alfvén velocity

$$v_A = \frac{B}{(4\pi n \gamma_p)^{1/2}} \quad , \tag{7.1}$$

where n is the particle density and $\gamma_p\ mc^2$ is the particle energy. In the model of Henriksen and Rayburn (1974), this condition leads to a maximum corotation Lorentz factor of $\gamma_{MAX} = \sqrt{2}$ or $\beta \leq .71$, and defines the 'shear-strength-limited' boundary of the magnetosphere. Hinata and

Jackson (1974) place even stricter limits on the extent of the corotation zone. It seems unlikely that large Lorentz factors are involved in corotation shearing, although relativistic shearing velocities will probably exist. How rapidly the velocity decreases outside the corotation zone has not been determined, but is probably dependent on the magnetic field structure and particle densities there. The magnetic field is predominantly dipole in the corotation zone, but there is also a toroidal component generated by the flow of charged particles along the open field lines. At the light cylinder, the toroidal field component becomes comparable to or greater than the poloidal component (Goldreich and Julian 1969) as the field lines are swept back. Therefore, the field is almost parallel to the velocity in the region of high shearing.

Shearing caused by particle streaming close to the stellar surface would involve much higher maximum velocities. Lorentz factors for the accelerated particles emitting curvature radiation are estimated to be $\gamma \sim 10^3 - 10^6$. If these particle streams are responsible for the observed radio emission, then the radiation will propagate through regions of highly relativistic shear immediately after it is emitted. Since the plasma is constrained to move along the magnetic field, a model with the field parallel to the shearing velocity is also relevant here.

The shearing in these regions probably does not involve smooth velocity profiles, as there is likely to be some turbulence. The plasma itself is thought to be highly turbulent throughout the magnetosphere, so that sharp gradients in the index of refraction may exist independent

of shearing effects. A relativistic beam of charged particles moving through a neutral plasma is subject to a variety of instabilities. The classic "two-stream" instability which results in charge clumping along the relative direction of motion has been invoked to explain coherent radio emission in pulsars. A particle stream moving along a curved magnetic field line has also been shown to be unstable to bunching (Goldreich and Keeley 1971). In addition, transverse electromagnetic instabilities may cause filamentation of the beams perpendicular to the streaming motion. Hardee and Rose (1974) found that for fast pulsars, this would occur inside the light cylinder and they estimate the scale size of the fastest growing unstable mode to be less than 1 meter.

Considering the instabilities possible in a relativistically moving plasma, it is reasonable to expect that any shearing would involve some degree of fluid turbulence, especially in the emission region. We can estimate the scale size of the smallest turbulent cells as roughly the scale ℓ of the bunches which are thought to emit coherent radio emission. If radiation is to be coherent, the bunch size must be on the order of the wavelength, and broadband coherence requires $\ell << \lambda$. Since broadband coherence is currently needed to explain the observed properties of pulsar radio emission, it is possible that the scale of turbulence in the emission region, $L_o << \lambda$. The question of whether the pulsar emission mechanism is broadband or narrowband, however, is still far from being settled (Buschauer and Benford 1979, Cordes 1979b). The turbulence scale at the light cylinder is harder to estimate but is probably also on the scale of the dominant plasma instability. The magnetic field at the edge of the corotation zone is likely to be tur-

bulent also, with rapid fluctuations occurring in its strength and direction.

An important parameter of the model considered in the preceding chapters is the ratio of the gyrofrequency to the plasma frequency, ω_B/ω_p, and we estimate its value in different parts of the magnetosphere. From the basic expressions,

$$\omega_p = \left\{\frac{4\pi n_e e^2}{m}\right\}^{1/2} , \qquad \omega_B = \frac{eB}{mc} ,$$

we have

$$\omega_p = 5.6 \times 10^4 \, n_e^{1/2} ,$$

$$\omega_B = 1.7 \times 10^7 \, B . \tag{7.2}$$

In a dipole field, $B \simeq B_o(r_o/r)^3$, where B_o is the surface field strength and r_o is the radius of the star. The particle density in the magnetosphere also falls off with r in the same way, so that $n_e \simeq n_o(r_o/r)^3$, where n_o is the particle (electron) density at the surface. Estimates of n_o vary over a large range of values from the conservative estimate of Goldreich and Julian (1969),

$$n_o \simeq \frac{\Omega B}{2\pi c} \sim 5 \times 10^{10} \text{ cm}^{-3}$$

to the more liberal $n_o \sim 5 \times 10^{13}$ cm^{-3} of Ruderman and Sutherland (1975) and $n_o \sim 10^{19}$ cm^{-3} of Henriksen and Rayburn (1974). If we take $n_o = 10^{15}$ cm^{-3} and $B_o = 10^{12}$ gauss, then

$$\frac{\omega_B}{\omega_p} \simeq 9 \times 10^6 \left(\frac{r_o}{r}\right)^{3/2} \tag{7.3}$$

In most parts of the corotation zone, $\omega_B >> \omega_p$, and the shearing plasma exists in the strong field regime. At the light cylinder, $r = R_L \simeq 5 \times 10^9$ P, and taking $r_o = 10^6$ cm.,

$$\frac{\omega_B}{\omega_p} \simeq 27 P^{-3/2} B_{12} n_{15}^{-1/2} \tag{7.4}$$

where B_{12} is the surface field in units of B_o and n_{15} is the surface particle density in units of n_o. Therefore, shearing plasma at the light cylinder will have $\omega_B \gtrsim \omega_p$, except in pulsars with weak surface fields or large particle densities.

The relatively simple models we considered in our calculations have avoided complexities which could obscure an understanding of the basic propagation effects in shearing media. Some of these complexities, unfortunately, are present in the pulsar magnetosphere. For example, it is unlikely that the rest frame plasma parameters are constant in space or time. The plasma frequency decreases with r because of the fall off in particle density, and beyond the corotation zone, ω_p may decrease to near zero before the velocity reaches zero. Our model maintained a constant ω_p in the rest frame which would be unrealistic in the corotation shearing. A symmetric velocity field is probably also unrealistic, although our results would be essentially the same for any single peaked profile with large enough gradients. The fact that turbulence may be present decreases the dependence of the results on a specific mean velocity profile. A minimum of two sharp gradients in velocity (or one in velocity and one in particle density) are required to produce the resonance effect above the plasma frequency. Turbulent shearing would

produce at least several of these reflection causing gradients. The magnetic field varies in strength and direction through the magnetosphere also, but in regions where $\omega_B >> \omega_p$, the variation would be gradual. At the light cylinder, where the field lines are being swept back, the field may change direction more rapidly.

If the shearing regions producing the propagation effects we have studied are relatively small, then plane parallel shearing may be a good approximation. If they are comparable to the size of the entire magnetosphere, though, spherical three-dimensional geometry would be more appropriate. A full three-dimensional treatment of wave propagation in the plane parallel shearing medium described in Chapter II is considerably more complicated. If $k_z \neq 0$, equation (2.10) for the x components of the fields contains both H_z and E_z, so that the boundary conditions would mix the polarizations and they would not propagate independently. The polarization of the transmitted pulses could therefore be quite different. In the pulsar magnetosphere, however, magnetic field effects on the polarization are probably more important. Deviations from plane parallel shearing would affect the angles at which the radiation enters successive layers of the medium. For normally incident waves having straight ray paths, there would be no effect due to curvature, but the differences in ray path and transmission characteristics could be significant for waves at oblique angles of incidence.

CHAPTER VIII

A MODEL FOR PULSE MICROSTRUCTURE

We now compare the results presented in Chapters III - VI with the existing observational data on single pulses. Properties of micropulses, observed in ten pulsars to date, are reviewed in §1, and in §2 we suggest a model for periodic microstructure based on propagation effects in a shearing plasma.

1. Observed Properties

Microstructure has been observed in about 80% of the nearby pulsars studied with high time resolution, at frequencies of several hundred MHz to several GHz, and is thought to be a general characteristic of the pulsar signal. Micropulses are the fine structure of single pulses, appearing as spikes of several hundred microsecond duration. The single pulse structure varies drastically from one pulse to the next, some pulses showing very intense micropulses while others show none at all. The microstructure observed in some pulsars is quasi-periodic. Table 1 shows the microstructure timescales and periods for the ten pulsars in which it has been observed. The timescale, Δt_μ, is obtained from the break point in the average autocorrelation function which defines a shoulder on the zero lag spike called the "micropulse feature". The periods, P_μ, appear as bumps or enhancements at certain time lags and, in general, vary from pulse to pulse. The microstructure in PSR 2016 + 28 has an average period of 0.9 ms. but the periods range from 0.3 ms. to 2.0 ms., with no apparent correlations between adjacent

drifting subpulses in the same pulse or between different pulses (Cordes 1976a). The micropulse time scales and periods tend to increase with pulsar period (as do subpulse time scales), but the correlation of P_μ with P is questionable because of the large spread in P_μ for each pulsar.

Polarization properties of single pulses have been studied with high time resolution and reveal fluctuations in the Stokes Parameters on the same time scale as the intensity variations. Autocorrelation analysis of the Stokes Parameters suggests that the state of polarization varies slowly over the micropulse duration, the position angle and sign of circular polarization changing most frequently on the edges of micropulses (Cordes and Hankins 1977). Single pulse profiles often show a 90° change in position angle coincident with a change in sense of circular polarization between two micropulses. This behavior seems to suggest the presence of orthogonal modes in the observed signal. Cordes, Rankin, and Backer (1978) found that in PSR2020+28, a positive or negative sign of the Stokes Parameter V was almost always associated with the same value of the position angle. Properties of mode switching in single pulses of other pulsars suggest that they also emit radiation in orthogonal modes.

The spectral properties of microstructure, and of single pulses in general, are not well determined due to the lack of simultaneous multifrequency observations. Nevertheless, these observations are very important in their potential for establishing the physics of the radiation mechanism and of magnetospheric propagation effects. PSR1133+16 and PSR0950+08 show microstructure over a large frequency range from 111 MHz to 3 GHz. The microstructure in three other pulsars, however, seems

to diminish with increasing frequency. The microstructure feature in the average autocorrelation function for PSR2016+28 disappears somewhere between 606 MHz, where it is weak, and 1410 MHz, where it is absent. The microstructure modulation index, measuring the strength of the micropulses, decreases steadily with increasing frequency (Cordes 1979a). Micropulses are not seen in PSR1919+21 above 318 MHz nor in PSR1944+17 at high frequencies. These observations suggest that the bandwidth of microstructure is smaller than the total flux bandwidth. Since different frequencies may be emitted at different distances from the star, the actual bandwidth of microstructure may be even smaller, and could be determined by the frequency range over which simultaneous microstructure is correlated. Rickett et al. (1975) found that the microstructure in PSR0950+08 is at least 50% correlated between 111 and 318 MHz, implying a bandwidth of at least 200 MHz. Ferguson and Seiradakis (1978) found the microstructure in PSR1133+16 to be 20% decorrelated between channels separated by 100 MHz at 2.7 GHz. It seems that microstructure bandwidths, at least in these pulsars, are around a few hundred MHz.

Some properties of the microstructure in several pulsars have been found to be highly dependent on pulse longitude. Cordes and Hankins (1977) performed autocorrelation analysis of the Stokes Parameters in different longitude regions and showed that the strength and polarization of the microstructure varied while the time scales remained constant. These observations also suggest a correlation between micropulse intensity and polarization fluctuations.

2. Microstructure as a Propagation Effect

At the present time, microstructure is an unpredicted and unexplained phenomenon. Models have been proposed to account for various isolated properties of micropulses but no comprehensive theory has emerged. The time scale could be caused either by a rotation of angular beams past the observer (Benford 1977) or by actual temporal modulations of the emission. In most pulsars, the position angle has been observed to rotate systematically through the average pulse profile. This behavior has been explained as a geometric effect within the context of the polar cap model (Radhakrishnan and Cooke 1969). Coherent curvature radiation from particle bunches moving along magnetic field lines is linearly polarized parallel and perpendicular to the field. The position angle at any given longitude is determined by the projection of the field onto the plane of the sky, and dipole fields will produce position angle rotations which generally agree with those observed. If subpulses and micropulses are caused by angular beams of radiating particles, then they should show similar position angle rotations. The position angle in single pulses rotates through the subpulses, so it seems that subpulses are due to angular beaming. This is apparently not the case for microstructure, if the position angle is constant over a micropulse duration, suggesting that models with subpulses due to angular beaming and micropulses due to temporal modulations might better explain the observations (Cordes 1975). Ruderman and Sutherland (1975) have accounted for micropulses in their model as the temporal modulations of current in the emission region caused by pair production avalanches above the polar cap. However, the typical time between spark

discharges producing the current is $\sim 10\,\mu s$, and is a factor of ten too small to account for the observed micropulse durations.

The orthogonal mode switching in single pulses has been attributed to propagation effects in the magnetosphere. Blandford and Scharlemann (1976) found that induced Thomson scattering is much stronger for radiation polarized parallel to a strong magnetic field than perpendicular to it. When the brightness temperature is high, induced scattering is dominant, and mode transitions will occur with optical depth changes. When the optical depth is large, the parallel mode is strongly scattered, leaving the observed radiation in the perpendicular mode. If the optical depth is $<< 1$, the radiation will be polarized in the dominant parallel mode.

We find that many of the observed properties of microstructure may be explained in the context of the model for pulse propagation in a shearing plasma. This model provides a mechanism for producing pure temporal modulations which are periodic. The observed microstructure periods at several hundred MHz require that

$$\omega P_{\mu} \sim 10^5 \ .$$

From equation (3.18), equating P_{μ} with P,

$$y_N \sim 10^5 \, \pi n_o \frac{c}{\omega} \tag{8.1}$$

so that a shearing region of size $y_N \lesssim 10^7$ cm. is necessary to produce the observed periods. This is about .01 times the distance from the polar cap to the light cylinder. If we associate the periodic components in the transmitted pulses with micropulses, then pulses of $t_w \lesssim 10^{-4}$ s are required as input to the shearing region. Curvature

radiation by a cloud or column of coherent particle bunches moving along a magnetic field line with radius of curvature R_c produces radiation along a given line of sight for a time $R_c/c\gamma$, where γmc^2 is the average particle energy. For a typical energy, $\gamma = 10^2$ and $R_c = 10^7$ cm, pulses of duration 3×10^{-4} s would be produced. Alternatively, t_w could be the coherent life span of the radiating bunches.

In the context of the noise model of Rickett (1975) and the results of Chapter VI, micropulses are amplitude modulations of a noise-like signal. If the radiation is broadband, then each particle bunch will produce a shot pulse of duration $\sim$ 1 nanosecond, equal to the inverse of the bandwidth ($\sim$ 1 GHz). Many of these "nanopulses" combine incoherently to produce a broad pulse which then passes through a shearing region on its way out of the magnetosphere. Depending on the mixture of emitted modes and the frequency, this pulse may then acquire periodic amplitude modulations and polarization fluctuations from multiple reflections. In the noise model, there is no upper limit to the duration of the incident pulse. It is possible for subpulses, with typical widths $\sim 10^{-3}$ s, to be the incident pulses, acquiring micropulse amplitude modulations on passing through a region of shearing plasma. Pulse to pulse variations in the strength of microstructure can be interpreted as the dependence of the strength and morphology of the amplitude modulations on the statistics of the random process.

According to the results of Chapter IV, the microstructure period should be frequency dependent if $\omega_p \gtrsim \omega_B$ and frequency independent if $\omega_B >> \omega_p$ in the shearing region. This allows the possibility of 1) testing the weak field model by looking for the frequency dependence pre-

dicted by equation (3.18), 2) setting limits on the quantities B_o and n_e if $\omega_p > \omega_B$, and 3) determining the location and size of the shearing region. According to equation (3.18), the microstructure period should decrease with frequency to the asymptotic value $y_N/\pi c$. If this is observed, then ω_p must be greater than ω_B in the shearing region. From the expressions for ω_B/ω_p in Chapter VII, this is unlikely except near the light cylinder, and even there it is unlikely, unless B_o is small or n_e is larger than previously thought.

The observed polarization properties can be explained in this model by means of the birefringence of the shearing plasma. In the field-free case, we found that a linearly polarized incident pulse acquires circular polarization and the transmitted pulse displays orthogonal mode transitions on the edges of the components. The polarization fluctuations are correlated with intensity changes because the position angle and circular polarization are determined by the relative amplitudes and phases of the O and X mode electric fields. In the presence of a magnetic field, the polarization fluctuations are more complex, but are also due to birefringence. Sharp mode changes still occur preferentially between components. The two orthogonal linear polarizations can independently acquire large amounts of circular polarization with opposite sign. These effects are strongest for $\omega_B \sim \omega_p$ and relax the condition on the orientation of the incident pulse position angle for the presence of polarization fluctuations in the transmitted pulse (cf. §III 3). It is generally true in this model that intensity fluctuations are a necessary but not sufficient condition for mode switching. This seems to be the case in observed single pulses,

which show microstructure with and without mode switching, but seldom mode switching in the absence of microstructure (Cordes and Hankins 1977).

Since propagation effects in this model become weaker with increasing frequency, it is predicted that periodic microstructure should make a smaller contribution to the total flux at high frequencies. Although this seems to be true for several pulsars, the bandwidths of microstructure inferred from cross-correlation analaysis cannot be easily accounted for in the smoothly shearing plasma model. Periodic intensity modulations can only be produced very close to ω_p in the absence of very steep gradients. This model also predicts strict and constant periodicities which is not the case observationally. The turbulence model of Chapter V, however, is able to account for both of these properties by introducing a physical cause for the required velocity gradients. As we have shown in Chapter VII, the existence of turbulence in the shearing region is not an unreasonable assumption. According to our calculations, turbulence on the scale of the wavelength is necessary to produce bandwidths $\sim \omega_p$. We suggested that fluctuations in streaming or shearing motions on this scale could result from the dominant plasma instabilities which are of scale size λ. The turbulence parameters required to give the observed minimum bandwidths can be estimated using equations derived in Chapter V. We distinguished between mildly relativistic, $\gamma \sim 1$, and highly relativistic, $\gamma >> 1$, turbulence. Near the light cylinder, it is probable that $\gamma \sim 1$, and equation (5.7) gives

$$\frac{\sigma_v}{L_o} \sim \left(\frac{\omega_{MAX}}{c} - \frac{\omega_p}{c}\right)^{3/2} \left(\frac{c}{\omega_p}\right)^{1/2} \frac{1}{\beta} \quad .$$

Assuming that $\omega_p = 10^8\ s^{-1}$, $\beta = 0.7$ and $(\omega_{MAX} - \omega_p) = 500$ MHz,

$$\frac{L_o}{\sigma_v} \sim 20 \text{ cm.}$$

so that $L_o \lesssim 20$ cm. will produce a fairly large bandwidth. In the emission region, $\gamma >> 1$, and equation (5.8) gives

$$\frac{L_o}{\sigma_v} \sim \left(\frac{\omega_{MAX}}{\omega_p}\right)^{-3} \frac{c}{\omega_p} \sim 2.4 \text{ cm.}$$

with $\omega_{MAX}/\omega_p = 5$ and $\omega_p = 10^8\ s^{-1}$. In this case, $L_o \lesssim 2$ cm. is required and, as mentioned previously, stronger turbulence is necessary to produce a similar bandwidth in the presence of highly relativistic velocities. The determination of the microstructure frequency range could place strict limits on the scale and degree of turbulence in the shearing region.

Turbulent shearing also predicts a variability in the microstructure period which reflects the time dependence of fluctuations in the velocity shear. The largest and dominant period results from reflections between gradients at maximum spacing (i.e., the size of the turbulent region), while smaller periods are also possible and result from closer spacings. This could explain the observed variation in the microstructure period from pulse to pulse (or from subpulse to subpulse). The mean period should depend on frequency in approximately the same way as in the turbulence free models. The periodic microstructure in all five pulsars in Table 1 has been observed to have a range of

periods at each frequency, with PSR0950+08 and PSR2016+28 having the largest ranges.

In this mechanism for producing periodic micropulses by temporal modulations, we have assumed that the pulses of radiation are incident on the shearing plasma almost perpendicular to the velocity. We mention another possible mechanism for producing periodic modulations within the context of this model, though it will not be as fully explored. In Chapter III, it was found that at grazing angles of incidence, the reasonance spacing in frequency approached zero but that spatial interference fringes approached a constant spacing (cf. eqs. [3.22] and [3.23]). When rotated past an observer, these spatial variations would become periodic temporal variations, with the period

$$P_\mu = \Delta\theta' \frac{P}{2\pi} \sim \frac{c}{n_o \omega y_N} P \quad . \tag{8.2}$$

For $P = 1\,s$, a shearing region of size $y_N \sim 3 \times 10^5$ cm is required to produce a microstructure period $P_\mu \sim 10^{-3}$ s. This mechanism would be appropriate if the shearing region were located in the radio emission region, because radiation emitted along field lines is travelling almost parallel to the velocity. Note that the microstructure period here is dependent on pulsar period, as well as on frequency. The frequency dependence differs from that predicted by the temporal mechanism by an extra factor of ω^{-1}.

TABLE 1

MICROPULSE TIME SCALES AND PERIODS

Pulsar	Δt_μ* (ms)	P_μ+ (ms.)	P(s.)
0525 + 21	3.00	--	3.74
0809 + 74++	0.10 - 0.20	4.0	1.292
0823 + 26	0.55	--	.531
0834 + 06	1.05	--	1.274
0950 + 08	0.18	0.5	.253
1133 + 16	0.58	1.2	1.188
1919 + 21	1.30	--	1.337
1944 + 17	0.30	0.9	.440
2016 + 28	0.28	0.9	.558
2020 + 28	0.10	--	.343

*From Cordes 1979a.

+From Cordes 1979a, positions of period distribution peaks at 430 MHz.

++From Popov and Hankins (unpublished data).

CHAPTER IX

CONCLUSIONS

The results of these numerical calculations have illustrated that propagation effects in the pulsar magnetosphere may be significant. The basic model, a field-free plasma undergoing laminar velocity shear, was chosen for its simplicity, and provides a mechanism for producing periodic temporal modulations of input pulses in a narrow frequency range. This shearing medium was found to be birefringent, with radiation polarized in the plane of shear undergoing multiple reflections from velocity gradients and radiation polarized perpendicular to the plane of shear unaffected by the motion. This birefringence produces polarization fluctuations in the transmitted pulse which are correlated with the periodic intensity variations.

We found that a magnetic field parallel to the velocity introduces more complex propagation modes which are neither linearly polarized nor constant through the medium. A shearing magneto-plasma does, however, preserve the orthogonality of the incident polarized modes and can convert linear to circular polarization. The period of the time structure in the transmitted pulse is frequency independent in the limit of a very strong field, but in the weak field regime shows the frequency dependence seen in the field-free case. A frequency dependence of the period is possible when $\omega_B \geq \omega_p$, but these cases are complicated by the presence of an absorption band encountered above a certain velocity. Because the cold plasma approximation breaks down at resonances, the amount of absorption cannot be determined and these cases could not be fully ex-

plored in this model. Due to the presence of more than one cutoff frequency, the periodic temporal modulations can occur in several widely spaced, though still narrow, frequency bands.

The introduction of turbulent velocity fluctuations in the shearing motion resulted in broadband temporal modulations as well as a variability in the period of the time structure. A more realistic shot noise model for the incident radiation produced a variability in the extent to which the modulations are expressed in the transmitted pulse structure. The noise model also allowed broad incident pulses to acquire shorter periodic temporal modulations, which was not possible with narrow band radiation.

The different models for the plasma, the shearing motion and the incident radiation were based on conditions believed to exist in the pulsar magnetosphere. In building these models, compromises were necessarily made between realism and simplicity. The field-free plasma model, being the simplest, affords the easiest understanding of basic propagation effects, but is too unrealistic to permit a comparison of the results with observation. Variations on this basic model were studied separately so that the effects of each could be understood. The most realistic model would include all of the variations, the magnetic field, turbulence, shot noise, simultaneously. Although we did not make a study of all of these effects together, several calculations were discussed in which two of the effects were present. Results obtained for shot noise propagating through a turbulent medium seemed to be consistent with a superposition of two independent random processes. In other words, the results are predictable from the parameters of each separate

process. The presence of velocity turbulence seems to randomize the polarization fluctuations caused by a magnetic field as well as producing different periodicities in the transmitted pulse. There is much more, though, which was not explored here (e.g., the effect of turbulence on the location of absorption bands, the superposition of different resonance bands which are much broader than their spacing).

There are effects not considered in these models which could significantly change the results we have obtained. Our model for turbulent shearing defined a spatial correlation scale but no temporal scale. It was therefore implicitly assumed that the fluctuations in velocity occur much more slowly than the propagation time of the pulse across the shearing region, but faster than the time between successive incident pulses. Each realization defines the location and strength of velocity gradients producing the multiple reflections. If they were variable during the course of the pulse propagation, the periodicities in the transmitted pulse might not be as strong. If fluctuations occurred slowly enough that the same gradients existed for successive pulses, then the period of the resulting time structure would not vary significantly from pulse to pulse.

We also did not consider the possibility of density variations in the plasma, which are undoubtedly present in the magnetosphere. Fluctuations in the particle density producing gradients in the index of refraction could cause reflections in much the same way as do velocity fluctuations. This could provide a mechanism for producing temporal modulations without shearing motions. A resonance effect caused by changes in density, though, would have a narrower frequency range.

There would be a similar upper limit on the frequency showing resonances from the size of the gradients in ω_p. There would, however, be a stricter lower limit on the frequency range, because frequencies below the highest value of ω_p would not propagate, unless the fluctuations were much smaller than the wavelength. In the case of velocity fluctuations, the effective plasma frequency is always less than or equal to the rest frame value (except at grazing angles of incidence).

In Chapter VIII, we suggested a model, based on the results of our calculations, for the micropulse amplitude modulations seen in single pulses. Several predictions emerged from this model as well as the possibility for placing limits on certain physical quantities describing the magnetosphere.

1) The bandwidth of microstructure should be smaller than the total bandwidth of the pulsar radio emission. This is perhaps the strongest prediction, resulting from the premise that the mechanism producing microstructure is separate from the radio emission mechanism.

2) If $\omega_B >> \omega_p$ in the shearing region, the micropulse period should be frequency independent. If $\omega_B \lesssim \omega_p$, the period should be frequency dependent. The angular beaming model also predicts a frequency dependence of the micropulse period (Cordes 1979a), but it is $\sim \omega^{-.25}$ which is much weaker than the dependence predicted by equation (3.18).

3) The spectrum of periodic microstructure should show sharp resonances with quasi-periodic spacing.

4) Micropulses should be independent of the subpulses that contain them. According to the model, subpulses are not conglomerations of independent micropulses but the input to the mechanism which produces periodic microstructure.

Observations of microstructure may be able to test these predictions.

1) The microstructure bandwidth can be determined by cross-correlating simultaneous single pulses over increasingly larger frequency intervals. If the bandwidth is smaller than the total flux bandwidth, the correlation coefficient will become negligibly small at some frequency interval. A frequency dependence of the microstructure period or width, however, could cause a decorrelation independent of the bandwidth.

2) Searching for a frequency dependence of the micropulse period is difficult, due to the wide spread of periods found at each frequency. The strong frequency dependence of period predicted by equation (3.18) near the plasma frequency may be observable.

3) Fine resolution spectra of pulses showing periodic microstructure would be expected to show resonances separated by the inverse of the micropulse period. This would not be a true verification of the model, however, because this kind of frequency structure should be present in the spectrum of a periodic signal, regardless of its origin. Our model only gives a physical cause for the existence of the frequency structure.

4) Observations determining that micropulses are independent of the subpulses in which they appear would give further support to the model. This could be shown most dramatically by establishing that micropulses appearing in a drifting subpulse are not correlated from pulse to pulse. Other observations could help to determine the origin of microstructure but could not prove or disprove the model presented here. These include further studies of the dependence of micropulse properties on pulse longitude and a search for microstructure in other pulsars to de-

termine if it is really a general characteristic of the pulsar signal.

If the model proposed in Chapter VIII for periodic microstructure proves to be generally correct, then several potentially important properties of the magnetosphere might be inferred. Observational determination of the microstructure bandwidths could set limits on the scale and degree of turbulence in the shearing region (cf. §VIII 2). A frequency independent period would imply that the shearing regions responsible for microstructure are located in the emission region where $\omega_B >> \omega_p$. A frequency dependent period would require the shearing region to be located near the light cylinder where $\omega_p \gtrsim \omega_B$, which might also indicate a low surface magnetic field or a high particle density in the shearing region. Finally, the largest microstructure periods observed at a given frequency would determine y_N, the size of the shearing region. If turbulence is necessary for the production of periodic microstructure, then y_N would be associated with the size of a region of turbulence in the magnetosphere. The boundaries of these regions might be determined by the locations of onset of various instabilities. For example, Benford and Buschauer (1977) propose that at a certain distance from the star, the onset of the filamentary instability will affect plasma streaming along open field lines. They find that this happens just inside the light cylinder for pulsars with either long periods or small magnetic fields. In this case, y_N would be the distance from the onset of instability to the location outside the corotation limit where either the particle density or the velocity falls off significantly. It should be mentioned that turbulence may not be necessary if, by some other cause, the required velocity gradients exist in

the path of the observed radiation.

Our results raise some theoretical questions on which further work is needed to put the model on a firmer foundation. First, it is quite possible that non-linear effects in wave and pulse propagation may be present, due to the high radiation densities in the magnetosphere. Intense radiation is capable of changing the properties of the plasma such that it can propagate more easily. Perhaps a strong pulse of radiation will ignore the steep gradients we have assumed will produce reflections leading to the resonance effect. A wave propagating through a shearing region can also take energy from the medium at one point and give up the energy at another, so that there is a transfer of energy and momentum between different parts of the medium. In the case of weak wave fields, these transfers of momentum have negligible effects on the overall motion. Intense waves or pulses, however, may produce changes in the velocity profile resulting in the creation or destruction of gradients or even in turbulence. If these effects are determined to be significant in pulsars, then the superposition principle, and thus the Fourier analysis used in these calculations is no longer valid. In addition, the non-linear plasma dispersion relation could be quite different from the linear dispersion relations used here.

A second question concerns the true behavior of waves and pulses at the plasma resonances they encounter, which has not been adequately described in the cold plasma approximation. There has been considerable study of wave behavior in finite temperature, inhomogeneous magnetoplasmas. This work suggests that a number of interesting phenomena can occur as radiation passes through resonances, such as mode conversion

and mode coupling, which may also happen in a shearing magneto-plasma.

Another poorly understood subject is relativistic turbulence. We have attempted to model a relativistic turbulent flow along the lines of non-relativistic turbulence, but the statistics may not be the same. The relationship between instability driven density fluctuations and velocity fluctuations in a relativistically streaming plasma must also be determined to better model the dynamics of turbulent shearing in pulsars. Clearly, more work on these problems is needed before propagation effects in the magnetosphere are fully understood.

REFERENCES

Adams, R.N. and Denman, E.D. 1966, Wave Propagation and Turbulent Media (New York: Elsevier).

Bailey, V.A. 1950, Phys. Rev., 78, 428.

Bellman, R. and Kalaba, R. 1956, Proc. Nat. Acad. Sci. USA, XLII, 629.

Benford, G. 1977, M.N.R.A.S., 179, 311.

Benford, G. and Buschauer, R. 1977, M.N.R.A.S., 179, 189.

Blandford, R.D. and Scharlemann, E.T. 1976, M.N.R.A.S., 174, 59.

Box, G.E.P. and Muller, M.E. 1958, Ann. Math. Stat. XXIX, 401.

Buschauer, R. and Benford, G. 1979 (preprint).

Chandrasekhar, S. 1960, Radiative Transfer (New York: Dover).

Chawla, B.R. and Unz, H. 1971, Electromagnetic Waves in Moving Magneto-Plasmas (University Press of Kansas).

Chen, H.C. and Cheng, D.K. 1966, IEEE Proc., 54, 62.

Cordes, J.M. 1975, Ph.D. Thesis, University of California, San Diego.

_____. 1976a, Ap.J., 208, 944.

_____. 1976b, Ap.J., 210, 780.

_____. 1979a, Aust. J. Phys., in press.

_____. 1979b, Space Sci. Rev., in press.

Cordes, J.M. and Hankins, T. 1977, Ap.J., 218, 484.

Cordes, J.M., Rankin, J. and Backer, D.C. 1978, Ap.J., 223, 961.

Ferguson, D.C. and Seiradakis, J.H. 1978, Astron. Astrophys., 64, 27.

Ginzburg, V.L. 1970, The Propagation of Electromagnetic Waves in Plasmas (New York: Pergamon).

Goldreich, P. and Julian, W.H. 1969, Ap.J., 157, 869.

Goldreich, P. and Keeley, D.A. 1971, Ap.J., 170, 463.

Hardee, P.E. and Rose, W.K. 1974, Ap.J. (Letters), 194, L35.

Henriksen, R.N. and Rayburn, D.R. 1974, M.N.R.A.S., 166, 409.

Hinata, S. and Jackson, E.A. 1974, Ap.J., 192, 703.

Ko, H.C. and Chuang, C.W. 1977, Radio Science, 12, 337.

_____. 1978, Ap.J., 222, 1012.

Lee, M.A. 1974 VIII, Ap.J., 194, 165.

Lee, M.A. and Lerche, I. 1974 XI, Ap.J., 194, 409.

_____. 1975 XII, Ap.J., 198, 477.

Lerche, I. 1974I, Ap.J., 187, 589.

_____. 1974 II, ibid, 597.

_____. 1974 III, Ap.J., 188, 627.

_____. 1974 IV, Ap.J., 191, 191.

_____. 1974 V, ibid, 753.

_____. 1974 VI, ibid, 759.

_____. 1974 VII, ibid, 763.

_____. 1974 IX, Ap.J., 194, 177.

_____. 1974 X, ibid, 403.

Manchester, R.N. and Taylor, J.H. 1977, Pulsars (San Francisco: Freeman).

Merzbacher, E. 1970, Quantum Mechanics (New York: Wiley & Sons).

Minkowski, H. 1910, Math. Ann., 68, 472 (see also Gott. Nach., 1908, p. 53).

Radhakrishnan, V. and Cooke, D.J. 1969, Ap. Letters, 3, 225.

Rickett, B.J. 1975, Ap.J., 197, 185.

Rickett, B.J., Hankins, T.H. and Cordes, J.M. 1975, Ap.J., 201, 425.

Ruderman, M. and Sutherland, P. 1975, Ap.J., 196, 51.

Scarf, F.L. 1961, Am. J. Phys., 29, 101.

Sturrock, P.A. 1971, Ap.J., 164, 529.

Tai, C.T. 1964, IEEE Proc., 52, 685.

Tang, T. 1970, Phys. Fluids, 13, 121.

Townsend, A.A. 1976, The Structure of Turbulent Shear Flow (Cambridge University Press).

Wait, J.R. 1970, Electromagnetic Waves in Stratified Media (New York: Pergamon).

Yeh, C. and Casey, K.M. 1966, Phys. Rev., 144, 665.